ASPECTS OF THE MHD STABILITY OF CORONAL AND LABORATORY PLASMAS

Leo J. Clifford

A Thesis Submitted for the Degree of PhD
at the
University of St Andrews

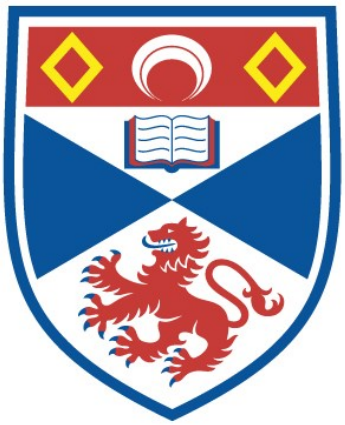

1993

Aspects of the MHD stability of coronal and laboratory plasmas

Leo J. Clifford

Thesis submitted for the degree of Doctor of Philosophy of the University of St Andrews

9th February 1993

ProQuest LLC.
789 East Eisenhower Parkway
P.O. Box 1346
Ann Arbor, MI 48106 – 1346

TL B3LY

Abstract

The magnetohydrodynamic (MHD) model is a simple mathematical model that treats a plasma as a perfectly conducting fluid acted upon by magnetic and pressure-driven forces. Many instablities in plasmas can be predicted using this model. In this Thesis, aspects of the linear stability of solar and laboratory plasmas are studied using the MHD model. Firstly, we investigate the thermal instability of coronal plasmas with line-tied magnetic fields and with anisotropical heat conduction, using an analytical analysis which concentrates on isobaric perturbations, and a time-dependent numerical code. We find that including perpendicular thermal conduction means that condensations are restricted to a narrow layer around the region where the local isobaric growth rate is largest and that, while the growth rate of the thermal mode is largely unaffected by perpendicular thermal conduction, this may be an important factor in determining the lengthscale for the width of condensations. Secondly, the effect of a finitely conducting wall on the linear stability of Spheromak and Reversed Field Pinch equilibria is investigated. We find growth rates for the modes that are present because of the finite resistivity of the wall, which grow proportionally to the "long" time constant of the wall. Finally, we apply a tractable method, derived by De Bruyne (1990), for investigating the stability of 2-D line-tied magnetic fields, to cylindrically symmetric spheromak equilibria. The method involves the solution of two sets of ordinary differential equations, integrated along the field lines, which give necessary and sufficient conditions for stability. The role of plasma pressure and of the width of the entrance region are investigated.

I, Leo Clifford, hereby certify that this Thesis has been composed by myself, that it is a record of my own work, and that it has not been accepted in partial or complete fulfilment of any other degree or professional qualification.

Signed Date 26-3-93

I was admitted to the Faculty of Science of the University of St Andrews under Ordinance General No 12 on 6th October 1985 and as a candidate for the degree of Ph.D. on 5th October 1989.

Signed Date 26-3-93

I hereby certify that the candidate has fulfilled the conditions of the Resolution and Regulations appropriate to the Degree of Ph.D.

Signature of Supervisor Date 26/3/93

In submitting this thesis to the University of St Andrews I understand that I am giving permission for it to be made available for use in accordance with the regulations of the University Library for the time being in force, subject to any copyright vested in the work not being affected thereby. I also understand that the title and abstract will be published, and that a copy of the work may be made and supplied to any *bona fide* library or research worker.

Contents

Chapter 1

Stability theory using the MHD model

Any theory advanced by theorists must, at some point, be related to observations of the physical world. Theorists working in the field of plasma physics have two main sources of experimental data: laboratory devices used in the search for nuclear fusion and the Sun. Although the magnetic configurations, parameters and boundary conditions vary widely between solar and terrestrial plasmas, any realistic model of plasma behaviour would explain observed features in each.

One model of plasma behaviour is the magnetohydrodynamic (or MHD) model. This simple model treats the plasma as a perfectly conducting fluid acted upon by magnetic and pressure-driven forces. It serves as a useful tool for predicting equilibria and large-scale instabilities in a large variety of magnetic topologies. Most work published by theorists investigating phenomena observed on, or in the Sun, has made use of the MHD model. Also, many macroscopic instabilities in fusion devices are predicted by the MHD model

(Bateman, 1978).

Questions of stability and instability are important for many phenomena both in the solar corona and in laboratory plasma containment devices. Stability theory has two main roles: to account for the stability of observed structures with long lifetimes and to discriminate against theoretical models that cannot be reconciled with observations. This in turn provides quantitative bounds on physical parameters that cannot be accurately measured.

Reviews of MHD stability in laboratory plasmas can be found in Wesson (1978) and Freidberg (1982). For coronal configurations reviews have been written by Van Hoven (1981), Birn and Schindler (1981) and Hood (1990, 1991). This Chapter introduces the MHD approximation and examines how we can use this model to investigate stability.

1.1 The MHD approximation

The MHD model is one of the simplest models used to describe the interaction between a highly conducting fluid and a magnetic field. In the MHD approximation, the behaviour of a continuous plasma is described by a simplified form of Maxwell's equations together with Ohm's law, the equations of mass continuity, equations of motion and energy, and an equation of state, for which we take the perfect gas law.

1.1.1 The MHD equations

The continuity equation expresses conservation of mass. The momentum equation is taken with viscosity assumed to be negligible. The convective derivative

$$\frac{D}{Dt} \equiv \frac{\partial}{\partial t} + \mathbf{v} \cdot \nabla$$

represents the rate of change with time following the plasma in its motion. The continuity equation is

$$\frac{D\rho}{Dt} = -\rho \nabla \cdot \mathbf{v} \tag{1.1}$$

and the momentum equation is

$$\rho \frac{D\mathbf{v}}{Dt} = -\nabla p + \frac{1}{\mu_0} (\nabla \times \mathbf{B}) \times \mathbf{B} + \rho \mathbf{g}. \tag{1.2}$$

The energy equation may be written as

$$\frac{\rho^\gamma}{\gamma - 1} \frac{D}{Dt} \left(\frac{p}{\rho^\gamma} \right) = -L \tag{1.3}$$

where the energy loss function L is the net effect of all the sinks and sources of energy. The induction equation arises from combining Ohm's law with Faraday's law and is written:

$$\frac{\partial \mathbf{B}}{\partial t} = \nabla \times (\mathbf{v} \times \mathbf{B}) + \eta \nabla^2 \mathbf{B} \tag{1.4}$$

and the perfect gas law is:

$$p = \frac{\mathcal{R}}{\widetilde{\mu}} \rho T \tag{1.5}$$

We have eliminated the electric current density using Ampere's law:

$$\mathbf{J} = \frac{1}{\mu_0} \nabla \times \mathbf{B}$$

The state of the system at any point in space and time is given by the variables $\mathbf{v}$, $\mathbf{B}$, p and ρ where $\mathbf{v}$ is the macroscopic fluid velocity, $\mathbf{B}$ is the magnetic field, p is the

thermal pressure and ρ is the mass density. The constant γ represents the ratio of specific heats. For an ideal gas with three degrees of freedom, $\mathcal{R}$ and $\tilde{\mu}$ are the ideal gas constant ($\mathcal{R} = 8.25 \times 10^3 m^2 s^{-2} deg^{-1}$) and mean molecular weight respectively, ($\tilde{\mu}$ is 0.5 for a pure hydrogen gas and 0.6 in the solar corona). $\rho = n m_H$ where n is the number density and m_H is the proton mass. μ_0 is the magnetic permeability ($\mu_0 = 4\pi \times 10^{-7} henry\ m^{-1}$), g the gravitational acceleration (for solar applications we write $\mathbf{g} = g(r)\hat{\mathbf{r}}$, where the unit vector $\hat{\mathbf{r}}$ acts radially outwards from the centre of the sun and the local gravitational acceleration may be written $g(r) = \frac{M(r)G}{r^2}$ in terms of the mass of the Sun inside a radius r and the gravitational constant $G = 6.62 \times 10^{-11} N m^2 kg^{-2}$), η the magnetic diffusivity ($\eta = 10^9 T^{-\frac{3}{2}} m^2 s^{-1}$ with the temperature T, measured in Kelvin) and σ the electrical conductivity ($\eta = 1/\mu_0 \sigma$).

The MHD equations describe how the variables advance in time. The motion of the plasma alters the magnetic field through Faraday's law and Ohm's law while the magnetic field acts on the motion of the plasma through the equation of motion. The plasma alters the pressure and mass density through the energy equation. The electric field and the current density are treated as auxiliary properties. A derivation of these equations and a discussion of the underlying assumptions can be found in Goedbloed (1983).

1.1.2 The energy equation

The term on the right hand side of equation (1.3) is known as the energy loss function. It is often ignored and the plasma assumed to be adiabatic. For the purposes of this Thesis, this term is only used in applications relating to the solar corona, thus the following discusses the term L under coronal conditions.

Temperature (K)	χ	α
$8 \times 10^5 \leq T \leq 10^7$	5.51 × 10−30	-1.0
$3 \times 10^5 \leq T \leq 8 \times 10^5$	3.94 × 10−21	-2.5
$8 \times 10^4 \leq T \leq 3 \times 10^5$	8.00 × 10−35	0.0
$1.5 \times 10^4 \leq T \leq 8 \times 10^4$	1.20 × 10−43	1.8
$T \leq 1.5 \times 10^4$	3.92 × 10−67	7.4

Table 1.1: The constants χ and α from Hildner (1974)

Here we consider the various terms combined in the energy loss function (L), which, in general, may be written as the rate of energy loss minus the rate of energy gain, namely

$$L = \nabla.\mathbf{q} + \mathcal{L} - \frac{j^2}{\sigma} - H \tag{1.6}$$

where $\mathbf{q}$ is the heat flux due to thermal conduction; $\mathcal{L}$ is the net radiation; j^2/σ is the ohmic dissipation and H is the unknown coronal heating function that may depend on T, ρ and $\mathbf{B}$. For coronal plasmas the radiative loss function has been estimated by several authors (see, for example, Hildner, 1974, and Table (1.1)). Normally $\mathcal{L}$ is approximated by a piecewise continuous function of the form $n^2Q(T)$, which represents the losses due to optically thin radiation and $Q(T)$ is normally approximated by

$$Q(T) = \chi T^{\alpha} \tag{1.7}$$

where χ and α are piecewise continuous constants. The shape of $Q(T)$ is important. This will be discussed in Chapter 2, together with the form of H that we choose.

The anisotropic thermal conduction term $\nabla.\mathbf{q}$ can be expressed in terms of conduction parallel and perpendicular to the magnetic field. A strong magnetic field makes thermal

heat conduction highly anisotropical. Conduction along a magnetic field line is unhampered, but conduction across the field is strongly impeded due to the spiraling of the ions around the magnetic field lines. We can write the heat conduction, using the conduction coefficients $\kappa_{\|}$ and $\kappa_{\perp}$, as

$$-\nabla \cdot \mathbf{q} = \mathbf{B} \cdot \nabla \left(\kappa_{\|} \frac{\mathbf{B} \cdot \nabla T}{B^2} \right) + \nabla \cdot \left(\kappa_{\perp} \frac{\mathbf{B} \times (\nabla T \times \mathbf{B})}{B^2} \right). \tag{1.8}$$

The conduction coefficients can be obtained from classical theory (Spitzer, 1962). Parallel conduction is mainly due to electrons, while ions contribute most to perpendicular conduction, which is strongly hampered by a strong magnetic field as the ions spiral around the magnetic field lines. For a fully ionized plasma, Spitzer (1962) gives

$$\kappa_{\|} = 10^{-11} T^{\frac{5}{2}} W m^{-1} K^{-1}$$

and in the corona, typically

$$\frac{\kappa_{\perp}}{\kappa_{\|}} \approx 10^{-12}.$$

1.1.3 Time-scales

From the MHD equations we can define time-scales over which various physical processes occur. Table (1.2) gives time-scale values for typical conditions inside the corona and a prominence.

In the corona, we take $B = 100G$, $\rho = 8.36 \times 10^{-13} kg\ m^{-3}$, $T = 2 \times 10^6 K$ and we choose a length-scale based on the typical length of a magnetic field line, $l = 5 \times 10^7 m$. In a prominence we take $B = 10G$, $\rho = 1.67 \times 10^{-10} kg\ m^{-3}$, $T = 2 \times 10^4 K$ and we choose a length-scale based on the typical width of a prominence, $l = 6 \times 10^6 m$. $\mathcal{R}$ is the gas constant.

Time-scale	Symbol	Definition	Coronal value	Prominence
Alfvén	τ_A	$l(\mu_0\rho)^{\frac{1}{2}}/B$	5	100
Sound	τ_S	$l/(\mathcal{R}T)^{\frac{1}{2}}$	200	300
Radiation	τ_{rad}	$1/(\gamma-1)p\chi T^{\alpha-2}$	3000	1
Conduction	$\tau_{\|}$	$pl^2/\kappa_{\|}T(\gamma-1)$	600	10^7

Table 1.2: Typical time-scales, in seconds (for isothermal sound speed, and conduction parallel to the magnetic field)

The Alfvén time-scale measures how fast magnetic perturbations travel along the field lines (Alfvén waves) while the sound time-scale indicates how fast pressure disturbances propagate as sound waves. The conductive and radiative time-scales quantify the rate of conductive heat transport along the field lines and the rate at which energy is radiated away by the plasma. There is also a perpendicular conduction time-scale which is defined as $\tau_\perp = pl^2/\kappa_\perp T(\gamma-1)$ and $\tau_\perp \approx \tau_{\|} \times 10^{12}$ in the corona.

1.1.4 Reduced forms of the equations

Simplified forms of the MHD equations are often considered. The most common form of simplified equations are the "ideal" MHD equations where the terms on the right hand side of equation (1.3) are neglected (i.e. $L = 0$) along with the resistive (or magnetic diffusion) terms in (1.4).

Neglect of the resistive term in the induction equation can be justified if we consider

the dimensionless parameter (known as the Lundquist number)

$$S = \frac{l_0 v_A}{\eta}$$

in terms of a typical Alfvén velocity v_A and length-scale l_0. The Lundquist number gives a comparison of the magnitude of the convection term in equation (1.4) and that of the diffusive term. This is a measure of the strength of coupling between the flow and the magnetic field. In the solar atmosphere $S \gg 1$ generally. When $S \gg 1$ the induction equation becomes approximately

$$\frac{\partial \mathbf{B}}{\partial t} = \nabla \times (\mathbf{v} \times \mathbf{B}) \tag{1.9}$$

and the frozen-flux theorem of Alfvén holds: "in a perfectly conducting plasma, magnetic field lines behave as if they move with the plasma". In this Thesis we assume that the induction equation has the simplified form. This in turn implies that there will be no heating due to ohmic dissipation.

Gravity is also often neglected since typical plasma length-scales are much shorter than the gravitational scale-height. However, gravity cannot be ignored in solar prominences for which gravity forces are balanced by the Lorentz force. Nevertheless, when studying the formation of prominences we study an instability in the surrounding corona and here gravity can be ignored. Gravity is not, therefore, considered in the work in this Thesis.

When the energetics of a process are not the prime consideration, the energy equation is often approximated by taking $L = 0$. We call the terms that contribute to the energy loss function L the "non-adiabatic" terms.

When the plasma is "thermally isolated" from its surroundings, in the sense that there is no exchange of heat (L =0), the change of state is said to be adiabatic. Equation (1.3)

shows that, following the motion, p/ρ^γ = constant, for each plasma element (sometimes "thermally isolated" refers instead to a state of vanishing heat flux across the boundaries). L is negligible when the time-scale for changes in p,ρ and T is much shorter than the time-scales for radiation, conduction and heating. This is often true for rapid changes associated with wave motions or instabilities. In general, the conductive and radiative time-scales are much longer than the Alfvén time-scale (i.e. nonadiabatic effects are small).

Force free fields

The inertial terms in the momentum equation (the left hand side of equation (1.2)) may be neglected when the flow speed is much smaller than the sound speed, the Alfvén speed and the gravitational free-fall speed. The force of gravity may be neglected and only pressure gradients considered when the height of the structure being investigated is much less than the scale-height. If, in addition, the plasma has a low beta, where

$$\beta = \frac{2\mu_0 p_0}{B_0^2} \tag{1.10}$$

is the plasma pressure (p_0) divided by the magnetic pressure, then the force-balance equation reduces to

$$\mathbf{j} \times \mathbf{B} = 0 \tag{1.11}$$

1.1.5 The linearized equations

Most of the literature concerned with MHD deals with the linearized system of equations. The linearized equations allow us to investigate the stability of a system subject to small-scale perturbations.

Investigations into the dynamics of a plasma conducted using the non-linear equations is limited by our mathematical knowledge of non-linear differential equations. If the system is linearized, many more techniques become available and often in a better grasp of the problem is achieved. However, we wish to be satisfied that linearization is appropriate. If our study is of an equilibrium state that lasts for a period much longer than typical time-scales occurring in the dynamics of the plasma then the approximation of a static equilibrium is quite appropriate. For such systems, three types of problems can be studied. Firstly, we need to find an equilibrium state, for the non-linear equations are appropriate, but the special properties of the equations of static equilibrium can be made use of. Secondly, the problem of stability with respect to small oscillations about the equilibrium state can be studied and thirdly the different waves of the system can be studied.

It is worthwhile defining precisely what we mean by the terms equilibrium and stability. Bateman (1978) stated that: "MHD equilibrium is the complete balance of forces at every point in space." To define instability, we say that an equilibrium is unstable if any small perturbations of the equilibrium grow in time. Because the theory deals with small perturbations, it is possible to expand the governing equations to obtain equations which are linear in the perturbed variables. (Terms involving products of the small perturbed variables are ignored.) The resulting problem can then be solved using the various techniques applicable to linear equations.

Once an instability has grown sufficiently large, nonlinear tems will become important. However, solutions of the full equations are very difficult to obtain and mostly involve numerical methods. To proceed, the equations of MHD are linearized by considering an arbitrarily small, Eulerian perturbation from a stationary equilibrium. All variables are

expressed as the sum of their equilibrium value and a small perturbation. For example

$$\mathbf{B} = \mathbf{B}_0(\mathbf{r}) + \mathbf{B}_1(\mathbf{r}, t)$$

where $\mathbf{B}_0$ is the equilibrium value of the magnetic field, and $\mathbf{B}_1$ is the change in the magnetic field. For a stationary equilibrium $\mathbf{v}_0 = 0$ and $\mathbf{v} \equiv \mathbf{v}_1$.

This yields the system of linearized equations

$$\frac{\partial \rho_1}{\partial t} = -\nabla \cdot (\rho_0 \mathbf{v}), \tag{1.12}$$

$$\rho_0 \frac{\partial \mathbf{v}}{\partial t} = -\nabla p_1 + \frac{1}{\mu}(\nabla \times \mathbf{B}_0) \times \mathbf{B}_1 + \frac{1}{\mu}(\nabla \times \mathbf{B}_1) \times \mathbf{B}_0, \tag{1.13}$$

$$\begin{aligned} \frac{1}{\gamma - 1}\left(\frac{\partial p_1}{\partial t} + \mathbf{v} \cdot \nabla p_0\right) &= \frac{\gamma}{\gamma - 1}\frac{p_0}{\rho_0}\left(\frac{\partial \rho_1}{\partial t} + \mathbf{v} \cdot \nabla \rho_0\right) + \mathbf{B}_0 \cdot \nabla\left(\kappa_{\|}\frac{(\mathbf{B}_0 \cdot \nabla T_1)}{B_0^2}\right) \\ &+ \nabla \cdot \left(\kappa_{\perp}\frac{\mathbf{B}_0 \times (\nabla T_1 \times \mathbf{B}_0)}{B_0^2}\right) - \frac{\partial \mathcal{L}}{\partial p_0}p_1 - \frac{\partial \mathcal{L}}{\partial T_0}T_1, \end{aligned} \tag{1.14}$$

$$\frac{\partial \mathbf{B}_1}{\partial t} = \nabla \times (\mathbf{v} \times \mathbf{B}_0), \tag{1.15}$$

$$\frac{p_1}{p_0} = \frac{\rho_1}{\rho_0} + \frac{T_1}{T_0} \tag{1.16}$$

where the terms $\partial \mathcal{L}/\partial p_0$ and $\partial \mathcal{L}/\partial T_0$ denote differentiation with respect to p_0 and T_0 respectively (with T_0 and p_0 held constant) at the equilibrium state. We take conduction coefficients as constants, which is valid for an isothermal equilibrium. For a non-isothermal equilibrium $\kappa_{\perp}$ and $\kappa_{\|}$ are functions of $\mathbf{B}$, T and ρ. For the equilibrium, the energy loss function is zero ($L = 0$). This effectively defines the heat loss H as a function of position ($\mathcal{L} = H$). Perturbations to H are neglected. We have derived the linearized equations without gravity or resistive terms for reasons which have been outlined above.

1.1.6 The non-dimensionalized equations

Sometimes it is useful to rewrite the linearized equations in terms of non-dimensionalized variables. In order to do this, we normalize the variables against typical values of the

variables in the plasma we are investigating.

We normalize the magnetic field components against a typical value B_0:

$$\mathbf{B}_0 = B_0\hat{\mathbf{B}}_0 \qquad \mathbf{B}_1 = B_0\hat{\mathbf{B}}_1$$

where the non-dimensionalized components of the magnetic field are denoted by $\hat{\mathbf{B}}_0$ and $\hat{\mathbf{B}}_1$.

Similarly, the thermodynamic variables can be non-dimensionalized

$$p_0 = p_0\hat{p}_0 \qquad p_1 = p_0\hat{p}_1$$

$$T_0 = T_0\hat{T}_0 \qquad T_1 = T_0\hat{T}_1$$

$$\rho_0 = \rho_0\hat{\rho}_0 \qquad \rho_1 = \rho_0\hat{\rho}_1$$

The perturbed velocity is normalized against a typical plasma length-scale, given as l, and a typical time-scale, which we shall choose to be τ_{rad} (any time-scale may be used).

$$\mathbf{v} = \frac{l}{\tau_{rad}}\hat{\mathbf{v}}$$

Now the time derivatives and spatial derivatives must be normalized against the same typical length-scale and time-scale

$$\nabla = \frac{1}{l}\hat{\nabla}$$

$$\frac{\partial}{\partial t} = \frac{1}{\tau_{rad}}\frac{\partial}{\partial \hat{t}}.$$

The linearized, non-dimensionalized equations can now be written:

$$\frac{\partial \hat{\rho}_1}{\partial \hat{t}} = -\hat{\nabla}\cdot(\hat{\rho}_0\hat{\mathbf{v}}), \tag{1.17}$$

$$\epsilon^2\hat{\rho}_0\frac{\partial \hat{\mathbf{v}}}{\partial \hat{t}} = -\frac{\beta}{2}\hat{\nabla}\hat{p}_1 + \left(\hat{\nabla}\times\hat{\mathbf{B}}_0\right)\times\hat{\mathbf{B}}_1 + \left(\hat{\nabla}\times\hat{\mathbf{B}}_1\right)\times\hat{\mathbf{B}}_0, \tag{1.18}$$

$$\frac{\partial \hat{p}_1}{\partial \hat{t}} + \hat{\mathbf{v}}\cdot\hat{\nabla}\hat{p}_0 = \gamma\frac{\hat{p}_0}{\hat{\rho}_0}\left(\frac{\partial \hat{\rho}_1}{\partial \hat{t}} + \hat{\mathbf{v}}\cdot\hat{\nabla}\hat{\rho}_0\right) + \frac{\tau_{rad}}{\tau_{\|}}\hat{\mathbf{B}}_0\cdot\hat{\nabla}\left(\frac{\left(\hat{\mathbf{B}}_0\cdot\hat{\nabla}\hat{T}_1\right)}{\hat{B}_0^2}\right)$$

$$+ \quad \frac{\tau_{rad}}{\tau_\perp}\hat{\nabla}\cdot\left(\frac{\hat{\mathbf{B}}_0\times\left(\hat{\nabla}\hat{T}_1\times\hat{\mathbf{B}}_0\right)}{\hat{B}_0^2}\right) - \hat{\mathcal{L}}_p\hat{p}_1 - \hat{\mathcal{L}}_T\hat{T}_1, \tag{1.19}$$

$$\frac{\partial\hat{\mathbf{B}}_1}{\partial\hat{t}} = \hat{\nabla}\times\left(\hat{\mathbf{v}}\times\hat{\mathbf{B}}_0\right), \tag{1.20}$$

$$\frac{\hat{p}_1}{\hat{p}_0} = \frac{\hat{\rho}_1}{\hat{\rho}_0} + \frac{\hat{T}_1}{\hat{T}_0}, \tag{1.21}$$

where $\hat{\mathcal{L}}_p = 2\hat{p}_0\hat{T}_0^{\alpha-2}$ and $\hat{\mathcal{L}}_T = (\alpha-2)\hat{p}_0^2\hat{T}_0^{\alpha-3}$

The parameter β has already been introduced, as have the time-scales τ_{rad}, $\tau_\perp$ and $\tau_\parallel$. The parameter ϵ is defined as

$$\epsilon = \frac{\tau_A}{\tau_{rad}} \tag{1.22}$$

and is a measure of the amount of coupling of the radiative mode to the MHD wave modes.

1.2 Methods for determining stability

When determining the stability of a system, two main methods of approach are used to solve the linearized equations. These are the normal mode method and the energy method.

1.2.1 Normal modes

To look for normal modes we decompose the time-dependent variables into a spectrum of Fourier components which have the form (taking the magnetic field as an example):

$$\mathbf{B}_1(\mathbf{r},t) = \mathbf{B}(\mathbf{r})\,e^{\sigma t} \tag{1.23}$$

This reduces the set of linearized equations to an eigenvalue problem for the eigenvalue σ. The boundary conditions determine which values of σ are allowed. If all the normal

modes have real frequencies ($\sigma^2 > 0$), the system is stable if $\sigma < 0$ and unstable if $\sigma > 0$. If the growth rates are imaginary ($\sigma^2 < 0$) then the equilibrium oscillates, and wave modes exist. For complex σ the equilibrium is said to be "overstable" if the real part is greater then zero.

1.2.2 The energy method

The second method, which is applied to ideal MHD problems, is the energy method. Developed by Bernstein *et al.* (1958), Hain, Lüst and Schlüter (1957), and Lundquist (1951), it has been applied extensively since. It states that an equilibrium is linearly stable if, and only if, there exists no continuous small perturbation that decreases the potential energy of the system from its equilibrium value. (We are using the ideal equations without gravity, which can be taken account of in the energy principle formulation, and the non-adiabatic terms which cannot.)

ξ-form of the equations

The energy method uses the useful transformation of writing the linearized ideal equations in terms of the displacement vector

$$\xi(\mathbf{x}, t) \equiv \int_0^t \mathbf{v}(\mathbf{x}, t')dt' \tag{1.24}$$

If we were using a Lagrangian coordinate system moving with the fluid, ξ would represent the displacement of a fluid element from its initial position. In an Eulerian system, on the other hand, the evolution of ξ characterizes the flow of a succession of different fluid elements past a fixed point. However, in both systems, the vector field ξ is well-defined and the distinction in interpretation is not relevant as long as the perturbation is arbitrarily

small.

The linearized equations for the perturbed magnetic field and pressure can be integrated once, and using the following boundary conditions:

$$\xi(\mathbf{x},0) = 0 \qquad \frac{\partial}{\partial t}\xi(\mathbf{x},0) \neq 0$$

$$\mathbf{B}_1(\mathbf{x},0) = 0 \qquad p_1(\mathbf{x},0) = 0$$

they become

$$\mathbf{B}_1 = \nabla \times (\xi \times \mathbf{B}_0) \tag{1.25}$$

and

$$p_1(\mathbf{x},t) = -\xi.\nabla p_0 - \gamma p_0 \nabla.\xi \tag{1.26}$$

Now we can combine the linearized equations into a single second-order partial differential equation for the displacement vector

$$\rho_0 \frac{\partial^2 \xi}{\partial t^2} = \mathbf{F}(\xi) \tag{1.27}$$

where $\mathbf{F}(\xi)$ is known as the linearized force function and is written:

$$\begin{aligned} \mathbf{F}(\xi) &= \nabla(\xi.\nabla p_0 + \gamma p_0 \nabla.\xi) + \frac{1}{\mu}(\nabla \times \mathbf{B}_0) \times [\nabla \times (\xi \times \mathbf{B}_0)] \\ &+ \frac{1}{\mu}(\nabla \times [\nabla \times (\xi \times \mathbf{B}_0)]) \times \mathbf{B}_0 \end{aligned} \tag{1.28}$$

The equation (1.27) is usually the starting point for linear stability analysis.

The energy principle

The system may be isolated form the rest of the world by using the boundary condition

$$\xi_\perp = 0 \tag{1.29}$$

along an equilibrium magnetic surface at the edge of the plasma or by allowing for a vacuum region bounded by a perfectly conducting wall.

Now we can derive the energy principle using equation (1.27) and the boundary condition (1.29). First, we multiply the equation of motion (1.27) by the time derivative of the displacement vector $\dot{\xi}$ and integrate over the volume of the plasma subject to the boundary condition (1.29)

$$\int \rho_0 \dot{\xi} \cdot \ddot{\xi} dV = \frac{\partial}{\partial t} \int \frac{1}{2} \rho_0 \dot{\xi}^2 dV \tag{1.30}$$

which becomes

$$\frac{\partial}{\partial t} \int \frac{1}{2} \rho_0 \dot{\xi}^2 dV = \int \dot{\xi} \cdot \mathbf{F}(\xi)\, dV \tag{1.31}$$

A system is said to be self-adjoint if we can integrate by parts to demonstrate the identity

$$\int \eta \cdot \mathbf{F}(\xi)\, dV = \int \xi \cdot \mathbf{F}(\eta)\, dV \tag{1.32}$$

for any choice of ξ and η, subject to the boundary condition. This integration by parts has been carried out by Kadomtsev (1966) among others. Using this property of self-adjointness, it follows that the total perturbed energy is constant in time.

$$\frac{\partial}{\partial t} \left[\int \rho_0 \dot{\xi}^2 dV - \frac{1}{2} \int \xi \cdot \mathbf{F}(\xi) dV \right] = 0 \tag{1.33}$$

where the potential energy is denoted by

$$\delta W \equiv -\frac{1}{2} \int \xi . \mathbf{F}(\xi)\, dV \tag{1.34}$$

The principle behind the energy method of stability analysis is straightforward. The total energy of the system is constant so if any displacement decreases the potential energy then there will be a corresponding rise in the kinetic energy, thereby indicating that the system

is unstable. Any test function will do provided that it satisfies the boundary condition and is integrable. If all perturbations lead to an increase in the potential energy (δW positive), then the system is linearly stable to exponentially growing modes. A rigorous proof of this is given by Laval, Mercier and Pellat (1965).

1.3 Outline of the Thesis

In this Thesis, we use the MHD model to research three separate topics. Firstly, we examine the so-called "thermal instability" - which arises due to the inverse dependence of the (optically thin) radiative energy loss on temperature, and is generally accepted to be important for the formation of prominences - in an equilibrium that includes magnetic field lines of finite length and anisotropical heat conduction. These are important factors in coronal magnetic fields and should be taken into account in any realistic model of prominence formation. In Chapter 2 we study the thermal instability in a one-dimensional Cartesian equilibrium with line-tied magnetic fields and with anisotropic heat conduction, using a particular class of disturbances known as "ballooning modes" (Connor, Hastie and Taylor, 1979). In Chapter 3 we study the same problem for a shearless field, both analytically, concentrating on the isobaric mode, and numerically, using a time-dependent code to advance the linearized MHD equations explicitly in time.

Secondly, we apply a simple technique (see Gimblett, 1986) to study the effect of surrounding models of Reversed Field Pinch and Spheromak equilibria with a wall of finite conductivity. In Chapter 4 we outline the method and present the results of the analysis.

Thirdly, we apply the two tests for stability derived by De Bruyne (1990) (giving

separate necessary and sufficient conditions for stability) to two-dimensional, analytic, Spheromak equilibria in cylindrical geometry. In Chapter 5 the method and the equilibria are described and the results discussed.

Finally, Chapter 6 presents some conclusions and suggestions for possible future work.

Chapter 2

The thermal instability with anisotropic heat conduction in line-tied magnetic fields

Amongst the most unusual phenomena observed on the Sun are prominences. Lumps of cool, dense material, these sit in the extremely hot and diffuse solar corona supported against gravity by magnetic forces. While the support and structure of prominences are both fascinating subjects, this Chapter addresses the problem of their initial formation. It has long been considered probable that one of the mechanisms for the formation of prominences in the solar corona is a thermal instability arising from the form of the radiative loss function. In this Chapter we investigate the thermal instability and include the effects of line-tied magnetic fields and of thermal conduction transverse to the magnetic field lines.

In the first section of this Chapter, the physical nature of prominences and the role of

condensations caused by the thermal instability in their formation are discussed. We then go on to examine the basic physical mechanism underlying the thermal instability and its mathematical formulation, and to review previous work on the subject. This body of literature generally lacks one fundamental ingredient for the construction of a physically reasonable model of the magnetic structures in the solar corona, namely the fact that most magnetic field lines in the corona are connected to the solar photosphere. For coronal loops and arcades in particular, all magnetic field lines enter the photosphere on two sides (unless a magnetic island has formed somewhere inside). Hence, these structures are anchored to the cooler photosphere. A more common term for the photospheric anchoring of the magnetic field lines is "line-tying". Under idealized conditions the effect of line-tying on coronal structures can be treated as boundary conditions for the perturbations of the equilibrium state.

Line-tying can be invoked to explain how thermal instabilities can lead to the formation of magnetically stable high-density structures (i.e. prominences) in the solar corona. Since the thermal instability time-scale is much longer than the Alfvénic time-scale in the solar corona, without line-tying any equilibrium would be destroyed by magnetic instabilities long before a thermal instability can form cool condensations. Line-tying is extremely stabilizing to ideal MHD modes (Raadu, 1972). This makes it possible for thermal instabilities to grow in the absence of magnetic disruptions.

This Chapter extends the work of Cargill and Hood (1989) who investigated the effects of the photospheric boundary on radiative modes. They considered a slab geometry so that the Alfvén mode is decoupled from the system. For an isothermal equilibrium they considered a special class of disturbances which give a clear picture of the effects of the

line-tied boundaries. These are the localized interchange modes which are the counterpart of the "ballooning-modes" in fusion research. These localized modes have derivatives perpendicular to the equilibrium magnetic field that are much larger than the parallel derivatives. The first detailed description of ballooning modes in laboratory plasmas was given by Connor, Hastie and Taylor (1979). This was followed by a more rigourous treatment by Dewar and Glasser (1983).

Cargill and Hood (1989) only considered the radiative modes on individual flux surfaces so that each flux surface grows at its own growth rate. A global growth rate can be found by including the thermal conduction perpendicular to the magnetic field lines. This is often ignored because of the smallness of the perpendicular conduction coefficient, but it may be a very important parameter and, indeed, Van der Linden (1992) has shown that it may give rise to the fine-scale structure observed in prominences.

2.1 Prominences

Prominences are lumps of cool, dense plasma located in the hot, diffuse corona. They have temperatures a hundred times lower than the surrounding coronal gas and densities a hundred or a thousand times higher. Prominences exist in a great variety of shapes and sizes. There are many classification schemes, which have been described by Tandberg-Hanssen (1974) and Jensen *et al.* (1979). Although none of the schemes are identical, they usually classify prominences into two main types: long-lived or "quiescent" prominences and short-lived or "active" prominences. Active prominences have lifetimes of only minutes or hours. They are dynamic structures usually associated with solar flares. They are extremely hard to model and indeed no satisfactory model exists. This Thesis

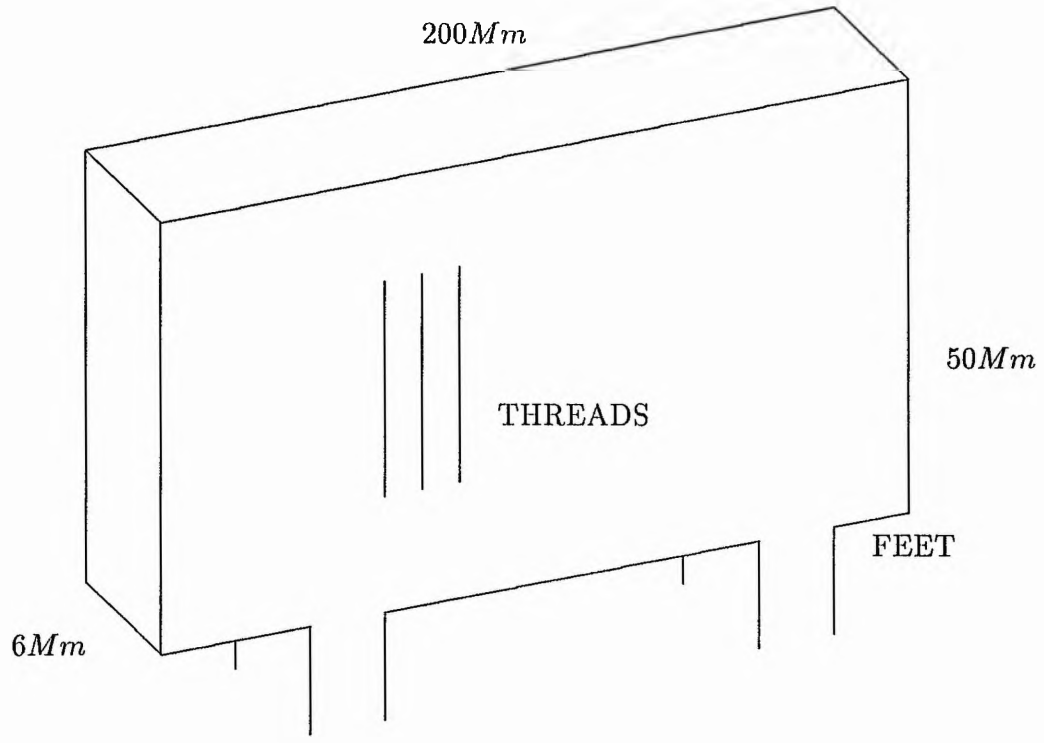

Figure 2.1: A simple-minded picture of a prominence

is concerned solely with quiescent prominences which are very stable with lifetimes that may stretch to many months.

A simple diagram of the geometry of a quiescent prominence is sketched in figure (2.1). Quiescent prominences always lie above a magnetic polarity-inversion line of reversal in the line-of-sight magnetic field in the photosphere (Babcock and Babcock, 1955). Their typical spatial scales are shown in the figure. The density is between 10^{16} and $10^{17}m^{-3}$, and the temperature is usually between 5000 and $8000K$ (Bommier, 1986).

When a prominence is observed on the limb, we can see that it consists of vertical threads, typically $5 - 7Mm$ long and 0.3 to $1.1Mm$ wide. These threads have been observed to lie across the magnetic field, but this is difficult to conceive theoretically as it

implies motion across magnetic field lines which contradicts the "flux-freezing" condition.

The magnetic field in a quiescent prominence is rather homogeneous, close to horizontal and inclined at about 20^0 to the prominence axis (Leroy, 1979). It has a typical magnitude of $5G$ and usually increases with height (Rust, 1967). Material continually falls slowly down the threads and down the "feet" into the chromosphere at speeds of only 1 $km\ s^{-1}$, much less than the free-fall speed. This lost mass must be being replaced somehow.

Magnetic fields in the corona are crucial to the formation and maintenance of prominences. Firstly, magnetic tension can support the prominence against gravity; secondly, by allowing sharp gradients to exist (because cross-field thermal conduction is very small) they can thermally insulate the plasma. Magnetic fields may also be a determining factor for the fine-scale structure or "threads" of a prominence (see, for example, Van der Linden, 1991).

In the course of a prominence's lifetime, its global structure remains virtually unaltered. A quiescent prominence may eventually erupt, but afterwards another prominence often forms in its place, indicating that the conditions for formation still exist. More than one mechanism for prominence formation has been put forward. A coherent mass injection from the photosphere or a "siphon-flow" owing to pressure imbalances at the footpoints of a magnetic arcade are two possible mechanisms. However, it is hard to conceive how a mass could move from the photosphere to the corona without destroying the magnetic field structure. A condensation of coronal plasma owing to an instability in the thermal equilibrium might also lead to prominence formation. Yet, the formation of a single prominence would consume a sizable fraction of the coronal mass (up to a tenth has been quoted). There are some observations of a "void" surrounding a number

of newly created prominences, but these voids are too small to account for the mass of the prominence. On the other hand, most prominences seem to be steadily losing mass to the photosphere by the steady downward flow already mentioned. This loss is regained by the condensation of coronal mass on the top of the prominence. So, the condensational instability must play at least some part in prominence formation and evolution.

2.2 Introduction to thermal instabilities

In this section we outline the physical mechanism behind the radiative (or thermal, or condensational) instability and its mathematical formulation. We also summarize the characteristics of the basic thermal instability in an infinite, uniform medium where the different waves and the thermal instability are uncoupled and their different properties can be determined in a straightforward way. An analysis in a uniform and infinite medium provides the key to an understanding of the thermal instability.

2.2.1 The thermal instability mechanism

The existence of a thermal instability in astrophysical plasmas was first pointed out by Parker (1953) and Kiepenheuer (1953). Using a simple analysis, Parker found that thermal instabilities could occur in a pure hydrogen plasma. Particular attention was paid to the possibility of this being a mechanism for prominence formation. This condensation process has been applied to many domains of astrophysics, for example, the solar wind (Parker, 1963), the formation of interstellar clouds (Field, 1962), and the formation of galaxies (Gold and Hoyle, 1959).

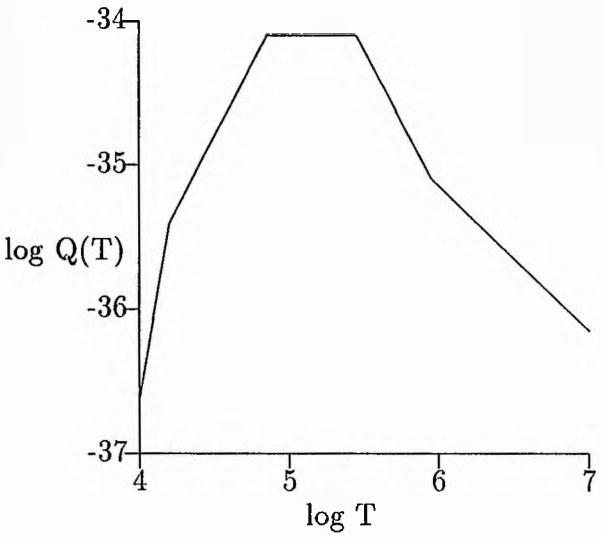

Figure 2.2: The approximate radiative loss fuction χT^{α} as a function of temperature.

Physical description

As discussed in Chapter 1, an equilibrium is stable only if it is stable to small perturbations of the variables. If the energy loss function L depends on the temperature such that a decrease in temperature results in an increase in L, then an instability exists. If the plasma cools locally, the energy loss increases and the plasma cools further.

In a hot hydrogen plasma, an instability can arise because of the form of the radiative energy losses. Following Hildner (1974) we can write the radiative loss in coronal plasmas as

$$n^2 Q(T) = n^2 \chi T^{\alpha} = \tilde{\chi} \rho^2 T^{\alpha} = \tilde{\chi} p^2 \frac{\tilde{\mu}^2}{R^2} T^{\alpha - 2} \tag{2.1}$$

where the piecewise continuous constants χ and α are shown in table (1.1) and illustrated in figure (2.2).

Other authors (e.g. McWhirter *et al.*, 1975; Raymond and Smith, 1977; Rosner *et al.*, 1978) have calculated different values for the constants χ and α, but the main property, that radiation increases rapidly by several orders of magnitude as the temperature falls from 10^6 to $10^5 K$, is common to all. Below a temperature of $10^4 K$ the radiation drops off and the plasma becomes optically thick. That the radiative loss function exhibits this behaviour is due to metallic ($z > 2$) atoms in the coronal plasma becoming progressively ionized as the temperature rises thereby radiating less energy (Rosner, Tucker and Vaiana, 1978). The fact that the chemical composition of the corona is unknown explains the differing evaluation of the constants offered by various authors.

Owing to the tendency of the plasma towards pressure balance, this temperature instability leads to condensation. As the temperature drops, the pressure drops. The plasma responds by setting up a flow that equalizes the pressure, resulting in increased density and a condensation. This condensation will occur if the instability time-scale is much larger than the sound travel time τ_S. For $\tau_S < \tau_{rad}$, pressure perturbations are nearly zero and the instability proceeds isobarically. If, however, $\tau_S > \tau_{rad}$, the above condition of pressure balance is not satisfied; the plasma has no time to set up flows in response to pressure changes and it evolves in an isochoric manner with no perturbed density. This can happen at temperatures of about $10^5 K$.

From the above arguments, we might expect that the corona is always thermally unstable. However, we have not considered the effects of thermal conduction in the plasma. Conduction would act to smooth out any temperature gradient, eliminating any instability when the conduction time-scale is shorter than the radiative time-scale. In the presence of a magnetic field, there are two conduction time-scales - perpendicular and

parallel to the magnetic field. The perpendicular time-scale is always much longer than the radiative time-scale, but conduction parallel to the magnetic field is extremely efficient at smoothing out temperature variations in the corona. Since this conduction time-scale is proportional to the square of the length of the field line, conduction will always stabilize the thermal mode over short distances. For the thermal instability to occur it requires either very long field lines so that $\tau_{||} > \tau_{rad}$, or special forms of disturbances that eliminate the perturbed parallel conduction term.

Thus far we have only discussed temperature drops and condensations, although in the linear regime a temperature increase could equally occur. However, non-linearly, only a condensation is likely as the parallel thermal conduction coefficient has the temperature dependence $\kappa_{||} = \kappa_0 T^{5/2}$. So, if the temperature were to increase, conduction would be enhanced and the temperature increase would be smoothed out.

The form of the heating function H is an unresolved problem in solar physics. In order to avoid possible spurious effects due to a specific parameterization, the heating is often taken as constant per unit volume or per unit mass. In this Thesis, we assume that the heating term is such that it is constant in time and that at equilibrium $L = 0$ everywhere (i.e. $H = H(x)$). Taking the heating as constant does not lose too much physics as the heating term must vary less with temperature change at coronal temperatures or there would be no instability.

Provided the radiative losses increase with density, the thermal instability may also be driven by a density perturbation. For then a small increase in density enhances the energy loss, yielding lower temperatures and, owing to pressure balance, a further increase in density. In practice, the destabilization caused by a density perturbation is much weaker

than that caused by the temperature perturbation.

In a non-ideal plasma where heating due to Ohmic dissipation is important, an instability can arise because of the temperature dependence of j^2/σ (e.g. Sparks and Van Hoven, 1987).

2.2.2 Basic equations and methods

In investigating the thermal instability in the corona we use the non-dimensionalized, linearized equations of MHD with the non-adiabatic terms included. The non-adiabatic terms are those terms that give rise to the thermal instability and so must be included. To recap, the equations are:

$$\hat{\sigma}\hat{\rho}_1 = -\hat{\nabla}\cdot(\hat{\rho}_0\hat{\mathbf{v}}), \tag{2.2}$$

$$\epsilon^2\hat{\rho}_0\hat{\sigma}\hat{\mathbf{v}} = -\frac{\beta}{2}\hat{\nabla}\hat{p}_1 + \left(\hat{\nabla}\times\hat{\mathbf{B}}_0\right)\times\hat{\mathbf{B}}_1 + \left(\hat{\nabla}\times\hat{\mathbf{B}}_1\right)\times\hat{\mathbf{B}}_0, \tag{2.3}$$

$$\begin{aligned}\hat{\sigma}\hat{p}_1 + \hat{\mathbf{v}}\cdot\hat{\nabla}\hat{p}_0 &= \gamma\frac{\hat{p}_0}{\hat{\rho}_0}\left(\frac{\partial\hat{\rho}_1}{\partial\hat{t}} + \hat{\mathbf{v}}\cdot\hat{\nabla}\hat{\rho}_0\right) + \frac{\tau_{rad}}{\tau_{\|}}\hat{\mathbf{B}}_0\cdot\hat{\nabla}\left(\frac{\left(\hat{\mathbf{B}}_0\cdot\hat{\nabla}\hat{T}_1\right)}{\hat{B}_0^2}\right)\\ &+ \frac{\tau_{rad}}{\tau_{\perp}}\hat{\nabla}\cdot\left(\frac{\hat{\mathbf{B}}_0\times\left(\hat{\nabla}\hat{T}_1\times\hat{\mathbf{B}}_0\right)}{\hat{B}_0^2}\right) - \hat{\mathcal{L}}_p\hat{p}_1 - \hat{\mathcal{L}}_T\hat{T}_1,\end{aligned} \tag{2.4}$$

$$\frac{\partial\hat{\mathbf{B}}_1}{\partial\hat{t}} = \hat{\nabla}\times\left(\hat{\mathbf{v}}\times\hat{\mathbf{B}}_0\right), \tag{2.5}$$

$$\frac{\hat{p}_1}{\hat{p}_0} = \frac{\hat{\rho}_1}{\hat{\rho}_0} + \frac{\hat{T}_1}{\hat{T}_0}. \tag{2.6}$$

We have Fourier analysed with respect to the time dependence of the variables and the growth rate has been normalised against the time-scale τ_{rad} (i.e. $\hat{\sigma} = \tau_{rad}\sigma$).

2.2.3 The thermal instability in an infinite uniform medium

In a uniform, magnetized medium there are a number of solutions to the coupled thermal/MHD equations, namely a purely growing (or decaying) thermal mode and the three

MHD wave modes. Of the wave modes, the Alfvén mode decouples (in Cartesian geometry), since it does not involve perturbations of the thermodynamic variables.

The first rigorous and detailed treatment of the radiative instability was provided by Field (1965). His treatment of the thermal instability in an infinite, homogeneous medium is a cornerstone of the subject. An analysis in a uniform and infinite plasma provides us with the key ingredients for understanding non-uniform plasmas.

For a uniform field all coefficients of the Eulerian quantities are constants, in the linearized equations. If we select a Cartesian coordinate system in which $\hat{\mathbf{B}}_0 = \left(0, 0, \hat{B}_0\right)$, and the perturbations have components only in the x,z plane, we can write the perturbed variables as:

$$\hat{T}_1(x,z) = \hat{T}_1 \cos(k_\perp x)\cos(k_\parallel z), \tag{2.7}$$

$$\hat{p}_1(x,z) = \hat{p}_1 \cos(k_\perp x)\cos(k_\parallel z), \tag{2.8}$$

$$\hat{\rho}_1(x,z) = \hat{\rho}_1 \cos(k_\perp x)\cos(k_\parallel z), \tag{2.9}$$

$$\hat{\mathbf{B}}_1(x,z) = (\hat{B}_{1x}\sin(k_\perp x) sin(k_\parallel z), 0, \hat{B}_{1z}\cos(k_\perp x)\cos(k_\parallel z)), \tag{2.10}$$

$$\hat{\mathbf{v}}_1(x,z) = (\hat{v}_\perp \sin(k_\perp x)\cos(k_\parallel z), 0, \hat{v}_\parallel cos(k_\perp x)\sin(k_\parallel z)), \tag{2.11}$$

where $k_\perp$ and $k_\parallel$ are the wave numbers perpendicular and parallel to the equilibrium magnetic field.

In a uniform medium we have no measure of distance, so we define the time-scales in terms of wavelengths, and the time-scales defined in table (1.2) must be modified and can be rewritten

$$\tau_\parallel = \frac{p l_1^2}{\kappa_\parallel T(\gamma - 1)},$$

$$\tau_\perp = \frac{p l_2^2}{\kappa_\perp T(\gamma - 1)},$$

$$\tau_A = \frac{l_3}{v_A},$$

where $l_1 = 2k_{||}/\pi$, $l_2 = 2k_{\perp}/\pi$ and $l_3 = \sqrt{l_1^2 + l_2^2}$.

The equations become

$$\begin{aligned}
-\frac{\beta}{2}k_{\perp}\hat{p}_1 + \epsilon^2\hat{\rho}_0\hat{\sigma}\hat{v}_{\perp} &= k_{||}\hat{B}_0\hat{B}_{1x} + k_{\perp}\hat{B}_0\hat{B}_{1z}, \\
-\frac{\beta}{2}k_{||}\hat{p}_1 + \epsilon^2\hat{\rho}_0\hat{\sigma}\hat{v}_{||} &= 0, \\
\hat{\sigma}\hat{\rho}_1 + k_{\perp}\hat{\rho}_0\hat{v}_{\perp} + k_{||}\hat{\rho}_0\hat{v}_{||} &= 0, \\
\hat{\sigma}\hat{B}_{1x} &= -\hat{B}_0 k_{||}\hat{v}_{\perp}, \\
\hat{\sigma}\hat{B}_{1z} &= -\hat{B}_0 k_{\perp}\hat{v}_{\perp}, \\
\frac{\hat{p}_1}{\hat{p}_0} &= \frac{\hat{\rho}_1}{\hat{\rho}_0} + \frac{\hat{T}_1}{\hat{T}_0}, \\
\hat{\sigma}\hat{p}_1 &= \gamma\frac{\hat{p}_0}{\hat{\rho}_0}\hat{\sigma}\hat{\rho}_1 - k_{||}^2\frac{\tau_{rad}}{\tau_{||}}\hat{T}_1 - k_{\perp}^2\frac{\tau_{rad}}{\tau_{\perp}}\hat{T}_1 - \hat{\mathcal{L}}_p\hat{p}_1 - \hat{\mathcal{L}}_T\hat{T}_1.
\end{aligned}$$

After elimination, our system of equations gives us a fifth degree polynomial for the growth rate $\hat{\sigma}$:

$$\begin{aligned}
&\left(k_{||}^2\frac{\tau_{rad}}{\tau_{||}} + k_{\perp}^2\frac{\tau_{rad}}{\tau_{\perp}} + \hat{\mathcal{L}}_T\right)\left(\epsilon^4\hat{\sigma}^4 + \epsilon^2\hat{\sigma}^2\left(\frac{\hat{B}_0^2k^2}{\hat{\rho}_0} + \beta\frac{\hat{p}_0}{\hat{\rho}_0}\right) + \frac{\beta}{2}\frac{\hat{p}_0}{\hat{\rho}_0^2}\hat{B}_0^2k^2\right) + \\
&\hat{\sigma}\left(\epsilon^4\hat{\sigma}^4\hat{\rho}_0 + \epsilon^2\hat{\sigma}^2\left[B_0^2k^2 + \beta\gamma\hat{p}_0\right] + \frac{\gamma\beta}{2}\frac{\hat{p}_0}{\hat{\rho}_0}\hat{B}_0^2k^2\right) + \hat{\mathcal{L}}_p\epsilon^2\hat{\sigma}^2(k^2B_0^2 + \epsilon^2\hat{\sigma}^2\hat{\rho}_0) = 0,
\end{aligned} \tag{2.12}$$

where $k^2 = k_{||}^2 + k_{\perp}^2$. This equation is equivalent to the dispersion equation obtained by Field (1965) for an infinite, magnetized plasma. It describes the non-adiabatic slow and fast magneto-acoustic waves and the thermal mode (which is always real). Neglect of the non-adiabatic terms in equation (2.12) reduces the equation to a dispersion equation for ideal fast and slow modes. The Alfvén mode has been uncoupled from the system and can be thought of as propagating in the y-direction.

Equation (2.12) has at least one positive real solution (i.e. a thermal instability) if

$$k_{\|}^2 \frac{\tau_{rad}}{\tau_{\|}} + k_{\perp}^2 \frac{\tau_{rad}}{\tau_{\perp}} + \hat{\mathcal{L}}_T < 0. \tag{2.13}$$

This inequality is the isobaric ($\hat{p}_1 = 0$) instability criterion, first obtained by Field (1965). Thermal conduction is always stabilizing, while the contribution from the radiative loss is destabilizing if $\hat{\mathcal{L}}_T < 0$, that is if $\alpha - 2 < 0$.

Neglecting the non-adiabatic terms in equation (2.12) makes the thermal mode collapse into the origin (σ=0) and the rest of the equation reduces to the dispersion equation for ideal slow and fast magneto-acoustic waves

$$\epsilon^4 \hat{\sigma}^4 \hat{\rho}_0 + \epsilon^2 \hat{\sigma}^2 \left[B_0^2 k^2 + \beta\gamma \hat{p}_0 \right] + \frac{\gamma\beta}{2} \frac{\hat{p}_0}{\hat{\rho}_0} \hat{B}_0^2 k^2 = 0. \tag{2.14}$$

When non-adiabatic motions are allowed these slow and fast modes are modified and are the complex solutions of equation (2.12). Field (1965) showed that they can become overstable when the isentropic instability criterion is satisfied:

$$k_{\|}^2 \frac{\tau_{rad}}{\tau_{\|}} + k_{\perp}^2 \frac{\tau_{rad}}{\tau_{\perp}} + \hat{\mathcal{L}}_T + \frac{\gamma}{\gamma - 1} \frac{p_0}{T_0} \hat{\mathcal{L}}_p < 0. \tag{2.15}$$

However, overstability of the fast and slow modes is unlikely to occur in practice because of the stability introduced by the p-derivative.

We can see from both the isobaric and isentropic instability criteria that thermal conduction inhibits the thermal instabilty once a critical wave number is exceeded. Stabilization due to perpendicular conduction requires much higher wave numbers than parallel conduction and so is often neglected. When boundary conditions are included in the problem the critical wave number translates into a critical length below which the thermal instability no longer exists.

Now if we let ϵ tend to zero in equation (2.12), then the dispersion equation reduces to (with $\hat{\rho}_0 = 1$):

$$\hat{\sigma} = -\frac{1}{\gamma}\left[k_{\parallel}^2 \frac{\tau_{rad}}{\tau_{\parallel}} + k_{\perp}^2 \frac{\tau_{rad}}{\tau_{\perp}} + \hat{\mathcal{L}}_T\right] + \mathrm{O}(\epsilon) \tag{2.16}$$

so that, for a uniform field, if $\epsilon \ll 1$, the fast and slow magneto-sonic modes are uncoupled from the thermal mode which grows isobarically.

2.2.4 The thermal continuum

It is well known in ideal MHD that mobile regular singular points in the linear differential equations lead to "continua", continuous bands of singular (wave) solutions to the equations (see e.g. Goedbloed, 1983). These continuous spectra are due to the non-uniformity of the equilibrium state. For uniform equilibria they collapse into points. Their existence is a *robust* feature and does not depend on the equilibrium profile or the geometry. The locations of the continua are affected by the equilibrium profile. These MHD continua are affected by non-ideal effects in different ways. For example, resistivity eliminates the Alfvén continuum, while isotropic thermal conduction causes a shift of the slow continuum (Hermans, 1987). In this section we illustrate the effects of the non-adiabatic terms on the continuous parts of the MHD spectrum in planar geometry. Without perpendicular thermal conduction there is a new continuum, known as the "thermal continuum". For a rigourous proof of the existence of the thermal continuum see Van der Linden (1991).

Consider a Cartesian system with x being the direction of non-uniformity. We can Fourier analyse with respect to the ignorable cooordinates y and z and assume that the solutions are of the form

$$f(\mathbf{r}) = f(x)\exp(ik_y y + ik_z z)$$

where f represents any of the unknowns, and k_y and k_z are components of the wave vector. For a horizontal magnetic field ($\hat{B}_x = 0$) the linearized equations (2.2) to (2.6) become

$$\begin{aligned}
\epsilon^2\hat{\rho}_0\hat{\sigma}v_x &= -\frac{\partial}{\partial x}\left(\frac{\beta}{2}\hat{p}_1 + \hat{B}_z\hat{B}_{1z} + \hat{B}_y\hat{B}_{1y}\right) + iF\hat{B}_{1x},\\
\epsilon^2\hat{\rho}_0\hat{\sigma}v_y &= -ik_y\frac{\beta}{2}\hat{p}_1 + \hat{B}_{1x}\frac{\partial\hat{B}_y}{\partial x} + ik_z\hat{B}_z\hat{B}_{1y} - ik_y\hat{B}_z\hat{B}_{1z},\\
\epsilon^2\hat{\rho}_0\hat{\sigma}v_z &= -ik_z\frac{\beta}{2}\hat{p}_1 + \hat{B}_{1x}\frac{\partial\hat{B}_z}{\partial x} - ik_z\hat{B}_y\hat{B}_{1y} + ik_y\hat{B}_y\hat{B}_{1z},\\
\hat{\sigma}\hat{\rho}_1 &= -ik_z\hat{\rho}_0\hat{v}_z - ik_y\hat{\rho}_0\hat{v}_y - \frac{d}{dx}(\hat{\rho}_0 v_x),\\
\hat{\sigma}\hat{B}_{1x} &= iFv_x,\\
\hat{\sigma}\hat{B}_{1y} &= ik_z(v_y\hat{B}_z - v_z\hat{B}_y) - \frac{d}{dx}(\hat{B}_y v_x),\\
\hat{\sigma}\hat{B}_{1z} &= ik_y(v_z\hat{B}_y - v_y\hat{B}_z) - \frac{d}{dx}(\hat{B}_z v_x),\\
\hat{\sigma}\hat{p}_1 &= -v_x\frac{d\hat{p}_0}{dx} + \gamma\frac{\hat{p}_0}{\hat{\rho}_0}\hat{\sigma}\hat{\rho}_1 + \gamma\frac{\hat{p}_0}{\hat{\rho}_0}v_x\frac{d\hat{\rho}_0}{dx} - \frac{F^2}{\hat{B}_0^2}\frac{\tau_{rad}}{\tau_{\parallel}}\hat{T}_1 - \frac{\tau_{rad}}{\tau_{\perp}}\frac{\partial^2\hat{T}_1}{\partial x^2}\\
&\quad + \left(\frac{F^2}{\hat{B}_0^2} - k^2\right)\frac{\tau_{rad}}{\tau_{\perp}}\hat{T}_1 - \hat{\mathcal{L}}_p\hat{p}_1 - \hat{\mathcal{L}}_T\hat{T}_1.\\
\frac{\hat{p}_1}{\hat{p}_0} &= \frac{\hat{\rho}_1}{\hat{\rho}_0} + \frac{\hat{T}_1}{\hat{T}_0},
\end{aligned}$$

where $F = \mathbf{k}\cdot\hat{\mathbf{B}}_0 = k_y\hat{B}_y + k_z\hat{B}_z$. These nine equations can be transformed, by substitution into a set of two first order and one second order equations:

$$\frac{d}{dx}\left(\frac{\beta}{2}\hat{\sigma}P'\right) = -\left(\epsilon^2\hat{\sigma}^2\hat{\rho}_0 + F^2\right)v_x, \tag{2.17}$$

$$\begin{aligned}
&\epsilon^2\hat{\sigma}^2\hat{\rho}_0\left(\epsilon^2\hat{\sigma}^2\hat{\rho}_0 + \hat{B}_0^2k^2\right)\hat{\sigma}P' + \frac{\beta}{2}\hat{p}_0k^2\left(\epsilon^2\hat{\sigma}^2\hat{\rho}_0 + F^2\right)\hat{\sigma}P' \;-\; \hat{\sigma}\frac{\hat{p}_0}{\hat{T}_0}\left(\epsilon^2\hat{\sigma}^2\hat{\rho}_0 + F^2\right)\epsilon^2\hat{\sigma}^2\hat{\rho}_0\hat{T}_1\\
&+\left(\epsilon^2\hat{\sigma}^2\hat{\rho}_0 + F^2\right)\left(\epsilon^2\hat{\sigma}^2\hat{\rho}_0\left[\frac{2}{\beta}\hat{B}_0^2 + \hat{p}_0\right] + F^2\hat{p}_0\right)\frac{dv_x}{dx} \;=\; 0,
\end{aligned} \tag{2.18}$$

$$\begin{aligned}
&\hat{\sigma}P'\left(1 + \frac{\hat{\mathcal{L}}_p}{\hat{\sigma}}\right)\left(\epsilon^2\hat{\sigma}^2\hat{\rho}_0 + \hat{B}_0^2k^2\right)\epsilon^2\hat{\sigma}^2\hat{\rho}_0 \;+\\
&\hat{\sigma}P'\left(\epsilon^2\hat{\sigma}^2\hat{\rho}_0 + F^2\right)\gamma\hat{p}_0\frac{\beta}{2}k^2 - \frac{1}{\beta}\frac{\hat{\mathcal{L}}_p}{\hat{\sigma}}\frac{d\hat{B}_0^2}{dx}\epsilon^2\hat{\sigma}^2\hat{\rho}_0\left(\epsilon^2\hat{\sigma}^2\hat{\rho}_0 + F^2\right)v_x \;+
\end{aligned}$$

$$\epsilon^2\hat{\sigma}^2\hat{\rho}_0\left(\epsilon^2\hat{\sigma}^2\hat{\rho}_0+F^2\right)\left(\frac{F^2}{\hat{B}_0^2}\frac{\tau_{rad}}{\tau_{\|}}+\hat{\mathcal{L}}_T\right)\hat{T}_1 \quad +$$

$$\left(\epsilon^2\hat{\sigma}^2\hat{\rho}_0+F^2\right)\left[\left(\epsilon^2\hat{\sigma}^2\hat{\rho}_0+F^2\right)\gamma\hat{p}_0+\frac{2}{\beta}\hat{B}_0^2\epsilon^2\hat{\sigma}^2\hat{\rho}_0\left(1+\frac{\hat{\mathcal{L}}_p}{\hat{\sigma}}\right)\right]\frac{dv_x}{dx} \quad -$$

$$\epsilon^2\hat{\sigma}^2\hat{\rho}_0\left(\epsilon^2\hat{\sigma}^2\hat{\rho}_0+F^2\right)\left[\frac{\tau_{rad}}{\tau_\perp}\left(\frac{F^2}{\hat{B}_0^2}-k^2\right)\hat{T}_1+\frac{\tau_{rad}}{\tau_\perp}\frac{d^2\hat{T}_1}{dx^2}\right] = 0, \quad (2.19)$$

where P' is the perturbed total pressure

$$P'=\hat{p}_1+\frac{2}{\beta}\hat{B}_y\hat{B}_{1y}+\frac{2}{\beta}\hat{B}_z\hat{B}_{1z}.$$

These three equations could be rewritten as a single fourth order equation by eliminating two of the variables.

As perpendicular thermal conduction is much smaller than parallel conduction we can neglect perpendicular conduction terms in a first approximation. Then the energy equation simplifies to an algebraic equation and the order of the system reduces from four to two. The perturbed temperature can then be eliminated to give:

$$\left(\epsilon^2\hat{\sigma}^2\hat{\rho}_0+F^2\right)^2\left(\gamma\hat{p}_0+\frac{\hat{T}_0}{\hat{\sigma}}\left(\frac{F^2}{\hat{B}_0^2}\frac{\tau_{rad}}{\tau_{\|}}+\hat{\mathcal{L}}_T\right)\right) \quad +$$

$$\frac{2}{\beta}\hat{B}_0^2\epsilon^2\hat{\sigma}^2\hat{\rho}_0\left(1+\frac{\hat{\mathcal{L}}_p}{\hat{\sigma}}+\frac{\hat{T}_0}{\hat{\sigma}\hat{p}_0}\left(\frac{F^2}{\hat{B}_0^2}\frac{\tau_{rad}}{\tau_{\|}}+\hat{\mathcal{L}}_T\right)\right)\left(\epsilon^2\hat{\sigma}^2\hat{\rho}_0+F^2\right)\frac{dv_x}{dx} \quad +$$

$$\hat{\sigma}P'\left(\epsilon^2\hat{\sigma}^2\hat{\rho}_0+\hat{B}_0^2k^2\right)\epsilon^2\hat{\sigma}^2\hat{\rho}_0\left(1+\frac{\hat{T}_0}{\hat{p}_0}\frac{\hat{\mathcal{L}}_T}{\hat{\sigma}}+\frac{\hat{\mathcal{L}}_p}{\hat{\sigma}}+\frac{\hat{T}_0}{\hat{\sigma}\hat{p}_0}\frac{F^2}{\hat{B}_0^2}\frac{\tau_{rad}}{\tau_{\|}}\right) \quad +$$

$$\hat{\sigma}P'\left(\epsilon^2\hat{\sigma}^2\hat{\rho}_0+F^2\right)\frac{\beta}{2}k^2\left(\gamma\hat{p}_0+\frac{\hat{T}_0}{\hat{\sigma}}\left(\frac{F^2}{\hat{B}_0^2}\frac{\tau_{rad}}{\tau_{\|}}+\hat{\mathcal{L}}_T\right)\right) \quad -$$

$$\frac{1}{\beta}\frac{\hat{\mathcal{L}}_p}{\hat{\sigma}}\epsilon^2\hat{\sigma}^2\hat{\rho}_0\frac{d\hat{B}_0^2}{dx^2}\left(\epsilon^2\hat{\sigma}^2\hat{\rho}_0+F^2\right)v_x = 0. \quad (2.20)$$

Equations (2.17) and (2.20) describe all linear perturbations of the equilibrium state. They can be rewritten as one second order differential equation in Sturm-Liouville form

$$\frac{d}{dx}\left(\frac{D}{N}\frac{dv_x}{dx}+\frac{1}{\beta}\frac{\hat{\mathcal{L}}_p}{\hat{\sigma}}\epsilon^2\hat{\sigma}^2\hat{\rho}_0\frac{d\hat{B}_0^2}{dx^2}\left(\epsilon^2\hat{\sigma}^2\hat{\rho}_0+F^2\right)v_x\right)+\frac{2}{\beta}\left(\epsilon^2\hat{\sigma}^2\hat{\rho}_0+F^2\right)v_x=0 \quad (2.21)$$

with

$$
\begin{aligned}
D &= \left(\epsilon^2\hat{\sigma}^2\hat{\rho}_0 + F^2\right)^2 \left(\gamma\hat{p}_0 + \frac{\hat{T}_0}{\hat{\sigma}}\left(\frac{F^2}{\hat{B}_0^2}\frac{\tau_{rad}}{\tau_{\|}} + \hat{\mathcal{L}}_T\right)\right) \\
&+ \frac{2}{\beta}\hat{B}_0^2\epsilon^2\hat{\sigma}^2\hat{\rho}_0\left(1 + \frac{\hat{\mathcal{L}}_p}{\hat{\sigma}} + \frac{\hat{T}_0}{\hat{\sigma}\hat{p}_0}\left(\frac{F^2}{\hat{B}_0^2}\frac{\tau_{rad}}{\tau_{\|}} + \hat{\mathcal{L}}_T\right)\right)\left(\epsilon^2\hat{\sigma}^2\hat{\rho}_0 + F^2\right) \qquad (2.22)
\end{aligned}
$$

and

$$
\begin{aligned}
N &= \left(\epsilon^2\hat{\sigma}^2\hat{\rho}_0 + \hat{B}_0^2k^2\right)\epsilon^2\hat{\sigma}^2\hat{\rho}_0\left(1 + \frac{\hat{T}_0}{\hat{p}_0}\frac{\hat{\mathcal{L}}_T}{\hat{\sigma}} + \frac{\hat{\mathcal{L}}_p}{\hat{\sigma}} + \frac{\hat{T}_0}{\hat{\sigma}\hat{p}_0}\frac{F^2}{\hat{B}_0^2}\frac{\tau_{rad}}{\tau_{\|}}\right) \\
&+ \left(\epsilon^2\hat{\sigma}^2\hat{\rho}_0 + F^2\right)\frac{\beta}{2}k^2\left(\gamma\hat{p}_0 + \frac{\hat{T}_0}{\hat{\sigma}}\left(\frac{F^2}{\hat{B}_0^2}\frac{\tau_{rad}}{\tau_{\|}} + \hat{\mathcal{L}}_T\right)\right) \qquad (2.23)
\end{aligned}
$$

Values of $\hat{\sigma}$ giving $D = 0$ correspond to true singularities of the differential equations, while $N = 0$ yields only apparent singularities. All $\hat{\sigma}$ that satisfy $D(x_0, \hat{\sigma}) = 0$ for some x_0 can give (singular) solutions to the eigenvalue problem. For proof see Van der Linden (1991).

The condition $D = 0$ gives rise to an Alfvén continuum, which is identical to the Alfvén continuum found in ideal (adiabatic) MHD (Goedbloed, 1983), and defined by

$$\left(\epsilon^2\hat{\sigma}^2\hat{\rho}_0 + F^2\right) = 0.$$

The slow, or "cusp", continuum of ideal MHD is modified however, and is absorbed into a third degree polynomial in $\hat{\sigma}$:

$$
\begin{aligned}
&\left(\epsilon^2\hat{\sigma}^2\hat{\rho}_0 + F^2\right)\left(\gamma\hat{p}_0 + \frac{\hat{T}_0}{\hat{\sigma}}\left(\frac{F^2}{\hat{B}_0^2}\frac{\tau_{rad}}{\tau_{\|}} + \hat{\mathcal{L}}_T\right)\right) \quad + \\
&\frac{2}{\beta}\hat{B}_0^2\epsilon^2\hat{\sigma}^2\hat{\rho}_0\left(1 + \frac{\hat{\mathcal{L}}_p}{\hat{\sigma}} + \frac{\hat{T}_0}{\hat{\sigma}\hat{p}_0}\left(\frac{F^2}{\hat{B}_0^2}\frac{\tau_{rad}}{\tau_{\|}} + \hat{\mathcal{L}}_T\right)\right) \quad = \quad 0. \qquad (2.24)
\end{aligned}
$$

The real solutions of this polynomial are the thermal continuum, and the complex solutions the modified slow continuum. In addition to this thermal continuum, the thermal subspectrum may contain discrete thermal modes above and below the thermal continuum on the real axis. In most cases, the thermal continuum determines the stability of

the system. Van der Linden (1991) shows that the stability of thermal continuum modes is governed by a local isobaric criterion and stability of the slow continuum is governed by the local isentropic criterion.

When perpendicular conduction is included the thermal continuum does not exist. Instead, it is replaced (for small $\kappa_\perp$) by a dense set of nearly singular discrete modes, the so-called "quasi-continuum modes". These modes reach up to the upper boundary of the thermal continuum so thermal stability is still governed by the local isobaric criterion.

For $\kappa_\perp \neq 0$ the set of equations consists of (2.17), (2.18) and (2.19) which contain mobile singular points. The continuous spectra that these define are the Alfvén continuum (again) and the isothermal cusp continuum. The latter continuum is different from the adiabatic slow continuum but is located on the imaginary axis. Other discrete modes exist outside the thermal quasi-continuum, but Van der Linden (1991) conjectures that the stability of the continuum provides necessary and sufficient conditions for the thermal stability of the system, although full proof of this statement has not as yet been found.

2.2.5 Thermal instabilities in the solar corona

Magnetic fields in the solar corona have two additional features which do not exist in the uniform, infinite medium so well analysed by Field (1965). These are the global structuring of the field and the finite extent of the field lines which emerge from and enter into the dense photosphere.

Studies of coronal, thermal instabilities have generally followed two different lines. In one approach, the coronal magnetic field is assumed to dominate so that the field is treated as rigid and basically confines the energy balance by defining the geometry of the system.

This allows us to concentrate on 1-D disturbances and non-isothermal initial atmospheres can be studied. In the second approach, the interaction between the magnetic-field and the thermal mode is investigated by allowing for magnetic field perturbations. This makes the stability calculation 3-D and, in order to make progress, attention is generally restricted to simple equilibria.

Rigid fields

Following on from the initial studies of Field (1965) and Heyvaerts (1974) on isothermal, uniform equilibria, Antiochos (1979), Habbal and Rosner (1979) and Hood and Priest (1980b) considered non-isothermal atmospheres. The results depended strongly on the choice of boundary conditions. Having investigated a variety of choices for the boundary conditions, Hood and Priest (1980b) found that the plasma becomes unstable if either the length of the field line or the plasma pressure exceed a certain value. Such studies have been carried further by various authors. Again, the results depend upon the choice of boundary conditions. So attempts have been made to model the coronal/photospheric boundary in a simple but realistic manner. One such investigation into the effects of different boundary conditions was carried out by Antiochos *et al.* (1985). This considered combinations of possible boundary conditions at the base. These conditions are: $T_1 = 0$ (the perturbed temperature), $dT_1/ds = 0$ (the perturbed conductive flux), $p_1 = 0$ (the perturbed pressure), and $v_1 = 0$ (the perturbed parallel velocity). It is assumed that the temperature in the corona is essentially constant. It was deduced that the only physically relevant solutions (for perturbations that penetrate the deeper, denser layers), are those

with

$$T_1 = 0 \qquad n_1 = 0 \tag{2.25}$$

at the boundary where n_1 is the perturbed number density. This implies that the perturbed pressure vanishes giving the isobaric mode. The choice $v_1 = 0$ seems to give a boundary layer near the base outside which (2.25) is satisfied.

Craig and McClymont (1987) showed that loops can be stabilized if there are sufficiently large pressure perturbations. They called this process "dynamical stiffness". Without gravity all loops are unstable, but with gravity the equilibria are stabilized by the stiffness introduced by stratification.

Magneto-thermal effects

When the equilibrium magnetic field is not uniform, currents and pressure gradients in the system can drive ideal MHD instabilities which grow on the ideal MHD time-scale. The resulting variations in the magnetic field and gas pressure can influence the thermal terms thereby producing a coupling between modes.

Work on thermal instabilities in a non-uniform field was first performed by Chiuderi and Van Hoven (1979). They considered a (Cartesian) slab geometry in which the Alfvén mode decouples. A Cartesian geometry is not an accurate representation of the pre-prominence coronal plasma which probably has the structure of a magnetic arcade, but a planar equilibrium simplifies the mathematics and allows us to form a clear picture of the physical processes behind the thermal instability. Chiuderi and van Hoven (1979) also neglected thermal conduction on the grounds that it has no stabilizing effect in a surface where $\mathbf{k} \cdot \mathbf{B}_0 = 0$ (i.e. $k_{\|} = 0$). The condition $\mathbf{k} \cdot \mathbf{B}_0 = 0$ is the well known ideal MHD

condition for a marginal stability mode-rational surface (Newcomb, 1960; Bateman, 1978). For an infinite sheared magnetic field, the thermal instability is *expected* to be enhanced at mode rational surfaces, but away from the mode rational surface thermal conduction becomes important and helps to stabilize the mode. Thus, the instability tends to localize near the mode-rational surface.

The work of Chiuderi and Van Hoven has been extended in a series of papers and effects such as resistive heating, non-linearity and perpendicular thermal conduction have been included. Sparks and Van Hoven (1988) have clarified much of this earlier work, pointing out that there exist essentially three important domains of behaviour. Well away from the mode rational surface, thermal conduction dominates and the plasma is thermally stable. Near the mode rational surface, conduction is reduced and an instability can develop. As discussed earlier, the sound (or, more correctly, the slow mode) travel time is shorter than the radiative time-scale and the instability is an isobaric mode. But at the singular layer itself the slow mode cannot propagate and pressure differences cannot be equalized. The instability is an isochoric mode here. But the faster growth rate occurs for the isobaric mode and so the instability develops with a maximium amplitude a short distance away from the singular layer. The instability will set in where the local isobaric growth rate is largest (Van der Linden, 1991).

Perpendicular thermal conduction is often ignored because of the small value of $\kappa_\perp$, although, as its inclusion increases the order of the system of differential equations from 2 to 4, it is not *a priori* evident that it is physically plausible to ignore it. Van der Linden (1991) has demonstated that the inclusion of perpendicular thermal conduction affects the growth rate of the thermal instability very little (which is determined by stability of

the thermal continuum), but that it is the dominant mechanism affecting the structure of the eigenmodes perpendicular to the equilibrium magnetic field. The length-scales in this direction are, therefore, small and could be responsible for the fine-scale structure observed in prominences. Similar ideas have been put forward by Oran *et al.* (1985), Steinolfson (1984) and Van Hoven *et al.* (1986).

Van der Linden (1991) has found that the thickness of the "fibrils" is proportional to $\kappa_\perp$ to the power $\frac{1}{4}$ and not $\frac{1}{2}$ as is largely assumed in qualitative arguments. This conclusion is very significant as it allows the length-scales introduced by perpendicular thermal conduction to be of the same order as the observed length-scales of fine-scale structure in prominences, and anomalously high perpendicular conduction does not need to be invoked. Van der Linden (1991) also shows how eigenmodes with different mode numbers across the magnetic field can have very similar growth rates, so that more than one mode may be excited by an instability.

Generally speaking, the finite length of coronal magnetic field lines has not been incorporated into much of the above mentioned work. Field lines in the corona are anchored at both ends in the dense photosphere. The boundary conditions that represent the photospheric base can be represented by the "line-tying" boundary conditions, discussed in section (2.3.1). One important consequence of line-tying is that there can be no mode rational surface except under special conditions (Hood and Priest, 1979, 1980a; Einaudi and Van Hoven, 1981; Hood, 1983). So thermal conduction is important everywhere and the different regimes discussed by Sparks and Van Hoven (1988) for the planar field case do not necessarily exist.

Investigating a slab geometry with boundary conditions representing the photospheric

base, Cargill and Hood (1989) used a class of localized modes known as "ballooning modes". Instead of finding that there is always an instability, they discovered that the instability only occurs when the field line length exceeds a critical value at which the conduction time-scale increases to the order of the radiative time-scale. This gives a more selective means for prominence formation, one which helps to explain why relatively few prominences are seen in the corona. Their main conclusions were that the least stable mode requires a parallel velocity at the photosphere, and that the least stable thermal mode evolves almost isobarically and decouples from the slow mode. They also showed how an increase in the equilibrium plasma pressure destabilizes the system.

Some work has been done on thermal instabilities in geometries other than artesian. Thermal instabilities in coronal loops, without boundaries, have been investigated by An (see, for example, An, 1982, 1984, 1986). The main effect of field line curvature is that the Alfvén mode is now coupled to the thermal and slow modes with the amount of coupling dependent on the time-scale ratios. Hood *et al.* (1993) have investigated a finite length coronal loop by concentrating on localized modes. They used a WKB approach that eliminates the fast mode. When the time-scales are comparable, there is substantial coupling between unstable Alfvén and thermal modes, and the modes can become complex overstable modes. By varying the magnitude of the wavenumber, an investigation of how a global mode is related to a localized mode has been carried out by Van der Linden *et al.* (1991).

2.3 Boundary conditions and localized modes

We want to investigate the thermal instability in the solar corona including the effects of the photospheric boundary and not ignoring the perpendicular thermal conduction. In order to do this we have developed the work of Cargill and Hood (1989) which addressed the thermal stability of coronal plasmas incorporating the effects of the photospheric boundaries. These boundary conditions (referred to as line-tying in connection with the MHD variables) force conditions on coronal perturbations at the photosphere owing to the large inertia there. In addition, the thermal conduction term requires boundary conditions on the thermodynamic variables.

The line-tying boundary conditions give conditions for the perturbed velocity at the boundary. When we also include the non-adiabatic terms, we need additional boundary conditions on the temperature perturbation.

In deriving the non-dimensionalized equations in Chapter 1, we introduced the parameter ϵ which is a measure of the coupling between the MHD wave modes and the thermal mode. When ϵ is small, as in the corona, the coupling is very weak and we can investigate the thermal mode using perturbations that eliminate the MHD modes from our analysis and allow us to concentrate on the thermal mode. One class of perturbations that enables this decoupling are known as ballooning modes.

The general equations for ballooning modes in the solar corona, including the effects of resistivity and viscosity along with conduction, gravity and plasma radiation were derived by Hood, Van der Linden and Goossens (1989). Hood *et al.* (1993) and Cargill and Hood (1993) have used these equations (neglecting resistivity, viscosity and gravity) to investigate thermal instabilities in coronal arcades and, as mentioned earlier, Cargill and

Hood (1989) investigated thermal instabilities in a slab geometry using these equations to investigate the effects of the line-tying boundary conditions on the thermal instability.

2.3.1 Line-tying

Most magnetic field lines in the corona are not infinite but emerge from and go back into the photosphere. The inertia of the dense photosphere dominates the photospheric-coronal boundary. The term "line-tying" is a good description of the physical effect of the photo-coronal boundary. The magnetic field lines are "tied" to the photospheric matter, as the magnetic flux is "frozen" to the plasma (for negligible resistivity). The inertia of the photospheric matter dominates at the interface, so perturbations of coronal origin cannot substantially move the footpoints of the magnetic field lines. Consequently, line-tying is strongly stabilizing.

The boundary condition that the component of the perturbed velocity perpendicular to the magnetic field is zero is generally accepted. Reasons for this are outlined below.

Going from the corona into the photosphere, the number density increases from 5×10^{14} to $10^{23} m^{-3}$ over a distance of $2 \times 10^{3} km$. When compared to the coronal scaleheight of $10^{5} km$ at a temperature of $2 \times 10^{6} K$, it is seen that the density rises almost discontinuously. To a first approximation we can treat the photospheric base as an interface. By considering coronal and photospheric time-scales we can estimate the effect of this interface on coronal disturbances.

The coronal Alfvénic time-scale is about $5s$. The corresponding photospheric time-scale is larger by a factor of approximately 1.4×10^{4} (assuming an average value for the magnetic field strength in the photosphere). The photosphere is unable to respond quickly

to Alfvénic disturbances generated in the corona.

We can argue this a different way. Consider an Alfvén wave propagating down from the corona. At the interface it is transmitted and reflected with amplitudes

$$A_t = \frac{2v_{A_p}}{v_{A_p} + v_{A_c}} A_i$$

and

$$A_r = \frac{v_{A_p} - v_{A_c}}{v_{A_p} + v_{A_c}} A_i$$

respectively in terms of the incident wave amplitude. v_{A_p} and v_{A_c} are the Alfvén speeds in the photosphere and corona. Neglecting any photospheric concentration of the magnetic field and using the densities quoted above, we have

$$A_t = 1.4 \times 10^{-4} A_i$$

$$A_r = -0.9999 A_i$$

and the wave is essentially totally reflected. As the Alfvén wave is a transverse wave this implies that the perpendicular velocity components vanish at the interface.

The boundary conditions for the velocity component along the field lines have been a source of controversy for many years. Einaudi and Van Hoven (1981, 1983) argued that $\mathbf{v}_{||}$ need not be zero at the photosphere, but that instead the energy is conserved. This set of boundary conditions is known as the "flow-through" line-tying conditions.

$$\mathbf{v}_\perp = 0, \qquad \mathbf{v}_{||} \neq 0 \tag{2.26}$$

But Rosner et al (1986) concluded that the best way to model the transition from corona to photosphere is to make all velocity components vanish. We call these the "rigid wall" conditions.

$$\mathbf{v}_\perp = 0, \qquad \mathbf{v}_{||} = 0 \tag{2.27}$$

Several authors have tried to determine the correct boundary conditions. Hood (1986) used the ballooning approximation to construct solutions to the MHD equations in a simple equilibrium where the corona-photosphere transition was modelled as a sharp density increase in a periodic cylinder. He found that as the ratio of photospheric to coronal density is increased, all velocity components decrease to zero. Thus he concluded that the rigid wall conditions are best for ideal MHD. This argument holds for fast instabilities, but Hood, Van der Linden and Goossens (1989) found that $\mathbf{v}_\perp$ must vanish but that $\mathbf{v}_\parallel$ may be non-zero for slower instabilities.

Temperature boundary condition

When the non-adiabatic terms are included in the differential equations, two more boundary conditions are needed in addition to those on the perturbed velocity components. There are two different sets of thermal boundary conditions that we may use:

$$T_1 = 0 \tag{2.28}$$

or

$$\frac{dT_1}{ds} = 0 \tag{2.29}$$

where s is a field-aligned coordinate.

This is another controversial issue, especially with regard to the studies of the thermal instability of single rigid magnetic field coronal loop models (Hood and Priest, 1980b; Antiochos, 1979; McClymont and Craig, 1985a,b). The first condition implies that there is a fixed point in space at which there is sufficient plasma to radiate away any incoming heat flux instantaneously. The second states that the plasma cannot radiate away any incoming heat flux, but manages to maintain a zero temperature gradient. The first

condition makes more physical sense as large temperature changes in the diffuse corona could only raise the photospheric temperature slightly. This, therefore, is the boundary condition that we will use.

Antiochos *et al.* (1985) studied thermal perturbations of static coronal loop models. They concluded that the most physical assumptions are that the temperature and density perturbations vanish there and that an allowance for parallel flow is the minimium requirement for a realistic boundary.

The rigid wall conditions are probably the most appropriate for high frequency perturbations and the flow-through conditions for low frequencies. If the photosphere can respond to pressure perturbations on a faster time-scale than the growth of the instability in the corona, then the flow-through conditions will be appropriate. As mentioned in the preamble, Cargill and Hood (1989) found that the least stable thermal mode requires a parallel velocity displacement at the photosphere, with the mode corresponding to a vanishing thermal pressure.

2.4 Derivation of the stability equations

If line-tying is enforced in the z-direction and the equilibrium magnetic field varies in the x-direction, two characteristic length-scales exist in the problem, so we cannot isolate individual Fourier components as we can for an infinite medium. One must either solve coupled linear partial differential equations or an infinite system of coupled ordinary differential equations.

For a one-dimensional equilibrium, line-tying makes the linear analysis intrinsically two dimensional. But, the ballooning approximation reduces the problem to a one dimensional

analysis for solutions in the flux surfaces.

Now we can proceed to outline the ordering of the perturbed variables in the ballooning approximation for an isothermal equilibrium in Cartesian geomatry. The solutions are assumed to have a slow variation along magnetic field lines but a rapid variation transverse to the field lines. To model this the perturbed variables have a WKB solution of the form:

$$f(\mathbf{r}) = \tilde{f}(\mathbf{r}) \exp(inS(\mathbf{r})) \tag{2.30}$$

where $n \gg 1$ and to eliminate stable wave modes $\mathbf{B_0} \cdot \nabla S = 0$. The amplitude factors satisfy the boundary conditions. n is the ratio of the equilibrium length-scale to the perpendicular length-scale. From the form of the WKB solution we can replace ∇ by $in\nabla S + \nabla$ where the second ∇ operates on the amplitude functions alone.

We now write the perturbed velocity and magnetic field as

$$\hat{\mathbf{v}} = \frac{\left(\hat{\mathbf{v}} \cdot \hat{\mathbf{B}}_0\right) \hat{\mathbf{B}}_0}{B_0^2} + \hat{\mathbf{v}}_\perp \tag{2.31}$$

and

$$\hat{\mathbf{B}}_1 = \frac{\left(\hat{\mathbf{B}}_1 \cdot \hat{\mathbf{B}}_0\right) \hat{\mathbf{B}}_0}{B_0^2} + \hat{\mathbf{B}}_\perp \tag{2.32}$$

where $\hat{\mathbf{v}}_\perp$ and $\hat{\mathbf{B}}_\perp$ are the components perpendicular to the equilibrium magnetic field. Now we assume that the components parallel are O(1) quantities and that the perpendicular components are $O(1/n)$. This decouples the Alfvén wave which is unlikely to be important as it is incompressible and does not couple to the other modes in a slab geometry.

The momentum equation (1.2) from the leading order gives

$$\hat{p}_1 + \frac{2}{\beta}\hat{\mathbf{B}}_0 \cdot \hat{\mathbf{B}}_1 = O(1/n) \tag{2.33}$$

This removes the fast magnetosonic mode and Chiuderi and Van Hoven (1979) showed that the condition (2.33) is approximately satisfied. The neglect of the fast mode is valid provided that the radiative time-scale is much longer than the fast mode transit time based on the short perpendicular wavelength, so that the plasma can even out total pressure fluctuations on a much shorter time-scale than the growth time for any radiative modes.

Cargill and Hood (1989) used these assumptions (without perpendicular conduction) to investigate the effects of line-tying on the radiative mode. Their equations apply to parallel motions along individual field lines, so the growth rate is calculated at each field line. Including a perpendicular conduction term allows us to find a global growth rate and to investigate the transverse structure of the eigenmodes.

2.4.1 The isobaric mode

We can now remove the slow mode if we assume that the perturbed plasma pressure vanishes to leading order

$$\hat{p}_1 = \mathrm{O}(1/n).$$

Pressure perturbations will be small if pressure can be equalized on a much faster time-scale than the growth of the radiative instability, i.e. $\tau_{rad} \gg \tau_s$. This condition is satisfied under coronal conditions. We expect the radiative mode to grow fastest for vanishing pressure perturbations, which corresponds to the isobaric growth rate.

After making this further assumption, the leading order equations are (after non dimensionalization):

$$\hat{\sigma}\gamma\frac{\hat{p}_0}{\hat{T}_0}\hat{T}_1 = \frac{\tau_{rad}}{\tau_{\|}}\frac{\left(\hat{\mathbf{B}}_0\cdot\hat{\nabla}\right)^2}{\hat{B}_0^2}\hat{T}_1 - n^2\left|\hat{\nabla}S\right|^2\frac{\tau_{rad}}{\tau_{\perp}}\hat{T}_1 - \hat{\mathcal{L}}_{\hat{T}}\hat{T}_1, \tag{2.34}$$

$$\hat{\sigma}\frac{\hat{T}_1}{\hat{T}_0} = \hat{\mathbf{B}}_0 \cdot \hat{\nabla}\hat{v}_{\|}. \tag{2.35}$$

The perpendicular thermal conduction term can be included if the condition

$$n^2\frac{\tau_{rad}}{\tau_{\perp}} = \mathrm{O}(1) \tag{2.36}$$

is satisfied. Notice that if we ignore the perpendicular conduction term, then the energy equation reduces to

$$\left(\frac{\tau_{rad}}{\tau_{\|}}\frac{B_z^2}{B_0^2}\frac{d^2}{dz^2} - \hat{\mathcal{L}}_{\hat{T}} - \hat{\sigma}\gamma\frac{\hat{p}_0}{\hat{T}_0}\right)\hat{T}_1 = 0, \tag{2.37}$$

which is equivalent to equation (3.6) of Hood and Priest's (1980b) study of the one-dimensional (field-aligned) thermal instability of a coronal loop. The solution of this equation (2.37) gives the isobaric growth rate found by Cargill and Hood (1989).

The vanishing pressure (isobaric) mode decouples the MHD modes from the thermal effects in our Cartesian geometry. Magnetic field effects enter only as structuring of the plasma. Without the perpendicular conduction term we recover equation (3.6) of Hood and Priest (1980b) who studied the one-dimensional rigid field thermal instability of a coronal loop. If the perturbed temperature does not vanish, then coupling to the slow mode occurs and the equilibrium is more stable than for the isobaric case.

To find the values of the growth rate $\hat{\sigma}$, it is sufficient to solve the equation (2.34). This would give us the eigenfunctions $\hat{T}_1$. The perturbed parallel velocity is then defined by equation (2.35).

Line-tying can be easily modelled since the operator $\hat{\mathbf{B}}_0 \cdot \hat{\nabla}$ enables us to write

$$\hat{\mathbf{B}}_0 \cdot \hat{\nabla} = \hat{B}_0\frac{\partial}{\partial s}$$

where s is a field-aligned coordinate and we can apply line-tying at $s = \pm s_L$.

2.5 Solution of the equations

We can now proceed to solve the equations subject to the boundary conditions discussed in section (2.3.1).

A general form of S that satisfies the condition $\hat{\mathbf{B}}_0 \cdot \hat{\nabla} S = 0$ is

$$S = y - \frac{\hat{B}_y}{\hat{B}_z} z + S(x) \tag{2.38}$$

and this gives

$$|\nabla S|^2 = \left[S'(x) - \left(\frac{\hat{B}_y}{\hat{B}_z} \right)' z \right]^2 + 1 + \frac{\hat{B}_y^2}{\hat{B}_z^2} \tag{2.39}$$

where

$$' \equiv \frac{d}{dx}.$$

2.5.1 Equilibrium and boundary conditions

As the conduction time-scale is proportional to the equilibrium pressure, and the radiative time-scale is inversely proportional to it, the stability of the system depends critically on the form of the equilibrium pressure.

We specify the equilibrium magnetic field in the form

$$\hat{\mathbf{B}}_0 = \left(0, \hat{B}_y(x), \hat{B}_z(x)\right)$$

and deduce the equilibrium plasma pressure, using the condition that the total equilibrium pressure is constant.

We use a variation of the field employed by Chiuderi and Van Hoven (1979):

$$\hat{\mathbf{B}}_0 = \left[0, \lambda \mathrm{sech}(x), (2 - \mathrm{sech}^2(x))^{\frac{1}{2}}\right] \tag{2.40}$$

Note that all the field lines thread the line-tied boundaries for all finite x. The parameter λ represents the relative importance of magnetic shear and gas pressure gradients. $\lambda = 0$ corresponds to straight magnetic field lines with an ambient pressure gradient directed away from $x = 0$ whereas $\lambda = 1$ corresponds to a sheared force-free magnetic field.

We can write the equlibrium plasma pressure as

$$\hat{p}_0(x) = 2 - \frac{1}{\beta}\left(\lambda^2 \mathrm{sech}^2(x) + 2 - \mathrm{sech}^2(x)\right) \tag{2.41}$$

and we will let $\beta = 1$, in common with previous papers (for example Chiuderi and Van Hoven, 1979), so that

$$\hat{p}_0(x) = \left(1 - \lambda^2\right) \mathrm{sech}^2(x). \tag{2.42}$$

We use an isothermal equilibrium, so the non-dimensionalized equilibrium temperature can be set equal to unity ($\hat{T}_0 = 1$). This equilibrium pressure profile has a simple maximum at $x = 0$, and we expect a condensation to set in here, as this is where the local isobaric growth rate is highest.

We impose line-tying boundary conditions at $z = \pm l_1$. Strictly speaking we should apply the boundary conditions at $s = \pm s_L$, but we can project onto the z-direction, as we evaluate along a field line, using

$$\frac{\partial}{\partial s} = \frac{\hat{B}_z}{\hat{B}_0}\frac{\partial}{\partial z}.$$

For the energy equation (2.34), we require the thermodynamic boundary conditions

$$\hat{T}_1 = 0 \qquad \text{at } z = \pm l_1. \tag{2.43}$$

This implies that

$$\frac{\partial v_\parallel}{\partial z} = 0 \quad \text{at} \quad \pm l_1,$$

that is we have the flow through boundary conditions. This comes about through our assumption of constant plasma pressure. Physically this means that the photosphere responds to pressure perturbations in the corona on a faster time-scale than the growth of the thermal instability in the corona. The condition will be satisfied if the radiative time-scale in the corona is much longer than the sound travel time in the photosphere, which is generally the case (see Table 1.2).

Cargill and Hood (1989) considered various different sets of thermal and dynamic conditions at the photosphere. They found that the least stable mode corresponds to a vanishing thermal pressure in the limit of the radiative growth time greatly exceeding the Alfvén transit time. They argued that on the radiative time-scale a parallel motion at the photosphere is allowed. Boundary conditions in the x-direction are that all perturbations go to zero for large x.

2.5.2 Solving the energy equation

If we choose typical values for the time-scales and the constant γ, then the energy equation (2.34) contains two unknowns S' and $\hat{\sigma}$. By choosing a value of x and a value for $\hat{\sigma}$, we can integrate equation (2.34) numerically and iterate on the parameter S' to satisfy the boundary condition (2.43). By repeating this process for a range of values for x, we can plot values of the function S' against x for our chosen value of $\hat{\sigma}$.

Figure (2.3) shows plots of S'^2 against x for various values of $\hat{\sigma}$. For values of $\hat{\sigma}$ below a critical value σ_{crit}, say, S'^2 has two zeroes. As $\hat{\sigma}$ increases, the distance between the two zeroes of S'^2 becomes narrower and at σ_{crit} the curve just touches the x-axis at $x = 0$. For $\hat{\sigma} > \sigma_{crit}$, $S'^2$is always negative. This is typical WKB-like behaviour. From the form of

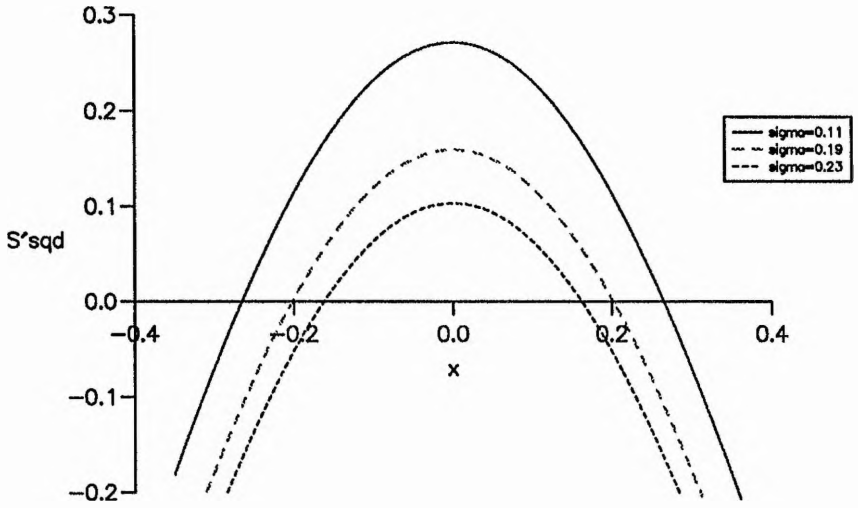

Figure 2.3: S'^2 against x for three values of $\hat{\sigma}$ ($\hat{\sigma} = 0.11, 0.19$ and 0.23), with $\lambda = 0.4$, $\gamma = \frac{5}{3}$, $l_1 = 2$, $\frac{\tau_{rad}}{\tau_{\parallel}} = 1$ and $n^2\frac{\tau_{rad}}{\tau_{\perp}} = 1$.

the perturbations (2.30), we can see that when S' is imaginary the eigenfunctions behave evanescently, and when S' is real the eigenfunctions will have oscillatory behaviour. The region of oscillatory behaviour is always localized around $x = 0$, where the equilibrium pressure (and the local isobaric growth rate) is highest. So introducing perpendicular thermal conduction into the analysis of Cargill and Hood (1989) has restricted condensations to a narrow region centred on the peak of the equilibrium pressure profile.

When S' is imaginary for all x, the eigenfunctions behave exponentially for all x and the boundary conditions in x cannot be satisfied. Solutions that satisfy the boundary conditions must have real S' for some range of x. The solutions will grow in time if $\hat{\sigma} > 0$, and therefore will be unstable.

WKB theory (Dewar and Glasser, 1983; Nayfeh, 1983) tells us that only certain discrete values of $\hat{\sigma}$ can exist. These values of $\hat{\sigma}$ will satisfy the Bohr-Sommerfeld condition

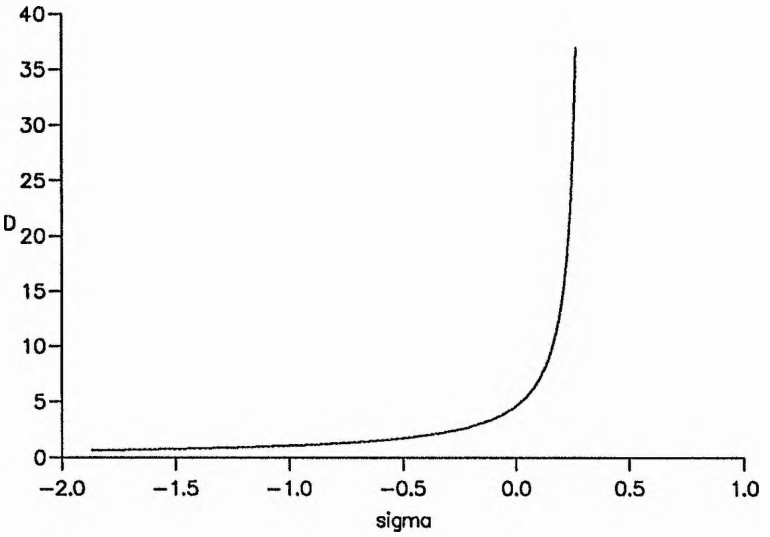

Figure 2.4: The growth rate $\hat{\sigma}$ plotted against n for $\lambda = 0.4$, $\gamma = \frac{5}{3}$, $l_1 = 2$, $\frac{\tau_{rad}}{\tau_{\parallel}} = 1$ and $n^2 \frac{\tau_{rad}}{\tau_{\perp}} = 1$.

for a two turning-point problem:

$$n \int_{-x_1}^{x_1} S'(\hat{\sigma}, t) dt = (m + \frac{1}{2})\pi \tag{2.44}$$

where $\pm x_1$ are the turning points where $S'^2 = 0$. So for any value of $\tau_{rad}/\tau_{\perp}$, with $n^2 \frac{\tau_{rad}}{\tau_{\perp}} = 1$, there is only one value of the growth rate $\hat{\sigma}$ for each mode number m. If $\hat{\sigma} > 0$ then that mode is unstable.

Figure (2.4) shows these allowable values of $\hat{\sigma}$ plotted against n for the mode number $m = 0$. The graph shows, as we would expect, that decreasing the perpendicular conduction time-scale decreases the growth rate of the instability, and for small values of n, the radiative mode is stable. However, we know that the perpendicular conduction time-scale is very large, so the physically interesting region is where n is large. As n increases in size the growth rate nears a limiting value. So for large n, changes in the value of the

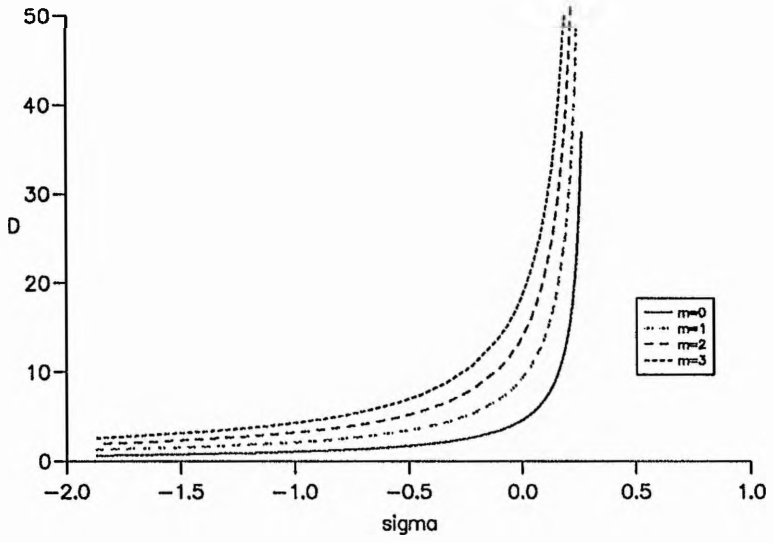

Figure 2.5: The growth rate $\hat{\sigma}$ plotted against n for the mode numbers $m = 0, 1, 2, 3$, with $\lambda = 0.4$, $\gamma = \frac{5}{3}$, $l_1 = 2$, $\frac{\tau_{rad}}{\tau_{\parallel}} = 1$ and $n^2 \frac{\tau_{rad}}{\tau_{\perp}} = 1$.

perpendicular conduction time-scale change the growth rate $\hat{\sigma}$ only a little.

We are also interested in the values of $\hat{\sigma}$ that we obtain for modes other than the fundamental mode. Figure (2.5) shows $\hat{\sigma}$ plotted against n for the mode numbers $m = 0, 1, 2$ and 3, where $\lambda = 0.4$, $\gamma = \frac{5}{3}$, $l_1 = 2$, $\frac{\tau_{rad}}{\tau_{\parallel}} = 1$ and $n^2 \frac{\tau_{rad}}{\tau_{\perp}} = 1$.

Figure (2.5) illustrates that the fundamental mode is always the most unstable mode. However, as n increases towards large values, the growth rates of the other modes approach that of the fundamental mode. We speculate that a perturbation that excited the fundamental mode may also excite other modes, modes which would grow at nearly the same growth rate as the fundamental mode.

A further graph shown is that of $\hat{\sigma}$ against n for the fundamental mode as we increase the shear of the magnetic field by changing λ. Figure (2.6) shows that as we increase the shear of the field (λ increasing towards 1), the radiative mode is stabilized. This

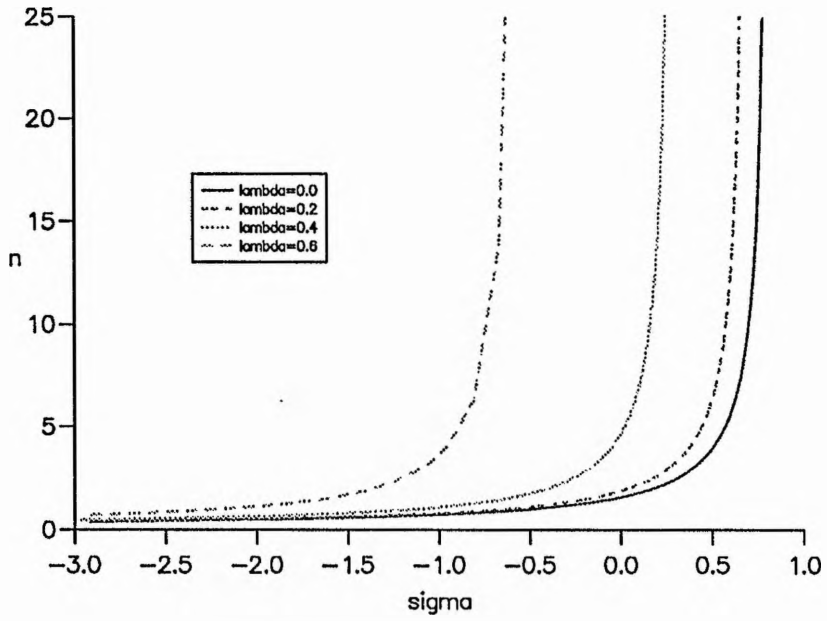

Figure 2.6: The growth rates $\hat{\sigma}$ plotted against n for different values of the shear parameter λ where $\gamma = \frac{5}{3}$, $l_1 = 2$, $\frac{\tau_{rad}}{\tau_{\parallel}} = 1$ and $n^2 \frac{\tau_{rad}}{\tau_{\perp}} = 1$.

agrees with the results of Cargill and Hood (1989). Although greater shear implies longer field lines and so reduces the stabilizing influence of conduction, the equilibrium plasma pressure has been reduced. The radiative losses scale as p_0^2 and this is the more important factor.

Localized modes

For modes that are highly localized around $x = 0$, we can find an approximate analytic solution for S'^2 and for the growth rate $\hat{\sigma}$. For a symmetric equilibrium the problem is equivalent to that of minimizing the integral

$$\int_{-l_2}^{l_2} [\left(\hat{\sigma}\gamma\hat{p}_0 + n^2 \frac{\tau_{rad}}{\tau_{\perp}} \left[S'^2(x) + \left[\left(\frac{\hat{B}_y}{\hat{B}_z} \right)' z \right]^2 + 1 + \frac{\hat{B}_y^2}{\hat{B}_z^2} \right] + \hat{\mathcal{L}}_T \right) \hat{T}_1^2 + \frac{\tau_{rad}}{\tau_{\parallel}} \frac{\hat{B}_z^2}{\hat{B}^2} \left(\frac{\partial \hat{T}_1}{\partial z} \right)^2] dz = 0, \quad (2.45)$$

(we have mutiplied the differential equation by T_1 and integrated by parts). For an equilibrium that is symmetric about $z = 0$ this reduces to:

$$\int_{-l_2}^{l_2} \left[\left(\hat{\sigma}\gamma\hat{p}_0 + n^2 \frac{\tau_{rad}}{\tau_\perp} |\nabla S|^2 + \hat{\mathcal{L}}_T \right) \hat{T}_1^2 + \frac{\tau_{rad}}{\tau_\parallel} \frac{\hat{B}_z^2}{\hat{B}^2} \left(\frac{\partial \hat{T}_1}{\partial z} \right)^2 \right] dz = 0. \qquad (2.46)$$

If we pick a trial form of T_1 then we can find approximate values for $S'^2(x)$ that minimize the integral (2.46). So, let us assume that $\hat{T}_1$ has the form

$$\hat{T}_1(x,z) = \hat{T}_1(x)\cos(\frac{\pi}{2l_1}z),$$

and that $l_2 = 2$, then this integral gives the expression

$$n^2 \frac{\tau_{rad}}{\tau_\perp} S'^2 = 3\hat{p}_0^2 - \gamma\hat{\sigma}\hat{p}_0 - \frac{\pi^2}{4l_1^2} \frac{\tau_{rad}}{\tau_\parallel} \frac{\hat{B}_z^2}{\hat{B}^2} - n^2 \frac{\tau_{rad}}{\tau_\perp} \left[1 + \frac{\hat{B}_y^2}{\hat{B}_z^2} + \left(\frac{\hat{B}_y}{\hat{B}_z} \right)' \left(\frac{4}{3} - \frac{2l_1^2}{\pi^2} \right) \right]. \qquad (2.47)$$

The Bohr-Sommerfeld condition (2.44) can give us the growth rate $\hat{\sigma}$ for these localized modes if we approximate the equilibrium quantities using power series (e.g. $\hat{p}_0 = (1 - \lambda^2)(1 - x^2) + \mathrm{O}(x^4)$). Ignoring all terms of $\mathrm{O}(x^4)$ or higher, the condition $S'^2 = 0$ at $x = 0$ gives us the maximum value of $\hat{\sigma}$, $\hat{\sigma}_{max}$:

$$\hat{\sigma}_{max} = \frac{1}{\gamma} \left[3(1 - \lambda^2) - \frac{\pi^2}{4l_1^2} \frac{\tau_{rad}}{\tau_\parallel} \frac{1}{(1 - \lambda^4)} - n^2 \frac{\tau_{rad}}{\tau_\perp} \frac{(1 + \lambda^2)}{(1 - \lambda^2)} \right], \qquad (2.48)$$

and if we let the growth rate of a mode be $\hat{\sigma} = \hat{\sigma}_{max} - \hat{\sigma}_1$ where $\hat{\sigma}_1 = \mathrm{O}(x^2)$, then

$$\hat{\sigma}_1 = \frac{(2m+1)}{n} \frac{1}{\gamma} \left[3 + \frac{\pi^2}{4l_1^2} \frac{\tau_{rad}}{\tau_\parallel} \left(\frac{1 + 3\lambda^2}{(1 - \lambda^4)^2} \right) + n^2 \frac{\tau_{rad}}{\tau_\perp} \frac{\left(1 - \lambda^2 + \left(\frac{4}{3} - \frac{2l_1^2}{\pi^2} \right) 4\lambda^2 \right)}{(1 - \lambda^2)^2} \right]^{\frac{1}{2}}. \qquad (2.49)$$

Equations (2.48) and (2.49) show that if $n^2\tau_{rad}/\tau_\perp = \mathrm{O}(1)$ then $\hat{\sigma}_1 = \mathrm{O}(1/n)$. So as n becomes large, the growth rate of the system tends towards $\hat{\sigma}_{max}$, regardless of the mode number m.

The expression for $\hat{\sigma}_{max}$ clearly shows how increasing the effect of perpendicular conduction along the field lines, by decreasing the parallel conduction time-scale or decreasing

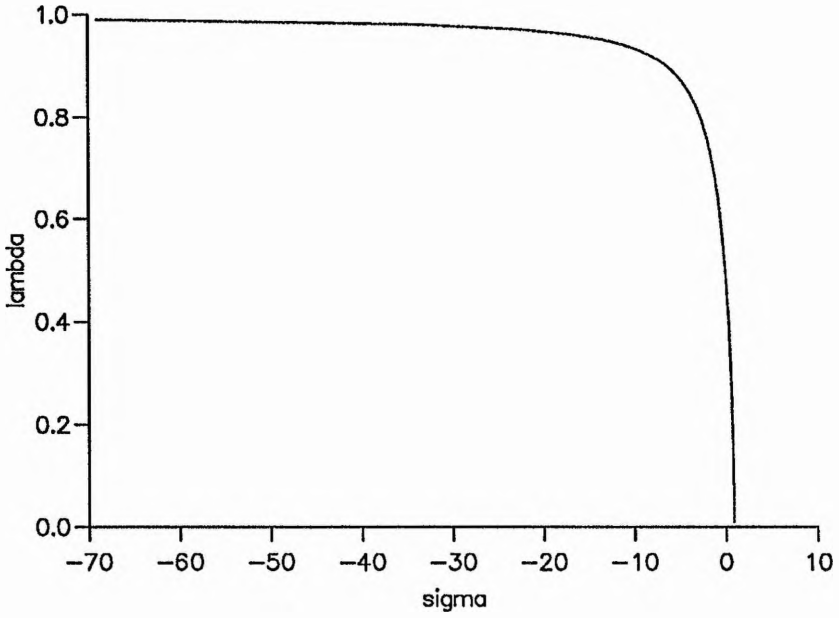

Figure 2.7: The growth rate $\hat{\sigma}$ plotted against λ for the "localized" solution, with $\gamma = \frac{5}{3}$, $l_1 = 2$, $\frac{\tau_{rad}}{\tau_{\parallel}} = 1$ and $n^2 \frac{\tau_{rad}}{\tau_{\perp}} = 1$.

the distance to the line tied boundaries, stabilizes the system. The effect on the growth rate of the thermal modes of varying the shear of the system by increasing λ is less clear from equation (2.48). Figure (2.7) shows how the growth rate $\hat{\sigma}_{max}$ changes as λ is varied. This shows that increasing the shear of the system has a stabilizing influence. We can also compare the values of $\hat{\sigma}_{max}$ against the values of the growth rates found when we numerically solved the energy equation. Figure (2.8) shows that the growth rates are tending towards the maximum values given by Equation (2.48). The expression for $\hat{\sigma}_{max}$ shows that if $n^2\tau_{rad}/\tau_{\perp} = \mathrm{O}(1)$, which was our condition for not ignoring the perpendicular thermal conduction in our analysis, then the perpendicular conduction, with this particular class of disturbances, has a significant effect on the growth rate of the thermal modes.

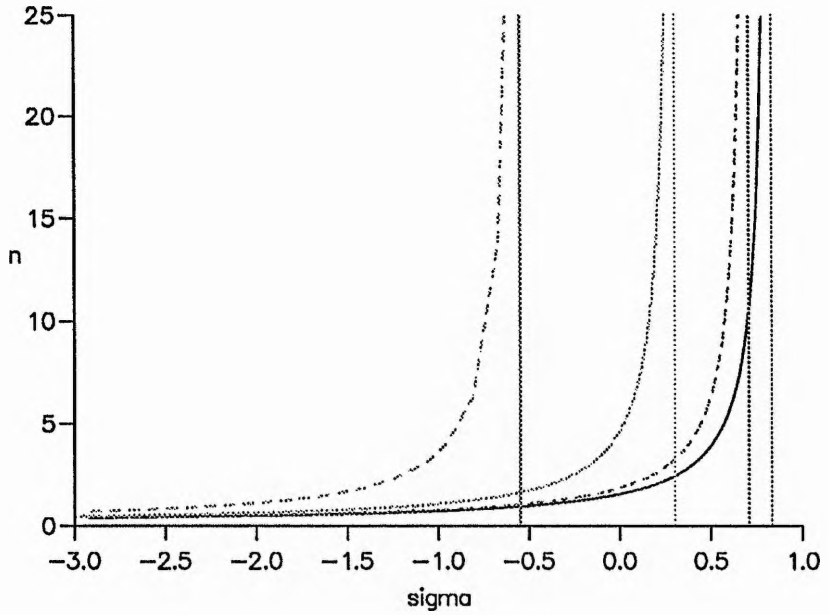

Figure 2.8: The growth rates $\hat{\sigma}$ plotted against n for different values of the shear parameter λ where $\gamma = \frac{5}{3}$, $l_1 = 2$, $\frac{\tau_{rad}}{\tau_\parallel} = 1$ and $n^2 \frac{\tau_{rad}}{\tau_\perp} = 1$. The straight lines show the approximate values of σ_{max} given by the "localized" solution.

2.6 Discussion

In this Chapter we have extended the work of Cargill and Hood (1989), who investigated the effects of the "line-tying" boundary conditions on the thermal instability, to include the influence of perpendicular thermal conduction. We used a particular class of perturbations that give rise to very small length-scales across the magnetic field. Concentrating on the simplest case, a slab geometry, means that the Alfvén mode can be decoupled from the system. We also neglected coupling to the fast and slow modes, and focussed on the isobaric mode, which Cargill and Hood (1989) found to be the most unstable mode for line-tied Cartesian equilibria. This mode exists when the radiative growth time greatly

exceeds the Alfvén transit time.

We have found that introducing perpendicular thermal conduction into the analysis of Cargill and Hood (1989) means that condensations are restricted to a narrow layer around the region where the local isobaric growth rate is largest. The general conclusions of Cargill and Hood (1989), namely that decreasing the length of the field lines and increasing the shear of the system are stabilizing factors, are unaffected.

We have also shown that the fundamental eigenmode is the fastest growing mode, but that other modes have growth rates very near to the value of the growth rate of the fundamental mode, and could grow alongside the fundamental mode.

Chapter 3

The thermal instability in a shearless equilibrium

In this Chapter we investigate thermal instabilities with particular emphasis on the effects of perpendicular thermal conduction, using a time-dependent numerical code and a numerical analysis based on an ordering of the perturbed variables. The numerical code has been developed in collaboration with Dr A. M. Milne. The code advances the set of linearized equations explicitly in time, and we believe that it could be extended to the non-linear MHD equations. The code has been written for a one-dimensional equilibrium, in Cartesian geometry, with two-dimensional perturbations. Advancing an equilibrium in time in the linear regime allows us to see clearly the linear growth of the system unobscured by nonlinear effects. An analytic analysis based on isobaric perturbations in a shearless Cartesian geometry is also considered, and the results from this compared with the output of the code. We show that perpendicular thermal conduction may be an important factor in determining the length-scale for the width of condensations caused

by the thermal mode, while the growth rate of the thermal mode is largely unaffected by perpendicular thermal conduction.

3.1 Basic equations and geometry

The basic equations we use are the linearized, non-dimensionalized MHD equations including the non-adiabatic terms. These are:

$$\frac{\partial \hat{\rho}_1}{\partial \hat{t}} = -\hat{\nabla} \cdot (\hat{\rho}_0 \hat{\mathbf{v}}), \tag{3.1}$$

$$\epsilon^2 \hat{\rho}_0 \frac{\partial \hat{\mathbf{v}}}{\partial \hat{t}} = -\frac{\beta}{2} \hat{\nabla} \hat{p}_1 + \left(\hat{\nabla} \times \hat{\mathbf{B}}_0\right) \times \hat{\mathbf{B}}_1 + \left(\hat{\nabla} \times \hat{\mathbf{B}}_1\right) \times \hat{\mathbf{B}}_0, \tag{3.2}$$

$$\begin{aligned} \frac{\partial \hat{p}_1}{\partial \hat{t}} + \hat{\mathbf{v}} \cdot \hat{\nabla} \hat{p}_0 &= \gamma \frac{\hat{p}_0}{\hat{\rho}_0} \left(\frac{\partial \hat{\rho}_1}{\partial \hat{t}} + \hat{\mathbf{v}} \cdot \hat{\nabla} \hat{\rho}_0 \right) + \frac{\tau_{rad}}{\tau_{\|}} \hat{\mathbf{B}}_0 \cdot \hat{\nabla} \left(\frac{\left(\hat{\mathbf{B}}_0 \cdot \hat{\nabla} \hat{T}_1\right)}{\hat{B}_0^2} \right) \\ &+ \frac{\tau_{rad}}{\tau_{\perp}} \hat{\nabla} \cdot \left(\frac{\hat{\mathbf{B}}_0 \times \left(\hat{\nabla} \hat{T}_1 \times \hat{\mathbf{B}}_0\right)}{\hat{B}_0^2} \right) - \frac{\partial \hat{\mathcal{L}}}{\partial \hat{p}_0} \hat{p}_1 - \frac{\partial \hat{\mathcal{L}}}{\partial \hat{T}_0} \hat{T}_1, \end{aligned} \tag{3.3}$$

$$\frac{\partial \hat{\mathbf{B}}_1}{\partial \hat{t}} = \hat{\nabla} \times \left(\hat{\mathbf{v}} \times \hat{\mathbf{B}}_0\right), \tag{3.4}$$

$$\frac{\hat{p}_1}{\hat{p}_0} = \frac{\hat{\rho}_1}{\hat{\rho}_0} + \frac{\hat{T}_1}{\hat{T}_0}. \tag{3.5}$$

For ease of writing we will drop the hats on our non-dimensionalized variables in the rest of this Chapter, so, except where otherwise stated, all the variables in this Chapter are non-dimensionalized.

The code is written for a planar geometry: axes x and z and all equilibrium quantities are functions of the dependent variable x. All perturbed quantities are functions of x and z with boundaries at $x = \pm l_2$ and $z = \pm l_1$.

3.2 The isobaric mode in a shearless field

We can perform an analytic normal mode analysis for perturbations in the same geometry as the numerical code; that is we have a one dimensional equilibrium, varying in the x direction with line-tying imposed in the z-direction, and perturbations that have x and z components. For a shearless, one dimensional equilibrium in a Cartesian geometry, we do not lose any physics by restricting our perturbations to two dimensions.

To make progress, we order the perturbed variables in a way similar to that in Chapter 2. This eliminates coupling between the radiative mode and the MHD wave modes. We assume that

$$v_{\|}, \rho_1, T_1 \quad = O(1) \tag{3.6}$$

$$\mathbf{v}_{\perp}, \mathbf{B}_1, p_1 \quad = O(\epsilon) \tag{3.7}$$

where

$$\epsilon = \frac{\tau_A}{\tau_{rad}}.$$

This ordering removes the Alfvén mode, the fast mode and the slow mode from the leading order equations. ϵ is a measure of the coupling of the radiative mode to the MHD modes, and when ϵ is small, as it is under typical coronal conditions, this has been shown to be a good approximation (e.g. Hermans, Hood and Clifford, 1990). Taking $p_1 = \mathrm{O}(\epsilon)$ means that we are concentrating on the isobaric mode.

The leading order equations are

$$\sigma\gamma p_0 T_1 = \frac{\tau_{rad}}{\tau_{\|}}\frac{\partial^2}{\partial z^2}T_1 + \frac{\tau_{rad}}{\tau_{\perp}}\frac{\partial^2}{\partial x^2}T_1 + 3p_0^2 T_1, \tag{3.8}$$

$$\sigma T_1 = \mathbf{B}_0 \cdot \nabla v_{\|} \tag{3.9}$$

for the equilibrium magnetic field $\mathbf{B}_0 = (0, 0, B_z(x))$, and an isothermal equilibrium ($T_0 = 1$). We have chosen $\alpha = -1$ which is a typical coronal value (so that $-\mathcal{L}_t = 3p_0^2$). The inclusion of the perpendicular conduction term is valid if the condition

$$\frac{\tau_{rad}}{\tau_\perp}\frac{\partial^2}{\partial x^2} \gg \epsilon$$

holds. The ratio $\tau_{rad}/\tau_\perp$ is small, but large temperature gradients can exist transverse to the magnetic field, so this condition involves no non-physical assumptions. The equation (3.8) can be solved to find the eigenvalues σ and the eigenfunctions T_1. Note that only the equilibrium plasma pressure enters the energy equation and not the equilibrium magnetic field. The latter is only important for structuring the plasma pressure.

3.2.1 Solution of the energy equation

Investigating a shearless equilibrium means that we can Fourier analyse in the z-direction, and the line-tying boundary conditions are equivalent to choosing a particular Fourier mode. So we let

$$T_1(x, z) = T_1(x)\cos\left(\frac{\pi z}{2l_1}\right). \tag{3.10}$$

where the length of the field lines in the z-direction is $2l_1$. Boundary conditions in the x-direction are that $T_1 = 0$ for large $|x|$, which we model by

$$T_1 = 0 \qquad \text{at} \quad x = \pm l_2 \tag{3.11}$$

for some l_2 large enough.

We can now write the energy equation (3.8) as a function of x only:

$$\delta^2\frac{\partial^2}{\partial x^2}T_1 = Q(x)T_1 \tag{3.12}$$

where $\delta^2 = \tau_{rad}/\tau_\perp$ and

$$Q(x) = \sigma\gamma p_0(x) + \frac{\tau_{rad}}{\tau_{||}}\left(\frac{\pi}{2l_1}\right)^2 - 3p_0^2(x). \tag{3.13}$$

The energy equation (3.12) has the form of a WKB problem for the small parameter δ. We therefore try to solve it using WKB techniques.

WKB solution

When $Q(x) > 0$, T_1 will behave evanescently. If $Q(x) > 0$ for all x, then the boundary conditions cannot be satisfied. But if $Q(x) < 0$ for some value of x, then T_1 will have periodic behavior for these values of x, and the boundary conditions can be satisfied. The equilibrium will be unstable if $\sigma > 0$.

For an equilibrium pressure that is symmetrical about $x = 0$ with a maximum value at $x = 0$, we have a two turning-point problem. Only certain values of σ that satisfy the Bohr-Sommerfeld condition are allowed, that is those values of σ where

$$\frac{1}{\delta}\int_{-x_1}^{x_1}\sqrt{-Q(\sigma,t)}dt = (m+\frac{1}{2})\pi \tag{3.14}$$

where $\pm x_1$ are the turning points given by $Q(x_1) = 0$. So instabilities may exist if $Q(x_1) = 0$ for some x_1.

If we choose the equilibrium plasma pressure

$$p_0 = \mathrm{sech}^2(x) \tag{3.15}$$

(the equivalent of the equilibrium field used in Chapter 2 with no shear), so that the equilibrium pressure has a maximum at $x = 0$, we can solve equation (3.14) numerically and plot δ against σ for the different mode numbers m, as for any value of δ, only one

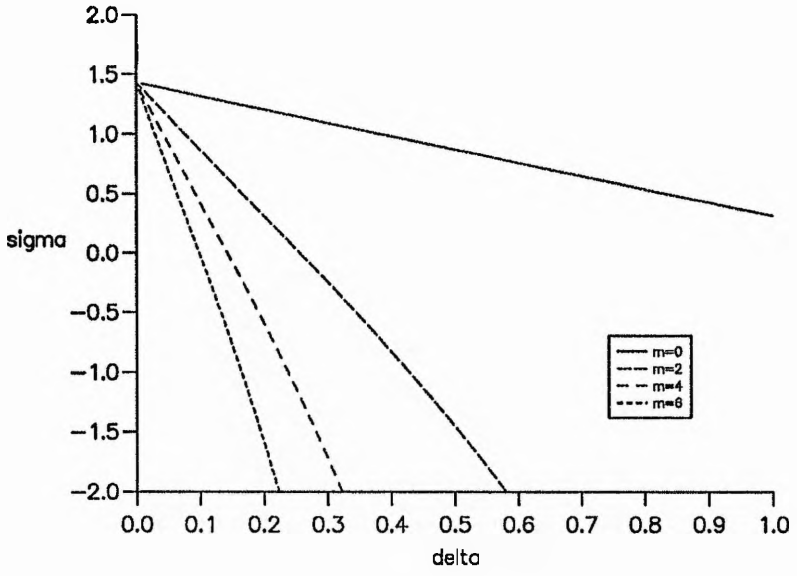

Figure 3.1: How the growth rate σ varies as the value of the perpendicular conduction time scale changes ($\delta^2 = \tau_{rad}/\tau_\perp$), solving the energy equation using WKB methods. Parameter values are $\tau_{rad}/\tau_{||} = 1$, $l_1 = 2$ and $\gamma = \frac{5}{3}$.

value of σ exists for each mode number m. By varying δ, a picture of how σ varies with m can be built up. Figure (3.1) shows σ against δ for the mode numbers $m = 0, 2, 4, 6$ with $\tau_{rad}/\tau_{||} = 1$, $\gamma = \frac{5}{3}$ and $l_1 = 2$. The graph shows that the fundamental mode (m=0) is the most unstable, remaining unstable as δ becomes fairly large. The most physically relevant case is when δ is small. We can see that as δ gets smaller, all the modes become unstable and have a growth rate similar to that of the fundamental mode. The point towards which they are accumulating is the single turning point condition

$$\sigma_{max} = \frac{1}{\gamma}\left(3 - \frac{\tau_{rad}}{\tau_{||}}\left(\frac{\pi}{2l_1}\right)^2\right). \tag{3.16}$$

This is the local isobaric growth rate at $x = 0$, in the limit $\kappa_\perp = 0$, where the local isobaric growth rate has its maximum value. So, the effect of including perpendicular thermal conduction is to restrict the fundamental mode to a narrow region around the

plane where the local isobaric growth rate is highest, but the effect on this growth rate is negligible. The correction to the maximum growth rate caused by the perpendicular thermal conduction can be derived using a simple, analytic analysis. The correction to the maximum growth rate for modes that are highly localized about $x = 0$ is obtained by approximating the equilibrium quantities using power series, so that

$$\mathrm{sech}^2(x) = 1 - x^2 + \mathrm{O}(x^4).$$

and $Q(x)$ becomes

$$Q(x) = -\sigma_1\gamma - \left[3 + \frac{\tau_{rad}}{\tau_{||}}\left(\frac{\pi}{2l_1}\right)^2\right] x^2 + \mathrm{O}(x^4),$$

with $\sigma = \sigma_{max} - \sigma_1$, and $\sigma_1 = \mathrm{O}(x^2)$. The Bohr-Sommerfeld condition (3.14) tells us that

$$\sigma_1 = \frac{\delta(2m+1)}{\gamma}\left[3 + \frac{\tau_{rad}}{\tau_{||}}\left(\frac{\pi}{2l_1}\right)^2\right]^{\frac{1}{2}}.$$

Values of σ for this localized solution are illustrated in Figure (3.2) and compared with the numerical results in Figure (3.3). The two methods give results that have a good agreement, particularly for small values of the δ.

Two conclusions emerge from these results. Firstly, for large values of the perpendicular conduction time-scale, condensation occurs where the local isobaric growth rate is highest, and the growth rate of the fundamental mode is very near to the growth rate predicted by the isobaric instability criterion in the limit $\kappa_\perp = 0$. Secondly, for large values of the perpendicular conduction time-scale, the growth rates of the eigenmodes other than the fundamental mode are very close to that of the fundamental mode, which is always the most unstable mode.

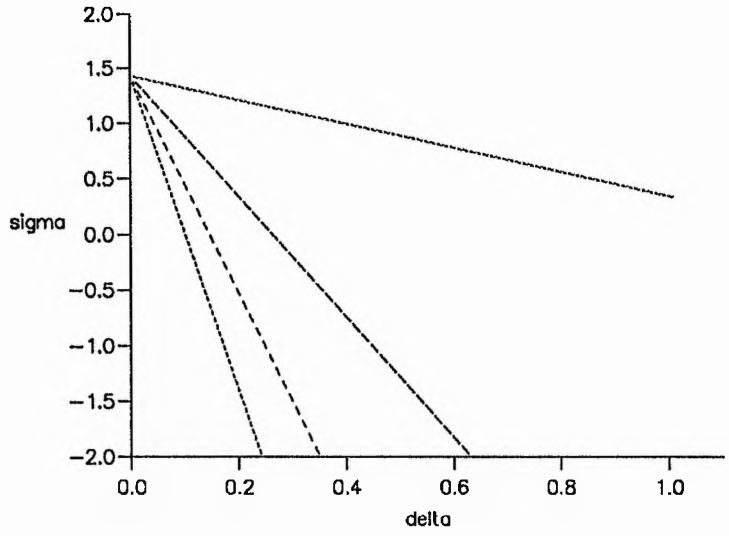

Figure 3.2: How the growth rate σ varies as the value of the perpendicular conduction time scale changes ($\delta^2 = \tau_{rad}/\tau_\perp$), for the localized solution, with $m = 0, 2, 4, 6$. Parameter values are $\tau_{rad}/\tau_{||} = 1$, $l_1 = 2$ and $\gamma = \frac{5}{3}$.

Numerical integration

Equation (3.12) can also be integrated numerically, and the values of the growth rate that satisfy the boundary condition (3.11) found. We use a Runga-Kutta scheme, integrating from $x = 0$ to $x = l_2$ and iterating on σ until the boundary condition (3.11) is satisfied. By varying δ, a picture of the growth rates that satisfy the boundary condition can be built up. The value of l_2 is changed as δ is varied. l_2 must be large enough that it simulates an infinite boundary, but not so large that the integration cannot proceed. So, for example, for $\delta = 0.5$, $l_2 = 10$ and for $\delta = 0.01$, $l_2 = 1$. The boundary conditions at $x = 0$ are $T_1(0) = 1$ and $dT_1/dx = 0$. This choice of boundary conditions means that only the growth rates of even numbered modes are found. The results are shown in Figure (3.4).

The results, shown together with the results obtained using the WKB analysis in

figure (3.5), again lead us to the conclusions made after solving the energy equation by the WKB method. Given that the WKB solution is accurate to $O(\delta)$, we would expect the two methods to give us the same general results, and to show good agreement for small values of δ. But, Figure (3.5) shows that the WKB solution is surprisingly accurate, even for larger values of δ.

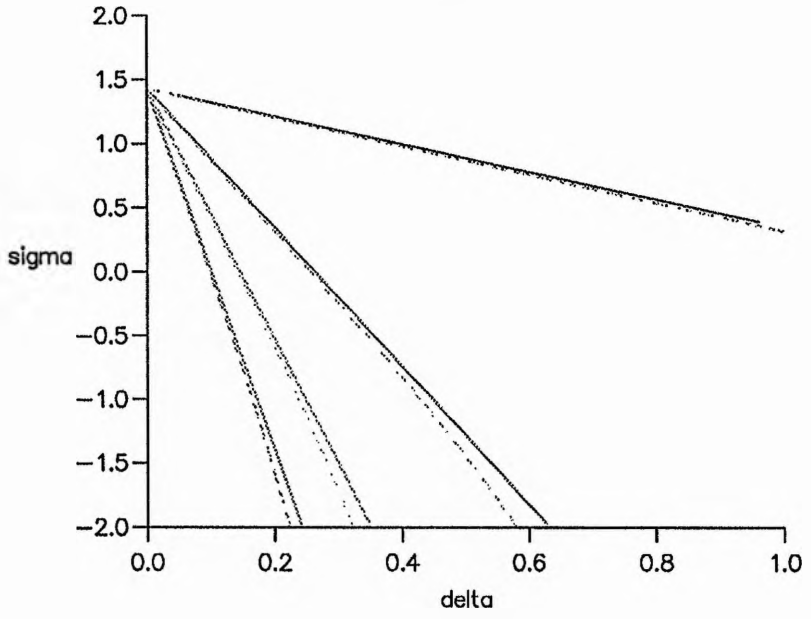

Figure 3.3: How the growth rate σ varies as the value of the perpendicular conduction time scale changes ($\delta^2 = \tau_{rad}/\tau_\perp$), solving the energy equation using WKB methods (dashed curves), and for the localized solution (solid curves). Parameter values are $\tau_{rad}/\tau_\parallel = 1$, $l_1 = 2$ and $\gamma = \frac{5}{3}$.

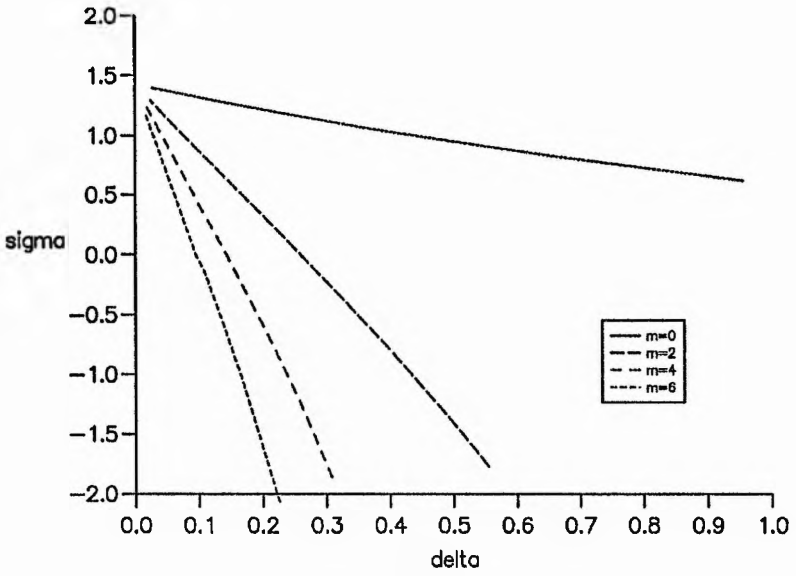

Figure 3.4: How the growth rate σ varies as the value of the perpendicular conduction time scale changes ($\delta^2 = \tau_{rad}/\tau_\perp$), solving the energy equation using numerical integration. Parameter values are $\tau_{rad}/\tau_\parallel = 1$, $l_1 = 2$ and $\gamma = \frac{5}{3}$.

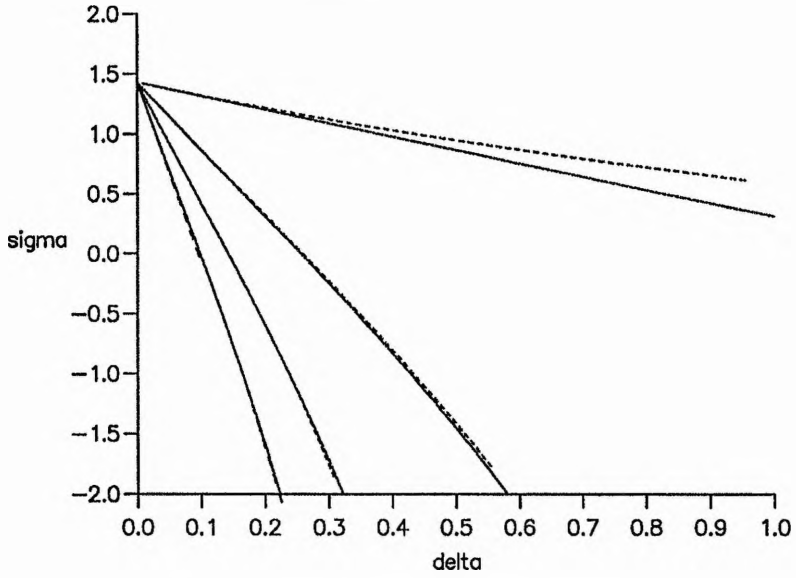

Figure 3.5: The WKB solution (solid curves) and the solution obtained by numerical integration (dashed curves) shown together. Parameter values are $\tau_{rad}/\tau_\parallel = 1$, $l_1 = 2$ and $\gamma = \frac{5}{3}$.

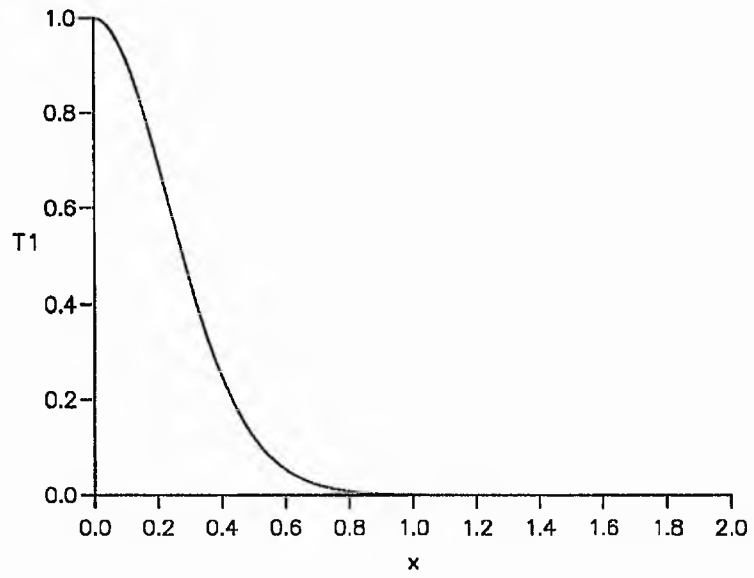

Figure 3.6: The fundamental eigenfunction, for $\delta = 0.1$. Parameter values are $\tau_{rad}/\tau_{\|} = 1$, $l_1 = 2$ and $\gamma = \frac{5}{3}$.

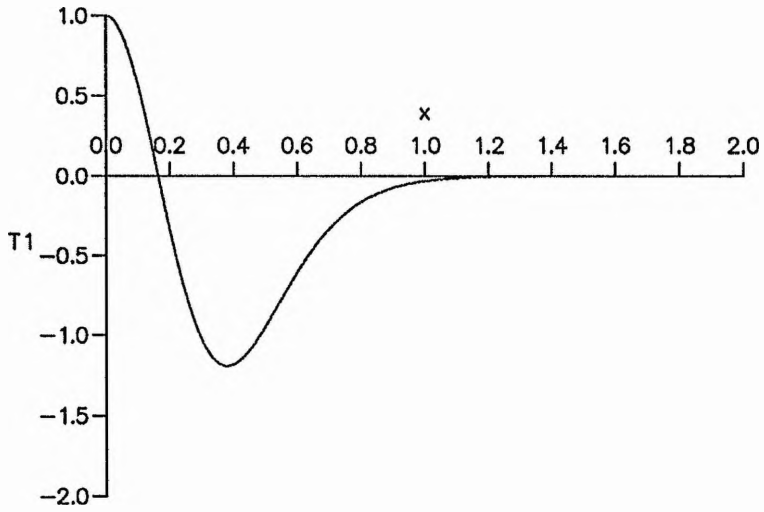

Figure 3.7: The second harmonic eigenfunction, for $\delta = 0.1$. Parameter values are $\tau_{rad}/\tau_{\|} = 1$, $l_1 = 2$ and $\gamma = \frac{5}{3}$.

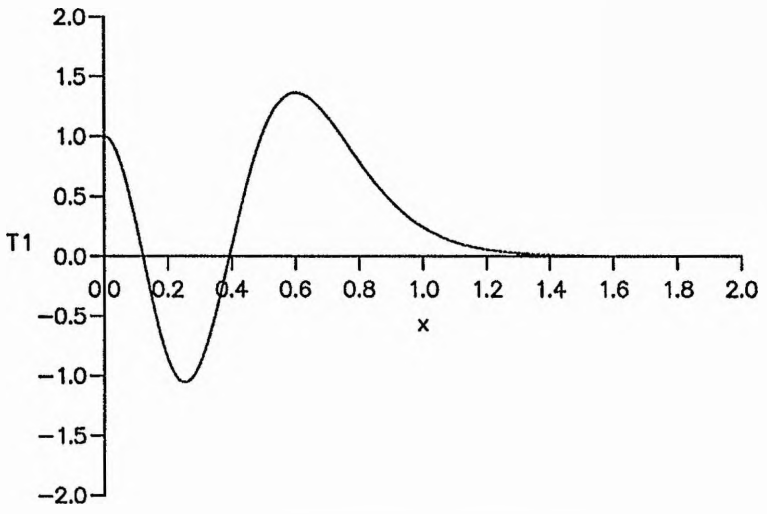

Figure 3.8: The fourth harmonic eigenfunction, for $\delta = 0.1$. Parameter values are $\tau_{rad}/\tau_{\|} = 1$, $l_1 = 2$ and $\gamma = \frac{5}{3}$.

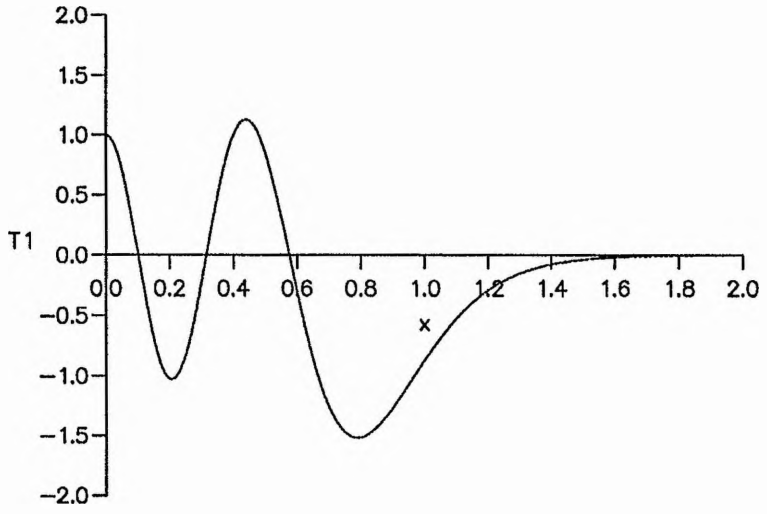

Figure 3.9: The sixth harmonic eigenfunction, for $\delta = 0.1$. Parameter values are $\tau_{rad}/\tau_{\|} = 1$, $l_1 = 2$ and $\gamma = \frac{5}{3}$.

3.2.2 Width of the condensations

The numerical integration of equation (3.12) allows us to examine the structure of the temperature perturbations transverse to the equilibrium magnetic field. Figures (3.6) to (3.9) show the perturbed temperature as a function of x for the mode numbers $m = 0, 2, 4, 6$ for $\delta = 0.1$. The perturbations are localized around $x = 0$. We can see that if modes other than the fundamental mode were to be excited by a perturbation, condensations of many different widths could exist.

These eigenfunctions allow us to investigate how the width of the perturbations change as we vary the value of the perpendicular conduction coefficient. We define the width of the fundamental mode to be the value of x where T_1 has decayed to half its value at $x = 0$. Then we plot the logarithm of these widths against the logarithm of $\delta^{\frac{1}{2}}$. The plot is shown in figure (3.10) and the straight line on the graph has a gradient of unity. The graph shows that, at least for small values of δ, the width of the perturbations is proportional to $\delta^{\frac{1}{2}}$. Now

$$\delta^{\frac{1}{2}} = \left(\frac{\tau_{rad}}{\tau_{\perp}}\right)^{\frac{1}{4}}$$

and we have non-dimensionalized the lengths against the typical plasma length-scale l, so

$$\frac{\text{width}}{\text{l}} \propto \left(\frac{\kappa_{\perp}}{\kappa_{\parallel}}\right)^{\frac{1}{4}}.$$

Further evidence from our analysis for the width of the eigenfunctions having a scalar law proportional to $(\kappa_{\perp}/\kappa_{\parallel})^{0.25}$ is found by considering the eigenmodes of the localized WKB solution. The transverse eigenmode form given by the localized solution is

$$\cos\left(\frac{1}{\delta}\int_0^x \left[3 + \frac{\tau_{rad}}{\tau_{\parallel}}\left(\frac{\pi}{2l_1}\right)^2\right]^{\frac{1}{2}} \left[x_1^2 - u^2\right]^{\frac{1}{2}} du\right),$$

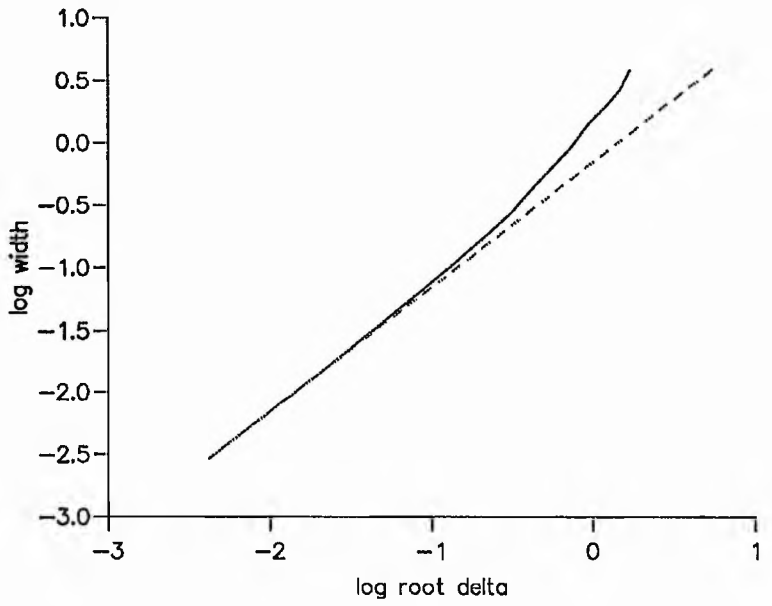

Figure 3.10: A logarithmic plot of the width of the fundamental eigenfunction against the logarithm of sqrt(delta).

where

$$x_1^2 = \frac{\delta(2m+1)}{\left[3 + \frac{\tau_{rad}}{\tau_{\|}}\left(\frac{\pi}{2l_1}\right)^2\right]^{\frac{1}{2}}}.$$

This expression allows us to find the approximate width of the eigenfunction. For $m > 0$ the first zero of the eigenfunction is given by

$$(m+\frac{1}{2})\left[\sin^{-1}\left(\frac{x}{x_1}\right) + \frac{x}{x_1}\left(1 - \frac{x^2}{x_1^2}\right)^{\frac{1}{2}}\right] = \frac{\pi}{2},$$

so that

$$x = \frac{\pi\sqrt{\delta}}{4\sqrt{(2m+1)}\left[3 + \frac{\tau_{rad}}{\tau_{\|}}\left(\frac{\pi}{2l_1}\right)^2\right]^{\frac{1}{4}}}$$

for small x, and we can see that the position of the zero scales as $\delta^{0.5}$.

For larger values of δ, this relation does not seem to hold, but this is not the most interesting physical case as classical values of δ are very small. This proportionality of the

width of the condensations to the quarter power of $\kappa_\perp/\kappa_\parallel$ means that even for classical values of $\kappa_\perp$, where $\kappa_\perp/\kappa_\parallel \approx 10^{-12}$ perpendicular length-scales can be generated which are of the same order as the width of the observed fine structure in prominences. Even finer scale structure which may or may not have been observed, could be caused by modes other then the fundamental mode being excited.

These results agree with those of Van der Linden (1992) who shows that, in general, the width of the condensations would be expected to scale with $\kappa_\perp^{1/3}$, but that near the maximum of the thermal continuum, the scaling is proportional to $\kappa_\perp^{1/4}$. As the most unstable mode is that given by the maximum of the thermal continuum, this is the dominant mode that we pick up. Typical prominence length scales on the surface of the sun are

$$l = 10^4 - 10^5 km,$$

and using the classical value

$$\kappa_\perp = 10^{-12}\kappa_\parallel$$

widths of about $10 - 100km$ are predicted. This predicted length scale is the same order of magnitude as those given by recent observations. Our results from this work and in the previous Chapter also agree with Van der Linden (1991) in finding that condensations set in where the local isobaric growth rate is a maximum.

3.3 The time-dependent numerical code

Thermal instabilities have been studied increasingly frequently over the past few years using numerical simulations. These studies have always been for nonlinear systems. Some

recent papers include: An et al (1988), Poland and Mariska (1988), Mok et al (1990). Many different approaches have been used. Klimchuk, Antiochos and Mariska (1987) used an equilibrium code (with $\partial/\partial t = 0$) to provide input to a dynamic code. Mok, Schnack and Van Hoven (1991) first produced a chromosphere-to-corona equilibrium using the rigid wall boundary conditions, then fixed the temperature of the loop and changed to the flow through conditions and advanced the loop in time. Two dimensional sheared-field filament condensation simulations have been performed by Van Hoven, Sparks and Schnack (1987) and Sparks, Van Hoven and Schnack (1990). Sparks, Van Hoven and Schnack (1990) performed a numerical experiment showing the two dimensional development of the thermal instability in a sheared force-free Cartesian field. They showed how narrow condensed regions could form with characteristic prominence densities and temperatures.

For the numerical experiment presented in this Chapter, the system of linearized equations is approximated using finite differences. Spatial derivatives are given by central differences. The system is advanced explicitly in time using a Lax-Wendroff method. Timesteps have the stepsize Δt. We use a rectangular grid with stepsizes Δx and Δz. Values of the variables are represented at each timestep by the superscript n, and the values in the i^{th} cell in the x-direction and j^{th} cell in the z-direction by subscripts i and j respectively. For the linearized equations we have an Eulerian system so the values of the variables within each cell can be approximated by point values at the centre of each cell.

The perturbed variables are represented by:

$$\begin{aligned} \rho_1 &= \rho^n_{i,j} \qquad p_1 = p^n_{i,j} \qquad T_1 = T^n_{i,j} \qquad v_{1z} = vz^n_{i,j} \\ B_{1x} &= Bx^n_{i,j} \qquad B_{1z} = Bz^n_{i,j} \qquad v_{1x} = vx^n_{i,j} \end{aligned} \tag{3.17}$$

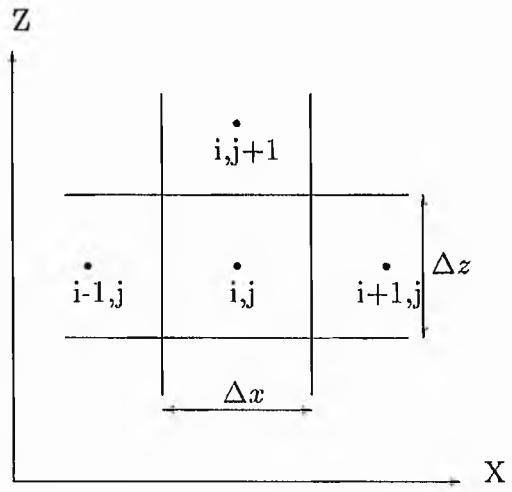

Figure 3.11: A typical cell at time level n. All values of the variables are given by a point value at the centre of each cell.

where $\mathbf{B}_1 = (B_{1x}, 0, B_{1z})$ and $\mathbf{v} = (v_{1x}, 0, v_{1z})$. Equilibrium quantities are represented by values at the centre of each cell, and have the superscript 0 i.e.

$$\rho_0 = \rho^0_{i,j} \qquad B_0 = B^0_{i,j} \qquad p_0 = p^0_{i,j}$$

where $\mathbf{B}_0 = (0, 0, B_0)$ and $T_0 = 1$ as we have an isothermal equilibrium.

3.3.1 Equations in component form

For our numerical discretization it is helpful if we write the system of equations in component form

$$\frac{\partial \rho_1}{\partial t} = -\frac{\partial}{\partial x}(\rho_0 v_{1x}) - \rho_0 \frac{\partial v_{1z}}{\partial z}, \tag{3.18}$$

$$\frac{\partial B_{1x}}{\partial t} = B_0 \frac{\partial v_{1x}}{\partial z}, \tag{3.19}$$

$$\frac{\partial B_{1z}}{\partial t} = -\frac{\partial}{\partial x}(B_0 v_{1x}), \tag{3.20}$$

$$\frac{\partial v_{1x}}{\partial t} = -\frac{1}{\epsilon^2}\frac{1}{\rho_0}\frac{\beta}{2}\left[\frac{\partial \rho_1}{\partial x} + \frac{\partial}{\partial x}(\rho_0 T_1)\right] - \frac{1}{\epsilon^2}\frac{1}{\rho_0}\left[\frac{\partial}{\partial x}(B_0 B_{1z}) - B_0 \frac{\partial B_{1x}}{\partial z}\right], \tag{3.21}$$

$$\frac{\partial v_{1z}}{\partial t} = -\frac{1}{\epsilon^2}\frac{1}{\rho_0}\frac{\beta}{2}\left[\frac{\partial \rho_1}{\partial z} + \rho_0\frac{\partial T_1}{\partial z}\right] + \frac{1}{\epsilon^2}\frac{1}{\rho_0}B_{1x}\frac{\partial B_0}{\partial x}, \tag{3.22}$$

$$\frac{\partial T_1}{\partial t} = (1-\gamma)\left[\frac{\partial v_{1x}}{\partial x} + \frac{\partial v_{1z}}{\partial z}\right] + \frac{1}{\rho_0}\frac{\tau_{rad}}{\tau_{\|}}\frac{\partial^2 T_1}{\partial z^2} + \frac{1}{\rho_0}\frac{\tau_{rad}}{\tau_{\perp}}\frac{\partial^2 T_1}{\partial x^2} - 2\rho_1 - \alpha\rho_0 T_1. \tag{3.23}$$

These equations are the starting point for a discretization. For the linearized case, we can reduce our equations to a set of one dimensional operators, as explained in Appendix A, involving advection equations and sources. To solve these advection equations we choose the Lax-Wendroff method described below.

3.3.2 Lax-Wendroff explicit method

The Lax-Wendroff method is an explicit method of second order accuracy. It may be used for both initial-value and initial-value boundary-value problems. Consider the linear hyperbolic problem for one space variable

$$\frac{\partial U}{\partial t} + a\frac{\partial U}{\partial x} = 0 \tag{3.24}$$

where a is a positive constant. By Taylor's expansion, we have

$$U_i^{n+1} = U(x_i, t_n + k) = U_i^n + k\left(\frac{\partial U}{\partial t}\right)_i^n + \frac{1}{2}k^2\left(\frac{\partial^2 U}{\partial t^2}\right)_i^n + ...$$

where $x_i = ih$ and $t_n = nk, i = 0, \pm 1, \pm 2, ..., n = 0, 1, 2, ...$

The differential equation (3.24) can be used to eliminate the t-derivatives, so that

$$U_i^{n+1} = U(x_i, t_n + k) = U_i^n - ka\left(\frac{\partial U}{\partial x}\right)_i^n + \frac{1}{2}k^2a^2\left(\frac{\partial^2 U}{\partial x^2}\right)_i^n + ...$$

and then we can replace the x-derivatives by central difference approximations, to get the explicit difference equation

$$u_i^{n+1} = u_i^n - \frac{ka}{2h}(u_{i+1}^n - u_{i-1}^n) + \frac{k^2a^2}{2h^2}(u_{i+1}^n - 2u_i^n + u_{i-1}^n)$$

where u_i^n is the difference analogue of U_i^n.

This scheme is stable if the Courant-Friedrichs-Lewy (C.F.L.) condition is satisfied, that is if

$$0 < ap \leq 1$$

where $p = k/h$. The local truncation error is

$$\frac{1}{6}k^2\frac{\partial^3 U}{\partial t^3} + \frac{1}{6}ah^2\frac{\partial^3 U}{\partial x^3}.$$

The Lax-Wendroff approximation is easily extended to a set of simultaneous equations which we may represent as

$$\frac{\partial \mathbf{U}}{\partial t} + \mathbf{A}\frac{\partial \mathbf{U}}{\partial x} = 0$$

where $\mathbf{U} = [U_1, U_2, ..., U_N]^T$, $\frac{\partial \mathbf{U}}{\partial t} = \left[\frac{\partial U_1}{\partial t}, \frac{\partial U_2}{\partial t}, ..., \frac{\partial U_N}{\partial t}\right]^T$, and $\mathbf{A}$ is an $N \times N$ matrix with real constant elements. Hence

$$\mathbf{u}_i^{n+1} = \mathbf{u}_i^n - \frac{1}{2}p\mathbf{A}(\mathbf{u}_{i+1}^n - \mathbf{u}_{i-1}^n) + \frac{1}{2}p^2\mathbf{A}^2(\mathbf{u}_{i+1}^n - 2\mathbf{u}_i^n + \mathbf{u}_{i-1}^n). \tag{3.25}$$

The Lax-Wendroff method can readily be extended for use with linear hyperbolic problems in two space variables. Firstly, rewrite equation (3.25) in terms of the Lax-Wendroff operator L_n^x:

$$\mathbf{u}_i^{n+1} = L_n^x(\mathbf{u}_i^n).$$

For a set of simultaneous equations in two space variables represented by

$$\frac{\partial \mathbf{U}}{\partial t} + \mathbf{A}\frac{\partial \mathbf{U}}{\partial x} + \mathbf{B}\frac{\partial \mathbf{U}}{\partial y} = 0$$

an explicit method of second order accuracy is given by

$$\mathbf{u}_{i,j}^{n+2} = L_n^x L_n^y L_n^y L_n^x(\mathbf{u}_{i,j}^n)$$

where

$$L_n^y(\mathbf{u}_j^n) = \mathbf{u}_j^n - \frac{1}{2}p\mathbf{B}(\mathbf{u}_{j+1}^n - \mathbf{u}_{j-1}^n) + \frac{1}{2}p^2\mathbf{B}^2(\mathbf{u}_{j+1}^n - 2\mathbf{u}_j^n + \mathbf{u}_{j-1}^n),$$

because it can easily be shown that

$$\begin{aligned} L_n^x L_n^y L_n^y L_n^x(\mathbf{u}_{i,j}^n) &= \mathbf{u}_{i,j}^n - 2k\left(\mathbf{A}\left(\frac{\partial \mathbf{u}}{\partial x}\right)_{i,j}^n + \mathbf{B}\left(\frac{\partial \mathbf{u}}{\partial y}\right)_{i,j}^n\right) \\ &+ 2k^2\left(\mathbf{A}^2\left(\frac{\partial^2 \mathbf{u}}{\partial x^2}\right)_{i,j}^n + (\mathbf{AB}+\mathbf{BA})\frac{\partial^2 \mathbf{u}}{\partial x \partial y} + \mathbf{B}^2\left(\frac{\partial^2 \mathbf{u}}{\partial y^2}\right)_{i,j}^n\right), \end{aligned}$$

which is the Taylor series expansion to $O(k^3)$ accuracy.

3.3.3 Numerical diffusion

Using the central-difference approximation for spatial differentiation leads to extra oscillatory terms that are due entirely to the central difference approximation. To illustate this, consider $\partial U/\partial x$ approximated at (ih, nk) by

$$[U(x+h,t) - U(x-h,t)]/2h$$

then the system of differential equations approximating

$$\frac{\partial U}{\partial t} + a\frac{\partial U}{\partial x} = 0, \quad a > 0, \quad 0 < x < X, \quad t > 0.$$

$U(x,0) = g(x)$, $U(0,t) = b(t)$, at the mesh points ih, $i = 1,..,N$ along time level t is

$$\frac{d\mathbf{V}(t)}{dt} = -\frac{1}{2}a\mathbf{B}\mathbf{V}(t) + \frac{1}{2}a\mathbf{b}(t)$$

where $\mathbf{V}(t) = [V_1(t), V_2(t), ..., V_{N+1}(t)]^T$,

$$\mathbf{B} = \frac{1}{h}\begin{bmatrix} 0 & 1 & & & & & \\ -1 & 0 & 1 & & & & \\ & -1 & 0 & 1 & & & \\ & & & \ddots & & & \\ & & & & -1 & 0 & 1 \\ & & & & & -1 & 0 \end{bmatrix} \text{ of order } N \times N,$$

and $h\mathbf{b}(t) = [b(t), 0, 0, ..., -V_{N+1}(t)]^T$. V_{N+1} is the solution at $(N+1)h, t$ and would be known only for periodic boundary conditions. That part of the solution corresponding to the term

$$-\frac{1}{2}a\mathbf{B}\mathbf{V}(t) \qquad \text{is} \qquad \exp(-\frac{1}{2}at\mathbf{B})\mathbf{g}.$$

The eigenvalues λ_s, of $\mathbf{B}$ are $\lambda_s = 2i\cos(s\pi/N+1)$, $s = 1, .., N$, and are all different. Hence the N eigenvectors $\mathbf{v}_s$ of $\mathbf{B}$ are all linearly independent. This means that the initial vector $\mathbf{g} = [g_1, g_2, ..., g_N]^T$ can be written as

$$\mathbf{g} = \sum c_s \exp(-\frac{1}{2}at\lambda_s)\ \mathbf{v}_s,$$

but λ_s is complex and $\exp(i\theta) = \cos\theta + i\sin\theta$, showing that the solution $\mathbf{V}(t)$ contains oscillatory terms. In an attempt to circumvent this problem we add some second order spatial derivative terms into our source terms, which we call "numerical diffusion". We add a second order spatial derivative multiplied by the small parameter ξ to each equation that does not already have any diffusion terms. The value of ξ must be large enough to damp out the oscillatory growth rate but not so large that it affects the growth rate of the thermal mode. The value of ξ to take is mostly a matter of trial and error, but we can use the exact solutions in a uniform field to estimate it.

3.3.4 Numerical Boundary conditions

We model the boundary conditions by using imaginary points. For example, suppose that we have N cells in the x-direction. As we have an Eulerian system, the values of the perturbed variables in this cell can be taken as point values at the centre of the cell. Now let there be an imaginary point x_{N+1}.

If the value of the parameter ρ, say, has to be zero at the boundary, which is midway between the centres of the two cells, then we let $\rho_{N+1} = -\rho_N$. If the derivative of ρ is required to be zero on the boundary, then we let $\rho_{N+1} = \rho_N$.

The initial conditions are that all the Fourier modes are present, and the code is allowed to run long enough for the fastest growing mode to dominate.

3.3.5 Discretized equations

The full system of discretized equations is given in Appendix A.

3.3.6 Results for a uniform field

Figures (3.12) and (3.13) show typical output diagrams from our program for a uniform equilibrium. The growth rate of the system is calculated from the change in the total kinetic energy, which grows proportional to $\exp(2\sigma t)$. Figures (3.12) and (3.12) show results for a uniform equilibrium with the boundary condition $T_1 = 0$ at $z = \pm l_1$ and $x = \pm l_2$. The exact growth rate for this system can be calculated from the dispersion equation (2.12). Table (3.1) shows values of the growth rate given by the code and the exact growth rate calculated from equation (2.12) as we vary ϵ, keeping all the other parameters the same.

ϵ	Growth rate from code	Exact growth rate
0.08	1.03689	1.04260
0.06	1.04540	1.04990
0.04	1.05232	1.05532
0.02	1.05744	1.05865
0.01	1.05881	1.05950
0.008	1.05952	1.05960
0.006	1.06032	1.05968
0.004	1.05722	1.05973
0.002	1.05599	1.05977

Table 3.1: Growth rates for a uniform field, with $\frac{\tau_{rad}}{\tau_{\parallel}} = 1$, $\frac{\tau_{rad}}{\tau_{\perp}} = 1$, $\epsilon = 0.04$, $\beta = 1$, $\alpha = -1$, $l_1 = 2$ and $l_2 = 2$.

We can see that the code picks up the fundamental Fourier mode, which is the fastest growing. The growth rates obtained from the code are very accurate for small values of ϵ, becoming less so as ϵ increases, but still accurate to the second decimal place. This gives us confidence in the numerical code. Running the code for a uniform field where the growth rates of the system are known beforehand, allows us to estimate the value of the numerical diffusion coefficient ξ, and the best choice was found to be $\xi \approx 0.3\frac{2\Delta x^2}{\Delta t}$. Figure (3.14) shows output for the same parameter values as figure (3.12) but with $\xi = 0$. This clearly demonstrates the oscillatory nature of the spurious growth rates introduced by using central differences.

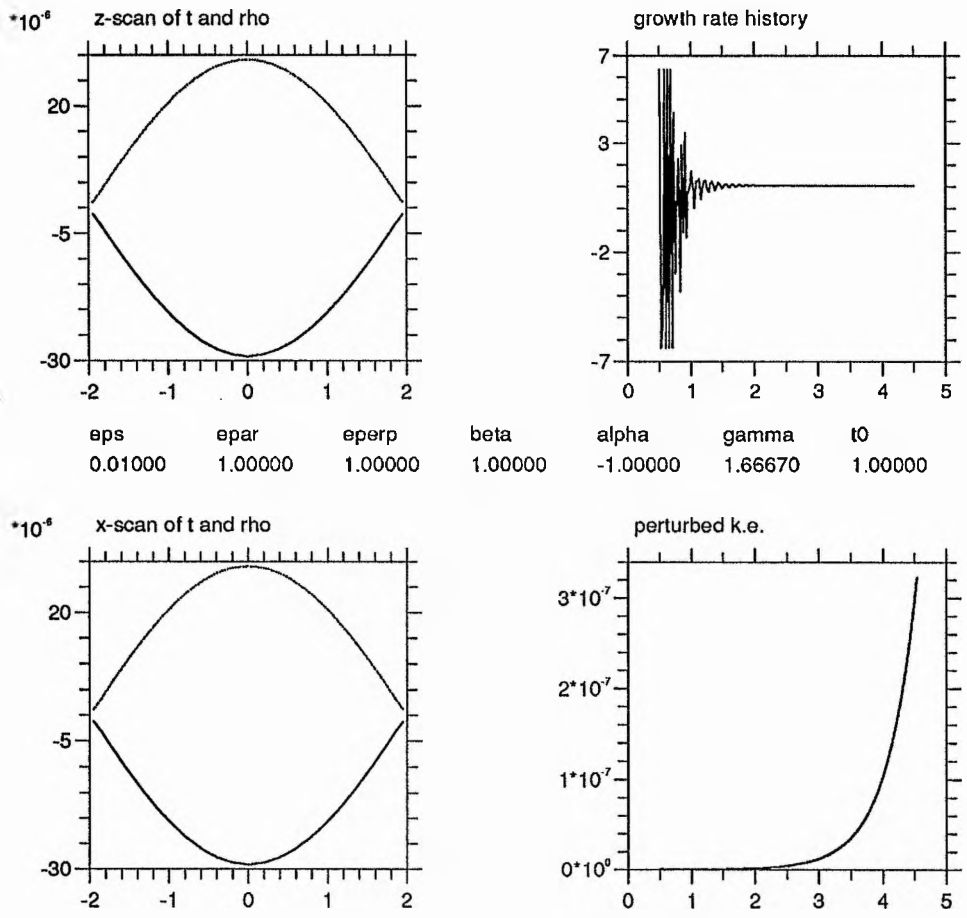

Figure 3.12: Results from the numerical code for a uniform equilibrium and the parameter values $\tau_{rad}/\tau_{\|} = 1$, $\tau_{rad}/\tau_{\perp} = 1$, $\epsilon = 0.01$, $\beta = 1$, $\alpha = -1$, $l_1 = 2$ and $l_2 = 2$. The left hand graphs show the pertured temperature (dotted line) and the perturbed density in the planes $x = 0$ and at $z = 0$. The right hand graphs show how the growth rate σ and the perturbed kinetic energy evolve in time.

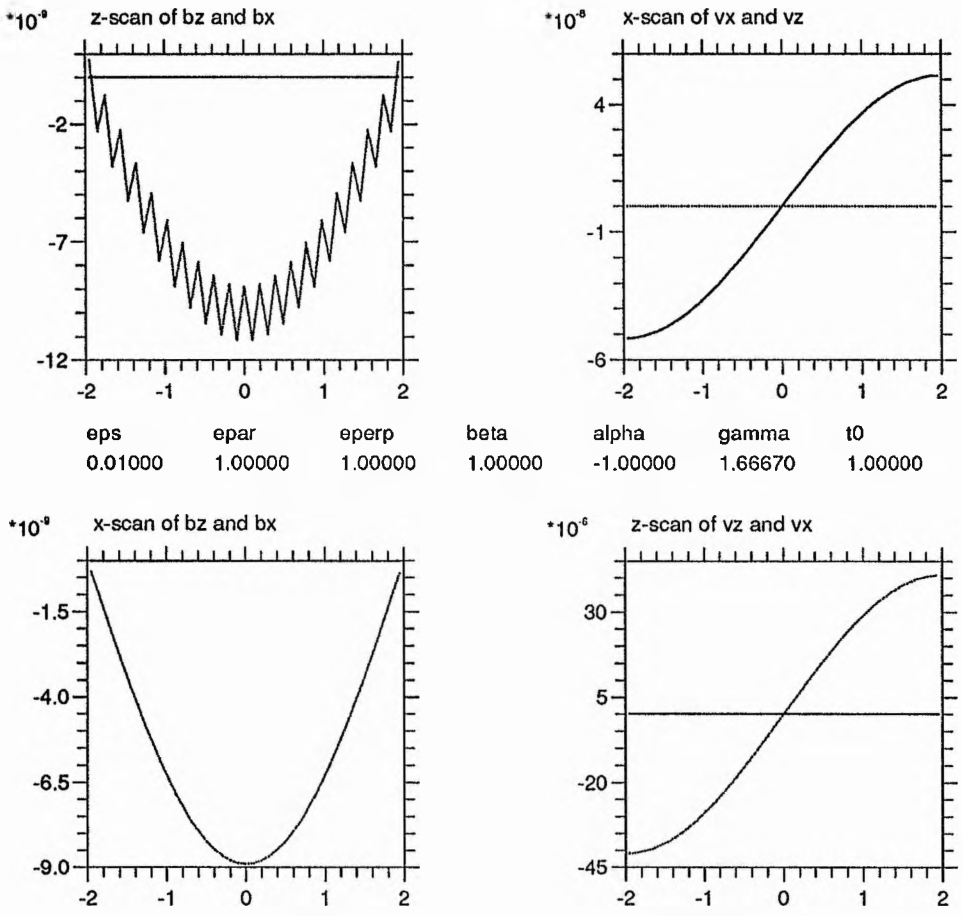

Figure 3.13: Results from the numerical code for a uniform equilibrium and the parameter values $\tau_{rad}/\tau_{||} = 1$, $\tau_{rad}/\tau_{\perp} = 1$, $\epsilon = 0.01$, $\beta = 1$, $\alpha = -1$, $l_1 = 2$ and $l_2 = 2$. The left hand graphs show the pertured magnetic field (B_z dotted line) in the planes $x = 0$ and at $z = 0$. The right hand graphs show v_x (dotted line) and v_z.

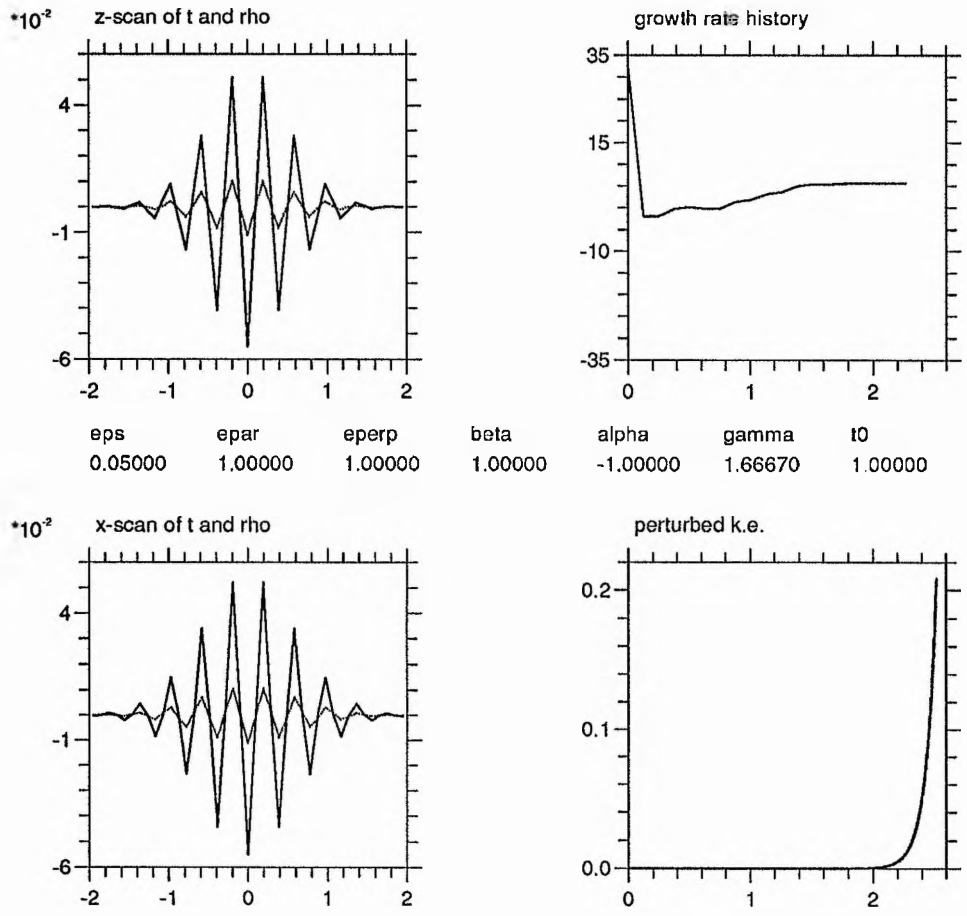

Figure 3.14: Running the numerical code for a uniform equilibrium without numerical diffusion

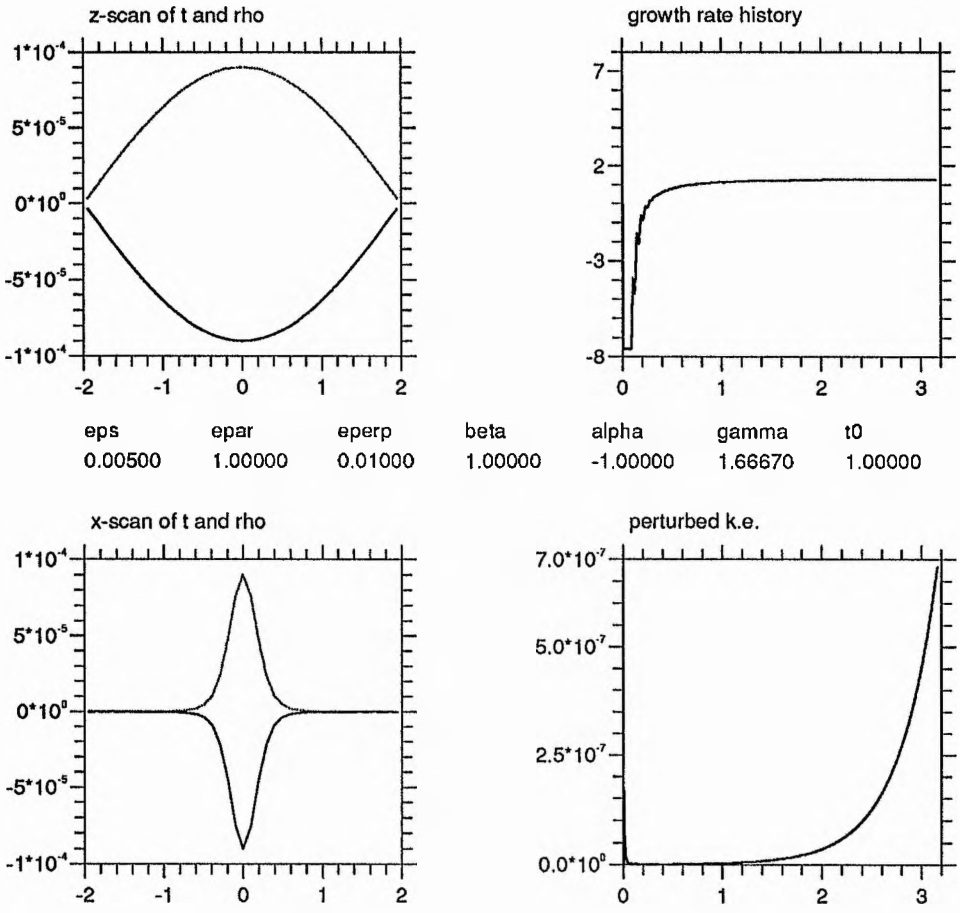

Figure 3.15: $\tau_{rad}/\tau_{\|} = 1$, $\tau_{rad}/\tau_{\perp} = 0.01$, $\epsilon = 0.005$, $\beta = 1$, $\alpha = -1$, $l_1 = 2$ and $l_2 = 2$. The left hand graphs show the perturbed temperature (dotted line) and the perturbed density in the planes $x = 0$ and at $z = 0$. The right hand graphs show how the growth rate σ and the perturbed kinetic energy evolve in time.

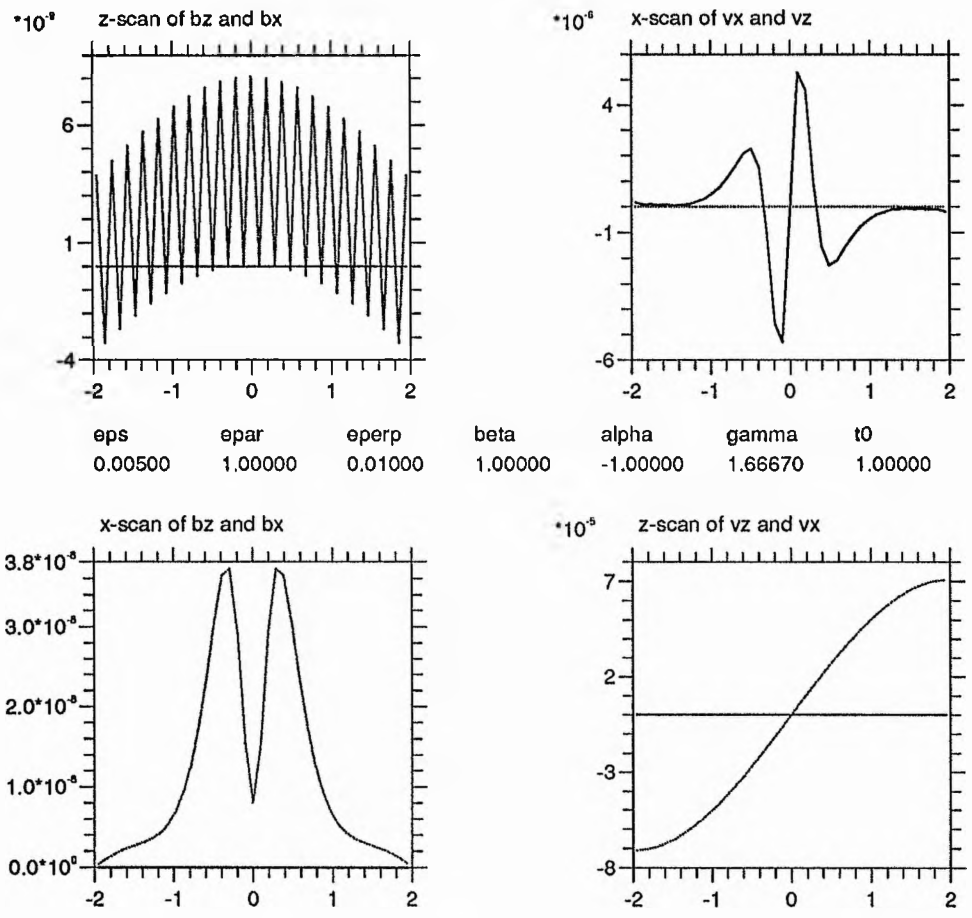

Figure 3.16: $\tau_{rad}/\tau_{||} = 1$, $\tau_{rad}/\tau_{\perp} = 0.01$, $\epsilon = 0.005$, $\beta = 1$, $\alpha = -1$, $l_1 = 2$ and $l_2 = 2$. The left hand graphs shows the pertured magnetic field (B_z dotted line) in the planes $x = 0$ and at $z = 0$. The right hand graphs show v_x (dotted line) and v_z.

3.3.7 Results for a non-uniform field

We have used the numerical code to investigate a non-uniform equilibrium, with the equilibrium plasma pressure having the same form as in the previous analytic work in this Chapter, that is,

$$p_0 = \mathrm{sech}^2(x)$$

and we choose an equilibrium magnetic field of the form $B_0 = (0, 0, B_z)$ where

$$B_z = \left|\sqrt{1 - \mathrm{sech}^2(x)}\right|.$$

The equilibrium plasma pressure has a maximum at $x = 0$ and is symmetrical about this axis. This is where we expect an instability to set in as it is where the isobaric growth rate is largest.

Figures (3.15) and (3.16) show typical output diagrams from the program. The boundary conditions are that all perturbed quantities are zero at $x = \pm l_2$ and that

$$T_1 = 0 \ \text{ at } \ z = \pm l_1.$$

Figure (3.15) illustrates that the fundamental Fourier mode is the fastest growing and that the instabilities are localised around $x = 0$. For these values of the parameters, the numerical code settles down to give a final growth rate $\sigma = 1.32$. From the numerical solution of equation (3.8), we predict the growth rate to be $\sigma = 1.31$. Thus, there is a good agreement.

Looking at figures (3.15) and (3.16), we can see that the magnitude of the perturbed variables bears out the ordering of the variables made in our analytic work. The figures give:

$$\rho_1, T_1, v_{\parallel} = \mathrm{O}(10^{-5})$$

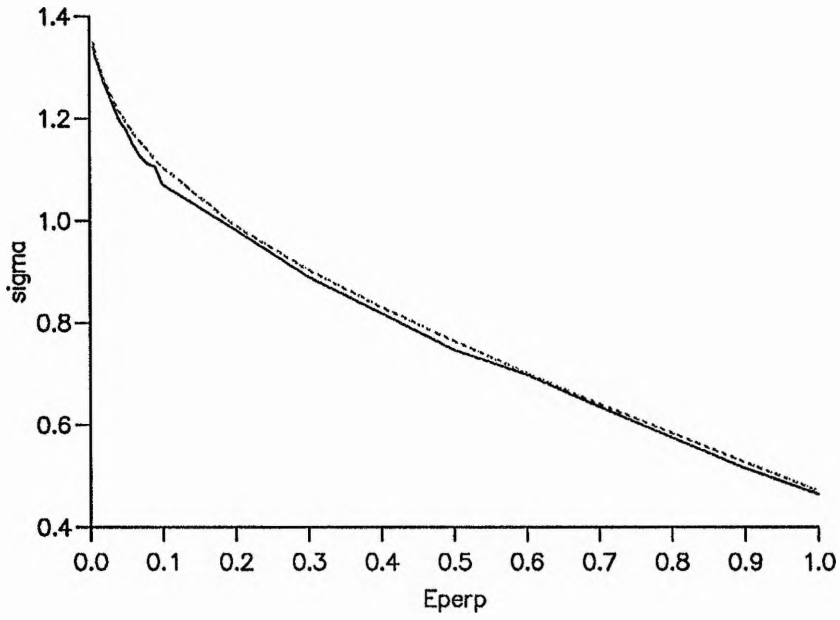

Figure 3.17: The growth rate (sigma) against $\tau_{rad}/\tau_{\perp}$ (Eperp) from the numerical integration of the energy equation (dashed curve) and from the numerical code (solid curve), with $\tau_{rad}/\tau_{||} = 1$, $\epsilon = 0.005$, $\beta = 1$, $\alpha = -1$, $l_1 = 2$ and $l_2 = 2$.

$$B_{1x}, B_{1z} = \mathrm{O}(10^{-9})$$

and

$$v_{||} \gg v_{\perp}.$$

So for this parameter regime, we have further evidence that the ordering of the perturbed variables in the analytic analysis is valid.

Figure (3.17) shows how the growth rates given by the numerical code compare with the growth rates given by the numerical solution of equation (3.8) as the value of the perpendicular conduction time-scale varies, with $\epsilon \ll 1$. We can see that for this parameter regime, where $\epsilon \ll \tau_{rad}/\tau_{||}$, the two approaches give very close results. We conclude that the growth rates of the fastest growing modes found by the numerical code are very accurate. We can also conclude that the ordering of the perturbed variables that we performed in our analytic analysis and the conclusions that we drew from this analysis

are valid for this parameter regime.

3.4 Discussion

In this Chapter we have investigated the thermal instability in a one dimensional, shearless, isothermal, equilibrium in a Cartesian geometry. Particular attention has been paid to the inclusion of thermal conduction perpendicular to the magnetic field, an important effect which has often been ignored in previous work. Our investigations have involved two approaches: an analytical approach based on an ordering of the perturbed variables and a time dependent numerical code.

In the analytic investigation, we ordered the perturbed variables in such a way as to decouple the radiative mode from magnetic effects. This clearly illustrated the effects of the perpendicular conduction. Using the numerical code, we investigated the thermal instability in the linearized equations and, for the same parameter regime as the analytic work, we found good agreement. The growth rates of the perturbations were very similar and the ordering of the perturbed variables was confirmed to be valid. The growth rates of the condensations found by running the time-dependent code were of a very high accuracy. We used both methods to investigate the growth rate of the thermal instability and the width of the condensations transverse to the magnetic field if perpendicular conduction is included in the analysis, in the parameter regime $\epsilon \ll \tau_{rad}/\tau_{\|}$. The effects of line-tying are incorporated by concentrating on a particular Fourier mode, the numerical code showing that the fundamental mode is always the fastest growing. Our main conclusions are as follows:

- The thermal instability gives rise to condensations that are highly localized about

the plane where the isobaric instability criterion is largest.

- The most unstable thermal mode grows almost isobarically and is decoupled from the magneto-acoustic modes.

- The growth rate of the system is largely unaffected by including the perpendicular conduction, the growth rate being close to the local isobaric growth rate with $\kappa_\perp = 0$.

- The width of the most unstable condensation is proportional to $(\kappa_\perp/\kappa_\parallel)^{\frac{1}{4}}$ when the perpendicular conduction coefficient is small. This relationship does not hold for larger values of $\kappa_\perp$, but these larger values are well above the classical value of $\kappa_\perp$. This means that perpendicular thermal conduction gives rise to length-scales across the magnetic field lines that are of the same order as the observed fine-scale structure in prominences. This implies that fine-structure could be a result of the formation process and does not occur after the prominence has been formed.

- The fundamental mode is the most unstable but other modes have growth rates very close to that of the fundamental mode, for small values of the perpendicular conduction coefficient $\kappa_\perp$.

The time-dependent numerical code that advances the system of linear equations explicitly in time using a Lax-Wendroff method has been shown to give extremely accurate predictions for the growth rate of the system. We may be interested in extending the code to investigate sheared equilibria or non-linear systems.

Chapter 4

Ideal instabilities caused by a resistive wall

In this Chapter the effect of a finitely conducting wall on the linear stability of an analytical Spheromak equilibrium and of an analytical Reversed Field Pinch (RFP) equilibrium is investigated. It has been shown by Pfirsch and Tasso (1971) that if a plasma is stable to a particular mode when surrounded by a perfect wall but unstable to it when the wall is removed, then surrounding the plasma with a wall of finite conductivity cannot stabilize the mode. For the purposes of determining marginal stability there is no difference between the absence of a wall and the presence of a finitely conducting wall. But physical considerations mean that any mode which exists because of the presence of a finitely conducting wall (that is, it is not present if the wall is perfect) should grow proportionally to the resistivity of the wall. The "long" time constant of the wall $\tau_w = a\delta/\eta_w$ is the relevant time scale (where the wall is situated at $r = a$, η_w is the resistivity of the wall, and the wall is of thickness δ). For low resistivity the growth rates of these modes will be small

and the modes will only be important if their growth time is shorter than the lifetime of the plasma configuration, which would be the case for reactor like conditions and thus motivates this work. For slowly growing instabilities the skin-depth is much larger than the thickness of the wall and it is appropriate to assume that the wall is a "thin-shell".

In Section (4.1) we introduce the concept of relaxation. This is used to derive the equilibria the stability of which is investigated. In Section (4.2) we introduce an analytic equilibrium in an infinite cylinder and in Section (4.3) we go on to describe the force-free configuration known as a Spheromak. In Section (4.4) we discuss the boundary conditions at a wall of finite conductivity in the limit of the thin-shell approximation. In Section (4.5) we investigate the effects of surrounding an RFP equilibrium with a thin wall of finite conductivity; derive the growth rates of the modes; and investigate the growth rates of these thin-shell modes for a Spheromak equilibrium.

4.1 Relaxation theory

Taylor's theory (Taylor, 1976) hypothesised that the relaxed state (minimum energy state) of a highly conducting plasma is determined by global helicity conservation. The helicity is defined as the integral

$$K = \int \mathbf{A} \cdot \mathbf{B} dV, \tag{4.1}$$

where $\mathbf{A}$ is the vector potential ($\nabla \times \mathbf{A} = \mathbf{B}$). The helicity K is a measure of the degree in which field lines interlink or twist around each other. In ideal MHD, K is conserved for every flux tube. In a highly conducting plasma (η small but non-zero) Taylor suggested

that the global helicity K_0 of the whole volume is approximately conserved, where

$$K_0 = \int_V \mathbf{A} \cdot \mathbf{B} dV, \tag{4.2}$$

and the integration is performed over the volume of the plasma. During relaxation the plasma energy decays, while the global helicity remains essentially constant. Energy decays much faster than helicity because of the turbulent fluctuations. For small-scale fluctuations energy dissipation is finite at scale lengths proportional to $\eta^{-0.5}$ while helicity dissipation is proportional to $\eta^{0.5}$ at this scale (Taylor, 1986).

The relaxed state of a slightly resistive turbulent plasma is found by minimizing the magnetic energy, given by

$$W = \frac{1}{2} \int (\nabla \times \mathbf{A})^2 dV \tag{4.3}$$

subject to the constraint $K_0 =$ a constant. For a plasma enclosed by a perfectly conducting shell, the corresponding equilibrium satisfies

$$\mathrm{j} = \mu \mathbf{B} \tag{4.4}$$

where μ is a constant, independent of position. For a plasma enclosed by a perfectly conducting shell (which also means that the toroidal flux ψ is invariant), the relaxed state depends on the single parameter μ. Given the boundary conditions, the final equilibrium can be predicted from Taylor's theory independent of the means of formation of the system.

Taylor's theory has been successfully applied to explain the generation of reversed toroidal fields in Reversed Field Pinches. Experimental evidence has shown Taylor's theory to give reasonable agreement with measured results in both Spheromaks (Jarboe *et al.*, 1983; Turner *et al.*, 1984; Hart *et al.*, 1985) and RFPs (e.g. Bodin and Newton,

1980). Three dimensional computer simulations of the relaxation process have also given support to Taylor's theory (Sykes and Wesson, 1977; Sato and Kusano, 1985).

4.2 Reversed Field Pinch equilibria

In an infinite cylindrical plasma column the solution of Equation (4.4) can be written (see Chandrasekhar and Kendall, 1957)

$$\mathbf{B} = \Sigma a_{m,k} \mathbf{B}^{m,k}(\mathbf{r})$$

where the constants $a_{m,k}$ are arbitrary and the individual magnetic field components are, when $\mu^2 > k^2$

$$B_r^{m,k} = \frac{-1}{(\mu^2 - k^2)^2}\left[kJ'_m(y) + \frac{m\mu}{y}J_m(y)\right]\sin(m\theta + kz),$$

$$B_\theta^{m,k} = \frac{-1}{(\mu^2 - k^2)^2}\left[\mu J'_m(y) + \frac{mk}{y}J_m(y)\right]\cos(m\theta + kz),$$

$$B_z^{m,k} = J_m(y)\cos(m\theta + kz),$$

with $y = r(\mu^2 - k^2)^{\frac{1}{2}}$, or when $\mu^2 < k^2$, the individual magnetic field components are

$$B_r^{m,k} = \frac{-1}{(k^2 - \mu^2)^2}\left[kI'_m(y) + \frac{m\mu}{y}I_m(y)\right]\sin(m\theta + kz),$$

$$B_\theta^{m,k} = \frac{-1}{(k^2 - \mu^2)^2}\left[\mu I'_m(y) + \frac{mk}{y}I_m(y)\right]\cos(m\theta + kz),$$

$$B_z^{m,k} = I_m(y)\cos(m\theta + kz),$$

with $y = r(k^2 - \mu^2)^{\frac{1}{2}}$.

This solution satisfies Equation (4.4) and is known as the "Bessel Function Model". We have not yet imposed any boundary conditions. At the plasma edge, the boundary condition that must be satisfied for an equilibrium is $B_r = 0$ at $r = a$ where $r = a$ is the

plasma boundary. The $m = 0, k = 0$ term of the above satisfies the boundary condition for any value of μ and has, in general, a non-zero toroidal flux. The other terms only satisfy the boundary condition for discrete values of μ and have no toroidal flux.

There are two distinct types of solutions which satisfy Equation (4.4) and the boundary condition and which correspond to a given toroidal flux (written as ψ). These are:

- The $m = 0$, $k = 0$ solution, which exists for any μ, is known as the "symmetric" solution. The appropriate value of μ is determined by the value of the invariant K/ψ^2.

- A "mixed" solution which consists of the $m = 0$, $k = 0$ solution and one of the other terms, so the solution is in the form $\alpha_0 \mathbf{B}^{0,0} + \alpha_{m,k}\mathbf{B}^{m,k}$ which exists only for fixed discrete values of μ and the invariant K/ψ^2 now determines the ratio $\alpha_{m,k}/\alpha_{0,0}$. The mixed solution having the lowest energy is the only one of interest and it occurs for $m = 1$, $ka \approx 1.23$ and $\mu = 3.11$ (Martin and Taylor, 1974), and is known as the "helical" solution.

For all values of K/ψ^2 that correspond to $\mu < 3.11$ the "symmetric" solution has the lowest energy and for larger values of K/ψ^2 the lowest energy state is the "helical" solution with $\mu = 3.11$.

4.3 The Spheromak

In fusion research to date, the Tokamak has emerged as the most feasible design for a magnetic fusion reactor. In the longer term, however, economic considerations are likely to become increasingly important and a quite different reactor topology may be required.

An ideal magnetic fusion reactor would combine the best features of Tokamaks and Mirror Machines, that is, closed magnetic field lines and an absence of conductors linking the plasma. An MHD-stable configuration that has closed toroidal flux surfaces and requires only poloidal-field coils would possess both these features. The low aspect-ratio limit of this type of configuration is called the "Spheromak", the high aspect-ratio limit giving the "Stabilized-Pinch" (Rosenbluth, 1958).

The Spheromak is the simplest form of magnetic containment device, the essential feature of which is that no conductors link the plasma. The magnetic field geometry is toroidal, consisting of nested toroidal flux surfaces surrounding the magnetic axis. The torus hole is a single line (the geometric axis of the Spheromak). The necessity for toroidal field coils is eliminated as the toroidal fields are generated by internal plasma currents.

The term "Spheromak" originated in the work of Rosenbluth and Bussac (1979) and Bussac *et al.* (1979). These papers examined theoretically a class of nearly force-free toroidal equilibria, which they named a "Spheromak". Rosenbluth and Bussac (1979) adopted an approach based on Taylor's principle and noted that the axisymmetric solution of Equation (4.4) in spherical geometry is (see Chandrasekhar and Kendall, 1957):

$$\mathbf{B} = \mathbf{r} \times \nabla\varphi + \frac{1}{\mu}\nabla \times (\mathbf{r} \times \nabla\varphi), \tag{4.5}$$

where φ are the spherical scalar eigenfunctions which satisfy

$$\nabla^2\varphi + \mu^2\varphi = 0, \tag{4.6}$$

and are given by

$$\varphi_m^n = j_m(\mu r) P_m^n(\cos\theta) \exp(in\phi). \tag{4.7}$$

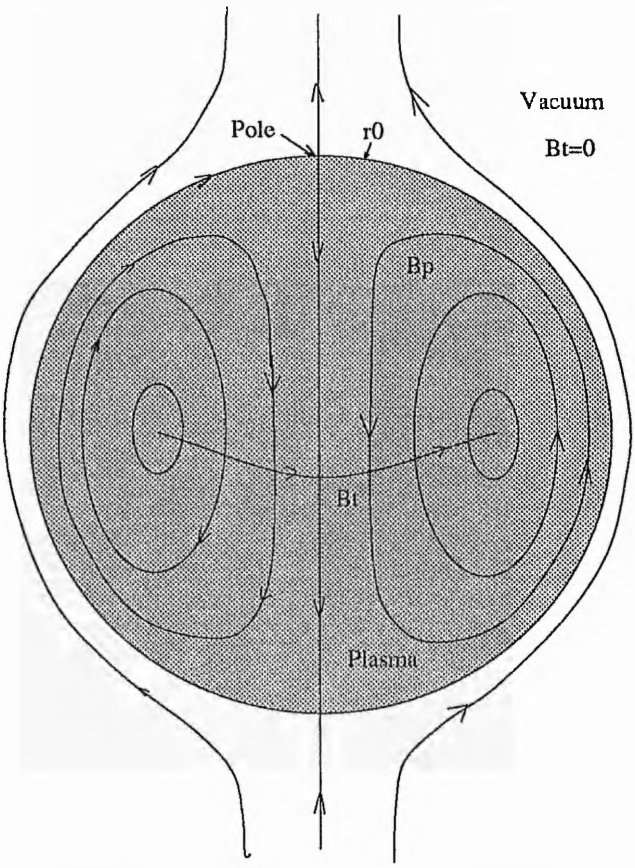

Figure 4.1: The "Classical" Spheromak, the $n = 0$, $m = 1$ solution.

$j_m(\mu r)$ is the spherical Bessel function

$$j_m(z) = \left(\frac{\pi}{2z}\right)^2 J_{m+\frac{1}{2}}(z). \tag{4.8}$$

Magnetic fields which satisfy Equation (4.4) are given by:

$$\begin{aligned}
\mathbf{B}_n^m &= b_m^n e^{in\phi}\Big[\left(m(m+1)P_m^n(\cos\theta)\frac{j_m(\mu r)}{\mu r}\right)\mathbf{e}_r \\
&+ \left(\frac{in}{\sin\theta}P_m^n(\cos\theta)j_m(\mu r) - \sin\theta P_m^{n'}(\cos\theta)\frac{1}{\mu r}\frac{d}{dr}(rj_m(\mu r))\right)\mathbf{e}_\theta \\
&+ \left(\sin\theta P_m^{n'}(\cos\theta)j_m(\mu r) + \frac{in}{\sin\theta}P_m^n(\cos\theta)\frac{d}{dr}(rj_m(\mu r))\right)\mathbf{e}_\phi\Big]
\end{aligned} \tag{4.9}$$

where b_m^n is a constant and $m \geq n$. The equilibrium solution given by $n = 0$, $m = 1$ is known as the "classical" Spheromak equilibrium and is illustrated in Figure (4.1) and for the sake of normalization we take $b_1^0 = 1$. This definition of the equilibrium implies that

the radius of the plasma is given by the first zero of $j_1(\mu r)$, which yields $\mu a = 4.493$.

4.4 Stability

Because relaxed states are states of minimum energy, all relaxed states are stable against perturbations that do not change the helicity, which includes all ideal MHD perturbations. For the Bessel Function Model of a Reversed Field Pinch, the equilibrium is stable against all ideal MHD modes when $\mu a < 3.11$. However, it ceases to be stable at this point, as the axisymmetric configuration in an infinite cylinder becomes linearly unstable to a resistive tearing mode at the point where it ceases to be the lowest-energy state (i.e, at $\mu a = 3.11$) (Whiteman, 1962; Gibson and Whiteman, 1968).

Rosenbluth and Bussac (1979) studied the stability of the force-free Spheromak equilibria described above against magnetically driven modes. The study was facilitated by the fact that energy minimizing perturbations continue to satisfy Equation (4.4) inside the plasma. The instability modes of principal interest were studied analytically by utilizing the configuration of figure (4.1) and introducing non-sphericity, finite β etc. as small perturbations. Internal modes and surface modes were considered.

Rosenbluth and Bussac (1979) showed that a prolate Spheromak is unstable and an oblate Spheromak stable to a tilt instability ($n = 1$), while the Spheromak is marginally stable to this mode when a perfect wall is placed on the plasma boundary. The Spheromak is stable to all other internal modes ($n > 1$). In the more realistic case where a vacuum region surrounds the plasma, new instabilities are possible. Their overall conclusion was that oblate Spheromaks can be completely stable for a conducting shell at about 1.15 times the plasma radius. This stabilizes resistive and kink modes. Pressure driven modes

were also investigated and a low limit on β found. This limit on β is improved in oblate Spheromaks. Subsequent investigations into the stability properties of a Spheromak have concentrated mainly on the tilt mode and beta limits. The stabilizing influences of an oblate shape and of a conducting shell have been verified experimentally. A good summary of theory and experiment is given by Bruhns (1986).

4.5 Instabilities caused by a resistive wall

Studies of the stability of Spheromak equilibria have usually assumed that any wall bounding the plasma is perfectly conducting as the resistive time-scale of the wall is longer than the plasma lifetime. However, if Spheromaks were to become important as fusion reactors, the resistivity of the wall would have to be considered.

Pfirsch and Tasso (1971) proved that an equilibrium that is unstable to MHD modes cannot be stabilized by introducing a finitely conducting wall. These instabilities will grow on a time-scale proportional to the vertical field penetration time-scale of the wall. Goedbloed, Pfirsch and Tasso (1972) considered the effect of placing a thin wall of finite conductivity (where the thickness of the resistive wall is very small relative to the radius) between the plasma and the superconducting wall. Pinch-like and Tokamak-like configurations were investigated. Robinson (1975, 1977) considered the effect of a "thin-liner" on the stability of a Reversed Field Pinch (RFP).

Jensen and Chu (1979) considered cylindrical cross-section Tokamak configurations surrounded by a resistive wall. They assumed that the instabilities grew on a time-scale long enough that inertial flows could be neglected and that the perturbed state is one of MHD equilibrium. This assumption is valid if the characteristic resistive time-scale of the

wall is low and with this assumption the solution of the problem is straightforward.

Hender, Gimblett and Robinson (1986) investigated the effects of a finitely conducting resistive wall on the MHD stability of Tokamaks and RFPs. They presented numerical and analytical results which showed the destabilizing effects of a resistive wall on some MHD stable (with an ideal wall) profiles. For some Tokamak configurations they found modes that may explain some observed activity in Tokamak experiments. Gimblett (1986) extended earlier research into the effects of these "thin-shell" modes in RFP equilibria to include the effect of bulk plasma rotation and mode rotation (plasma diamagnetism).

We follow the method of Jensen and Chu (1979) in assuming that the instabilities grow on a time-scale long enough that inertial flows can be neglected and that the perturbed state is one of MHD equilibrium and that energy minimizing perturbations satisfy Equation (4.4).

4.5.1 Electromagnetic boundary conditions at a "thin-shell"

In a wall of resistivity η_w, the perturbed magnetic field satisfies

$$\frac{\partial \mathbf{B}_1}{\partial t} = \eta_w \nabla^2 \mathbf{B}_1.$$

For a thin wall situated at $r = a$, with thickness δ where $\delta \ll a$ this becomes

$$\frac{\partial B_{1r}}{\partial t} = \eta_w \frac{\partial^2 B_{1r}}{\partial r^2},$$

assuming that the radial derivatives dominate and that curvature terms are negligible. For the general case see Aleksin and Romanov (1974) and Nalesso and Costa (1980). For the "thin-shell" approximation, where we treat the wall as a simple resistive layer (the electromagnetic skin depth $\gg \delta$) integrating this Equation yields the thin-shell boundary

condition

$$p\tau_w = \Delta', \tag{4.10}$$

where $\tau_w = a\delta/\eta_w$, p is the linear growth rate of the perturbed field ($B_{1r}(\mathbf{r},t) = B_{1r}(\mathbf{r})e^{pt}$) and Δ' is the normalized jump in the logarithmic derivative of the radial field

$$\Delta' = \frac{a}{B_{1r}}\left[\frac{\partial B_{1r}}{\partial r}\right]_{in}^{out}.$$

4.6 Growth rates for a Reversed Field Pinch

For the cylindrical force-free equilibria we restrict our attention to the "symmetric" equilibria ($\mu a < 3.11$). If we place a "thin-shell" on the plasma boundary (at $r = a$), the perturbed magnetic fields in the r-direction inside the plasma that satisfy Equation (4.4) are given by:

$$B_{1r}^{m,k} = \frac{-1}{(\mu^2 - k^2)^2}\left[k(J'_m(y) + a_1 Y'_m(y)) + \frac{m\mu}{y}(J_m(y) + a_1 Y_m(y))\right]\sin(m\theta + kz),$$

with $y = r(\mu^2 - k^2)^{\frac{1}{2}}$ when $\mu^2 > k^2$, or

$$B_{1r}^{m,k} = \frac{-1}{(k^2 - \mu^2)^2}\left[k(I'_m(y) + a_1 K'_m(y)) + \frac{m\mu}{y}(I_m(y) + a_1 K_m(y))\right]\sin(m\theta + kz),$$

with $y = r(k^2 - \mu^2)^{\frac{1}{2}}$ when $\mu^2 < k^2$.

For non-resonant perturbations, B_{1r} must be zero on the axis, so $a_1 = 0$. But if there is a resonance within the plasma ($\mathbf{k}\cdot\mathbf{B} = 0$), then we assume that $B_{1r} = 0$ at the resonance, defining a_1. Gimblett (1986) showed that, for resistive wall modes, if resistive effects are unimportant at the resonance then the calculation of the growth rate proceeds by assuming that $B_{1r} = 0$ at the resonance and integrating from there to the wall. We then employ Δ' at the wall and ensure continuity of the radial perturbed magnetic field

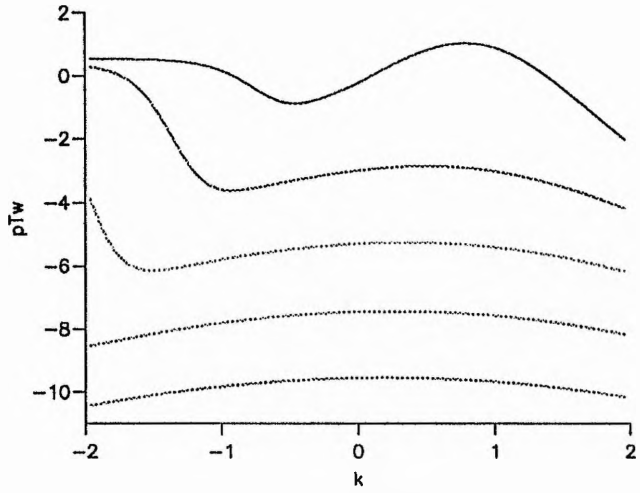

Figure 4.2: Growth rates of the resistive wall instability against k for $m = 1$ (upper curve), m=2,3,4 and m=5 (lower curve) for $\mu = 2.3$. (Resonances have been ignored for these results.)

to find the value of the growth rate of the mode $p\tau_w$. An on-axis resonance occurs for $k = -\mu/2$ (for $m = 1$) and there is a resonance within the plasma for values of k below this value.

The perturbed magnetic fields in the r-direction in the vacuum region outside the wall are given in terms of modified Bessel functions and can be written as

$$\tilde{B}_{1r}^{m,k} = \tilde{a}^{m,k} k K_m'(kr) \sin(m\theta + kz).$$

Figure (4.2) shows how the growth rate varies against k for different values of the mode number m with $a = 1$ and $\mu = 2.3$. This illustrates that the $m = 1$ mode is always the most unstable mode and we shall concentrate our attention on this mode. Figure (4.3) shows how the growth rate of the $m = 1$ mode varies against k for various values of μ. This graph shows that the mode has qualitively the same behaviour as Hender, Gimblett and Robinson (1989) found for resistive wall modes using numerical RFP equilibria (compare

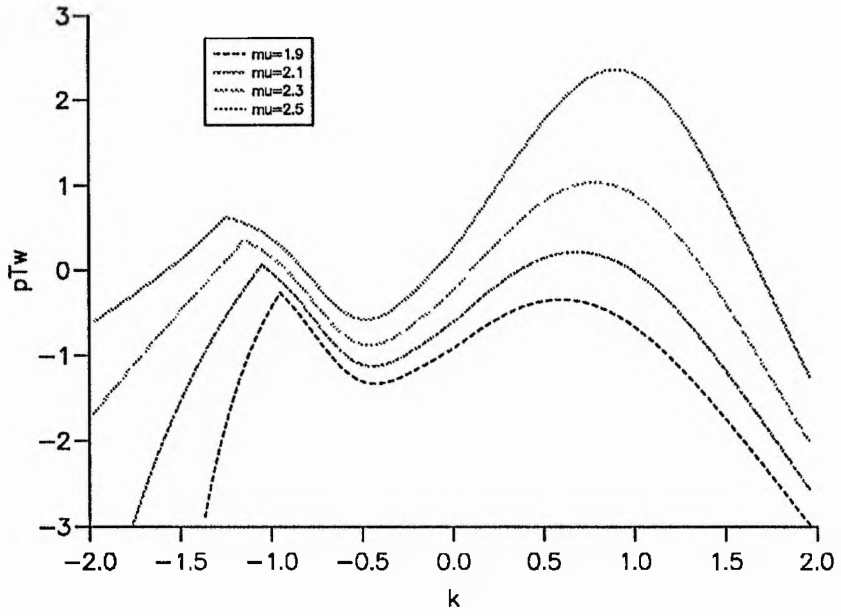

Figure 4.3: Growth rates of the resistive wall instability against k for $m = 1$ with different values of μ, including resonant perturbations.

with Figure 5 in Hender, Gimblett and Robinson, 1989). An ideal wall instability exists for non-resonant modes with both $k < 0$ and $k > 0$. Hender, Gimblett and Robinson (1989) classified the unstable modes into two classes, "within the axis" modes ($k < 0$) and "outside the wall" modes ($k > 0$). For larger values of μ the external modes are more important and have the highest growth rates but as μ decreases the internal modes become more important and eventually dominate. As μ approaches 3.11 our analysis is not valid as the "symmetrical" equilibrium becomes tearing-mode unstable at this point and the perturbed state is no longer one of MHD equilibrium.

4.7 Growth rates for a Spheromak

For a spherical force-free equilibrium we again restrict our attention to non-resonant perturbations. If we place a "thin-shell" on the plasma boundary (at $r = a$), the perturbed magnetic fields in the r-direction inside the plasma that satisfy Equation (4.4) are given by:

$$B_{1r}^{m} = b_{m}^{n} \mathrm{e}^{in\phi} \left(m(m+1) P_{m}^{n}(\cos\theta) \frac{j_m(\mu r)}{\mu r} \right) \mathbf{e}_r, \tag{4.11}$$

where $n \geq 0$ and $m \geq n$, and the perturbed magnetic fields in the r-direction in the vacuum region outside the wall are given by

$$\tilde{B}_{1r} = -(m+1) b_m r^{-(m+2)} P_m^n \mathrm{e}^{in\phi}.$$

Matching B_{1r} at the wall and using the boundary condition $p\tau_w = \Delta'$ then gives us an expression for the growth rate of the thin-shell resistive wall modes

$$p\tau_w = \frac{-k j_{m-1}(\mu a)}{j_m(\mu a)} \tag{4.12}$$

where $\mu a = 4.493$. At $\mu a = 4.493$, $j_m > 0$ for $m > 1$, and $j_1 = 0$ so that the instability is stable for $m \geq 2$ and there is no solution for $m = 1$. The soution found for the growth rate of the instability is also independent of the wave number n. This unexpected result, that the resistive wall mode are stable is probably because this analysis has only picked up the $n = 0$ modes, which Rosenbluth and Bussac (1979) showed to be stable to all modes in the absence of a conducting shell, except for a vertical displacement, which is marginally stable. So, for the $n = 0$ modes (and for these modes $m \geq 2$) there will be no instability caused by a conducting shell as the modes are stable in the absence of a conducting shell. To find the growth rates of the other modes ($n > 0$) another approach is needed.

4.8 Discussion

We have shown that a wall of finite conductivity can destabilize ideal MHD instabilities in an analytic RFP equilibrium, which would be stable were the wall perfectly conducting. The calculated growth rates of these instabilities give qualitatively the same results as those found in Hender, Gimblett and Robinson (1989) who investigated these modes using a numerical RFP profile.

For an analytic Spheromak equlibrium in spherical geometrey our approach seems only to pick up the $n = 0$ modes, which are stable in the absence of a wall, and so cannot be unstable in the presence of a conducting wall. A different approach is therefore required to investigate these modes.

Chapter 5

Simple tests for the MHD stability of Spheromak equilibria

A two dimensional ideal MHD equilibrium with line-tied field lines can be tested for stability using the analysis developed by De Bruyne and Hood (1989a,b) and De Bruyne (1990). They provided simple tests for the stability (sufficient condition) and instability (necessary condition) of line-tied two dimensional magnetic fields. In order to do this, they manipulated the energy integral for two dimensional equilibria into the form

$$\delta W = \frac{1}{2\mu_0}\mathcal{I} + \mathcal{J}$$

where $\mathcal{J}$ is a positive definite integral and $\mathcal{I}$ only involves derivatives along the equilibrium field lines. A sufficient condition for stability is then given by

$$\mathcal{I} > 0$$

for all field lines. The Euler-Lagrange equations found by minimizing $\mathcal{I}$ can be rewritten as a set of ordinary differential equations in which all the derivatives are along the field lines.

In order to derive a necessary condition, De Bruyne (1990) chose a trial function based on the "ballooning approximation". Substituting into δW and minimizing results in a set of Euler-Lagrange equations in which the only derivatives present are along the magnetic field lines. Thus, it is possible to obtain both a necessary and a sufficient condition for stability based on the solution of simple ordinary differential equations. This analysis is applied here to Spheromak equilibria. We begin with a short description of "gun-injected" Spheromaks, going on to derive ideal MHD equilibria capable of modelling their behaviour. Then the sets of ordinary differential equations that can be used to find bounds on stability are derived. Finally, these tests are applied to the Spheromak equilibria and the results discussed.

5.1 Gun-injected Spheromaks

Rarely spheroidal, Spheromaks tend to be squashed, oblate shapes, often nearly cylindrical and usually surrounded by a conducting wall known as the "flux-conserver". These laboratory magnetic fields can be modeled using ideal MHD in a two dimensional cylindrical geometry, a short, oblate Spheromak having nearly axisymmetric cylindrical geometry. We call a "Spheromak" any compact, nearly axisymmetric, nearly force-free equilibrium, that is, anything that is "Spheromak-like".

Since no current carrying coils or transformer arms limit the plasma in a Spheromak, indirect formation means must be used. There are currently four main methods of Spheromak formation all of which involve magnetic reconnection. The final state is to a large degree independent of the dynamics of formation, as predicted by Taylor's theory (Taylor, 1976).

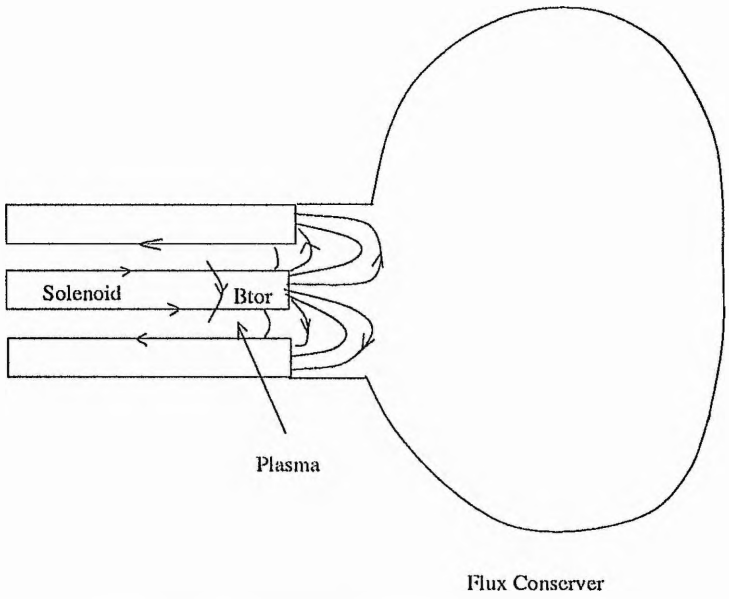

Figure 5.1: Gun injected formation 1: Plasma is formed between electrodes. The $\mathbf{j} \times \mathbf{B}$ force accelerates the plasma down the gun.

The most widely used method of Spheromak formation is known as "gun-injection". A gun injected Spheromak equilibrium consists of nested surfaces of closed field lines and open field lines, the latter remaining attached to the gun. The boundary conditions for these field lines at the gun are generally modeled by the "rigid-wall" line-tying condition.

In this Chapter, we are particularly concerned with the UMIST Spheromak, as the equilibria models we have used have been chosen in collaboration with Dr P. Browning and Mr J. Clegg. The UMIST Spheromak is a "gun-injected" Spheromak. The method of formation is illustrated in Figures (5.1) to (5.3). Figure (5.1) shows a coaxial plasma gun which feeds magnetized plasma through the annular gap between the inner and outer electrodes. The plasma is formed between the electrodes and the Lorentz force accelerates the plasma down the gun. The plasma drags out the field from the solenoid (Figure 5.2). As an equilibrium becomes established within the flux conserver, reconnection allows

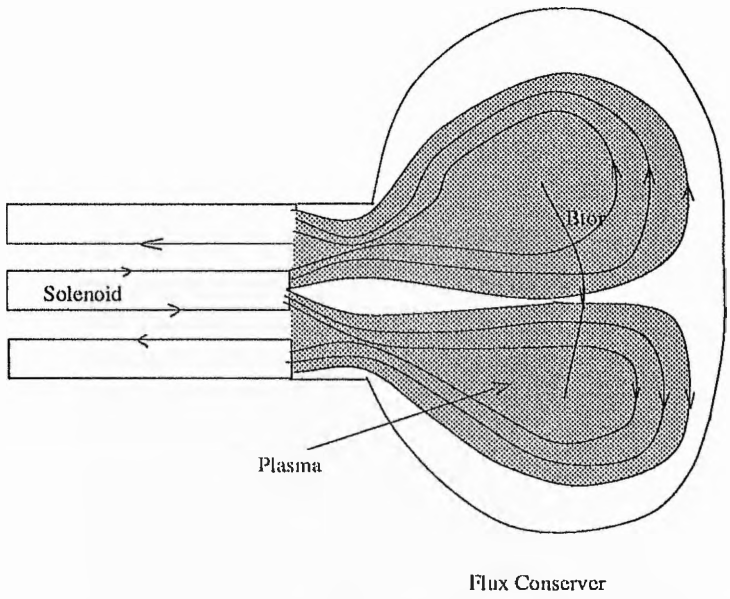

Figure 5.2: Gun injected formation 2: The plasma drags the magnetic field out from the solenoid, forming poloidal field.

the axial field lines from the gun to detach and to form the closed poloidal flux of the Spheromak (Figure 5.3).

The Spheromak configuration inside the flux conserver consists mainly of detached islands of poloidal field and is more or less axisymmetric. However, for this formation process there are always field lines that remain connected to the gun. These are of two types. Long, open field lines loop around the closed field, and short open field lines lie across the mouth of the gun. These open field lines can be considered line-tied at the gun (or entrance region) and we can use the line-tying boundary conditions.

There are several advantages to the magnetized gun. Not only is it relatively inexpensive and easy to build, but it also allows formation on time scales up to the resistive time scale for field dissipation and is capable of sustaining the equilibrium through helicity injection.

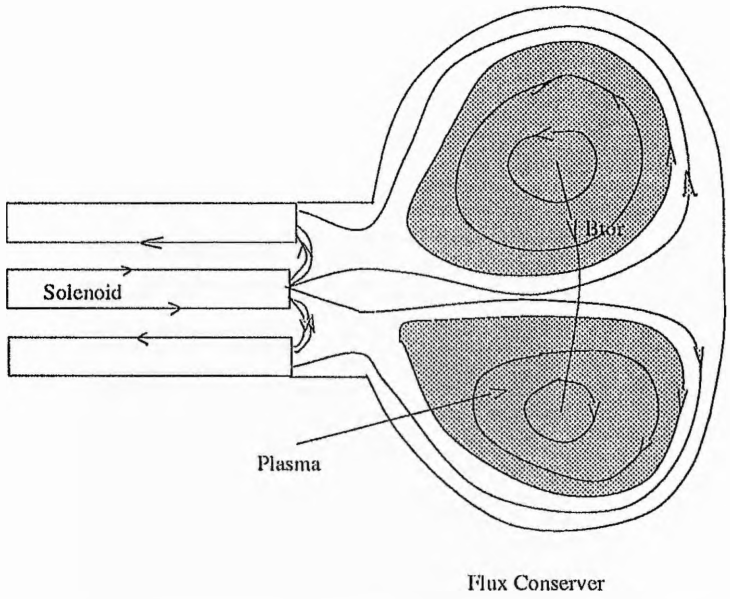

Figure 5.3: Gun injected formation 3: The magnetic field reconnects and amplifies to form closed surfaces.

5.1.1 Cylindrically symmetric analytic equilibria

One of the uses of the MHD model is for modeling equilibria and their evolution. As a first approximation current dissipation is often neglected and plasma flows are assumed to be slow compared to the Alfvén and sound speeds. To find a magnetostatic equilibrium to model the structure of interest, one needs to solve the equation of force balance, and in principle a steady energy balance equation. The stability of this equilibrium can then be studied.

Spheromak configurations formed inside the flux conserver of the UMIST Spheromak are nearly axisymmetric. We can model an equilibrium using cylindrical polar coordinates in two dimensions with the azimuthal direction being the ignorable direction. Firstly, we derive the equations that govern the equilibrium.

Consider ideal magnetohydrostatic equilibria governed by the equations

$$\nabla p = \mathbf{j} \times \mathbf{B},$$

$$\mathbf{j} = \frac{1}{\mu_0} \nabla \times \mathbf{B},$$

and

$$\nabla \cdot \mathbf{B} = 0$$

where p is the equilibrium plasma pressure, $\mathbf{j}$ the electric current density and $\mathbf{B}$ the magnetic induction. Now consider the non-dimensionalized forms of these equations, where we normalize against a typical plasma length scale l, a typical magnetic field strength B_0 and a typical plasma pressure p_0. The force balance equation becomes:

$$\beta \hat{\nabla} \hat{p} = \hat{\nabla} \times \hat{\mathbf{B}} \times \hat{\mathbf{B}}.$$

Note that here we have defined the plasma beta to be:

$$\beta = \frac{\mu_0 p_0}{B_0^2}.$$

To avoid factors of two in the equations this differs by a factor of two from the definition given in Chapter 1. Now we drop the hats.

Any axisymmetric field independent of θ may be expressed in terms of a flux function A, such that

$$B_r = -\frac{1}{r}\frac{\partial A}{\partial z}, \quad B_\theta = \frac{1}{r} G(A), \quad B_z = \frac{1}{r}\frac{\partial A}{\partial r}, \quad p = p(A) \tag{5.1}$$

where p is the plasma pressure and G and p are arbitrary functions of A.

This field automatically satisfies $\nabla \cdot \mathbf{B} = 0$ and the three components of the force balance equation

$$(\nabla \times \mathbf{B}) \times \mathbf{B} = \beta \nabla p \tag{5.2}$$

reduce to the Grad-Shafranov equation

$$r^2\nabla\cdot\left(\frac{\nabla A}{r^2}\right)+G\frac{dG}{dA}+r^2\beta\frac{dp}{dA}=0. \tag{5.3}$$

The flux function A is a useful quantity, since the projections of the field lines onto the r-z plane are given by contours of constant A.

For the Taylor state $\nabla\times\mathbf{B}=\mu\mathbf{B}$, with constant μ, $G(A)=\mu A$, and the Grad-Shafranov equation becomes

$$r^2\nabla\cdot\left(\frac{\nabla A}{r^2}\right)+\mu^2A+r^2\beta\frac{dp}{dA}=0. \tag{5.4}$$

We can assume that the plasma has relaxed to a Taylor state when the plasma boundary is not a flux surface by invoking the concept of "relative helicity". When the plasma boundary is not a flux surface the global helicity of the system is not well defined and Taylor's theory does not necessarily hold. But if we modify the definition of helicity then we can still apply Taylor's theory. Berger and Field (1984) defined a quantity known as the "relative helicity" of a system by imagining that the flux entering and leaving the system is extended outside as a vacuum field. The helicity of the system added to the helicity of this imaginary vacuum field is now a well defined quantity. If the boundaries of the system are perfectly conducting then changes in the magnetic field inside the system do not change this hypothetical vacuum field as the normal component of the magnetic field on the boundary does not change.

The relative helicity K_R is invariant during relaxation and the relaxed state is found by minimizing the energy subject to this invariance and using the boundary condition that the normal component of the magnetic field on the boundary does not change again

leads to the equation for the relaxed state:

$$\mathrm{j} = \mu \mathbf{B}. \tag{5.5}$$

Boundary conditions

On the magnetic axis ($r = 0$) $A = 0$, so that the toroidal field remains finite. On the time scale of an experiment no magnetic field will diffuse significantly into the flux conserver (Clegg *et al.* 1989), so we can assume that A is also zero at the flux conserver wall. For a cylindrical geometry we let the flux conserver wall be at $r = a$ and $z = 0$, and the entrance region at $z = L$. At $z = L$ $A \neq 0$ as flux is attached to the gun and A is as a function of r, i.e. $A = F(r)$ on $z = L$.

5.1.2 Form of the flux function

The plasma pressure is an arbitrary function of the flux function A. In order to derive analytic equilibria we let the plasma pressure p have the linear form

$$p = P_0 + P_1 A.$$

We can then solve Equation (5.4) with the boundary conditions defined above, to obtain

$$\begin{aligned} A &= -\frac{P_1 r^2}{\mu^2} + \frac{P_1 a^2}{\mu^2}\frac{rJ_1(\mu r)}{aJ_1(\mu a)} + \sum_{n=1}^{\infty} a_n r J_1(\frac{\alpha_n r}{a})\frac{\cosh(K_n(z-\frac{L}{2}))}{\cosh(K_n\frac{L}{2})} \\ &+ \sum_{n=1}^{\infty} \frac{2}{a^2 J_0^2(\alpha_n)} r J_1(\frac{\alpha_n r}{a})\frac{\sinh(K_n z)}{\sinh(K_n L)} \int_0^a F(r) J_1(\frac{\alpha_n r}{a}) dr \end{aligned} \tag{5.6}$$

where α_n $n = 1, 2, ...$ are the zeroes of the first Bessel function J_1,

$$K_n = \frac{\alpha_n^2}{a^2} - \mu^2,$$

(K_n may be real or imaginary) and the constants a_n are found by imposing the boundary conditions for z, which gives

$$a_n = \frac{2}{a^2 J_0^2(\alpha_n)} \int_0^a \left(\frac{P_1 r^2}{\mu^2} - \frac{P_1 a^2}{\mu^2} \frac{r J_1(\mu r)}{a J_1(\mu a)} \right) J_1(\alpha_n \frac{r}{a}) dr. \tag{5.7}$$

Using the orthogonality properties of Bessel functions (Abramowitz and Stegun, 1983), a_n becomes

$$a_n = -\frac{2P_1}{\mu^2 a J_0(\alpha_n)} \left[\frac{a^2}{\alpha_n} + \frac{\alpha_n}{K_n^2} \right].$$

When $P_1 = 0$ this solution for A reduces to the solution for the force-free case (see below).

5.1.3 Eigenvalues for force free equilibria

It is useful to discuss force free equilibria as this can tell us important information about the system. Force free configurations are governed by

$$(\nabla \times \mathbf{B}) \times \mathbf{B} = 0,$$

(i.e. $p = 0$) and the Grad-Shafranov equation becomes

$$r^2 \nabla \cdot \left(\frac{\nabla A}{r^2} \right) + G \frac{dG}{dA} = 0. \tag{5.8}$$

If no magnetic field is allowed to thread the boundaries, $\mathbf{B} \cdot \mathbf{n} = 0$ everywhere and the solution to (5.8) is an eigenvalue problem. The values of the eigenvalues $\mu_1, \mu_2, \ldots$ are determined by the geometry of the system.

In practice, some flux always enters and leaves the system and solutions for all values of μ exist (see, for example, Turner, 1984; Taylor, 1986; Browning, 1988). However, the eigenvalues are still important, particularly the first eigenvalue μ_1. It has been shown (Jensen and Chu, 1984) that as μ approaches the lowest eigenvalue μ_1, the system resonates and the poloidal flux, energy and helicity all tend to infinity. One can find solutions

analytically which have $\mu > \mu_1$, but the first eigenvalue appears to be a physical barrier, because in order to pass through μ_1 in a series of quasi-static equilibria, the energy required would be infinite. Also, for a given helicity, the minimum energy solution always has $\mu < \mu_1$.

5.1.4 Simple boundary source

To model a source with an effective entrance region width equal to that of the cylinder radius, we choose

$$F(r) = B_1 r J_1 \frac{(\alpha_1 r)}{a} \tag{5.9}$$

on $z = L$, where B_1 is a constant. The structure of the magnetic field lines is dependent on the value of μ. There are two important values of μ to consider. The first being where $\partial A/\partial z = 0$ at $z = L$, which we call μ_{min}, and the second being the first eigenvalue μ_1. μ can never rise beyond the first eigenvalue and three distinct equilibrium configurations exist for of $\mu < \mu_1$. These three regimes of behavior are:

- Open field lines only, where $\mu < \mu_{min}$. For the force free quilibrium, with $a = 1$ and $L = 1$, $\mu_{min} = 4.14$. All field lines are connected to the "gun" ($z = L$). This case is illustrated in Figure (5.4).

- Long open field lines connected to the "gun" surround closed field lines, where $\mu_{min} < \mu < \mu_1$. For the force free quilibrium, with $a = 1$ and $L = 1$, $\mu_1 = 4.95$. This case is illustrated in Figure (5.5).

- Only closed field lines exist, and $\mu = \mu_1$.

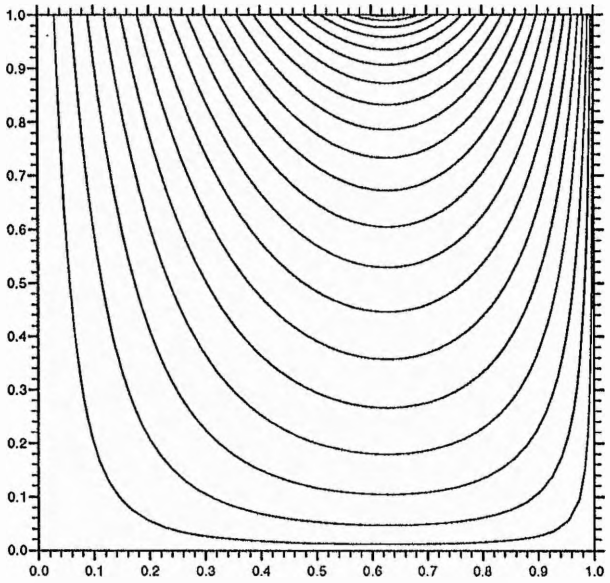

Figure 5.4: Contours of constant A (field lines projected onto the r, z-plane), for the "simple" boundary condition for $\mu = 3.0$, $\gamma = 5/3$, $\beta P_0 = \beta P_1 = 0$, $a = 1$ and $L = 1$.

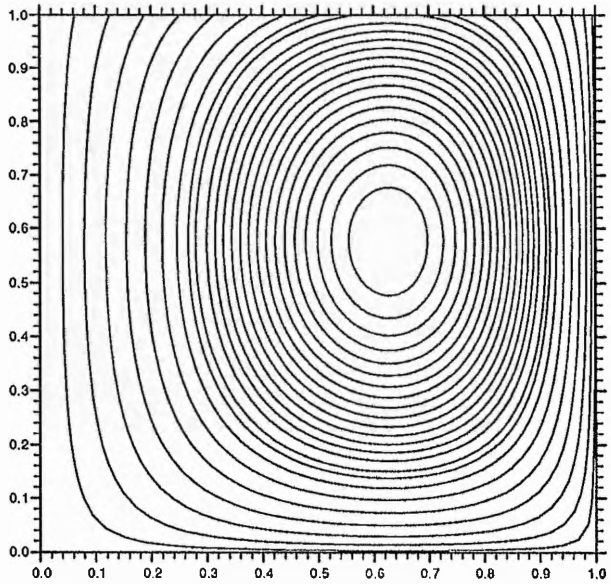

Figure 5.5: Contours of constant A (field lines projected onto the r, z-plane), for the "simple" boundary condition for $\mu = 4.7$, $\gamma = 5/3$, $\beta P_0 = \beta P_1 = 0$, $a = 1$ and $L = 1$.

5.1.5 Synthesised boundary source

A more realistic way to model the source input function is to write it as a two-fold sum

$$F(r) = B_1 r J_1(\alpha_1 \frac{r}{a}) + B_2 r J_1(\frac{\alpha_2 r}{a}) \quad \text{on} \quad \text{z = L.}$$

This tractable form approximates the effect of spatially restricting the source over a narrower radius than the cylinder. This models the real system's radial variation between entrance region and the flux conserver. We can change the ratio B_2/B_1 to model changes in the effective entrance region width. With this source function we also have a flux saddle point and this leads to short open field lines.

As μ varies, this source function gives different regimes of behavior:

- For a value of μ below a certain value μ_{min}, say, only long open field lines exist, as illustrated in Figure (5.6). For the force free quilibrium, with $a = 1$ and $L = 1$, $\mu_{min} = 4.46$. (For $B_2/B_1 > 0$, $\mu_{min} > 4.14$, for force free equilibria. μ_{min} is always higher than 4.14 for $B_2/B_1 > 0$.)

- At $\mu = \mu_{min}$ a point of inflection occurs somewhere inside the cylinder. Further increases in μ will push a local maximum away from the source and a saddle point (or X-point) towards the source at $z = L$.

- At a certain value of μ, μ_{max}, say, the saddle point reaches the boundary at $z = L$. For $\mu_{min} < \mu < \mu_{max}$ closed field lines, long open field lines and short open field lines are present, as illustrated in Figure (5.7).

- At $\mu = \mu_{max}$ short open field lines are excluded as the X-point touches the boundary at $z = L$. As μ increases further, the closed field line proportion increases until long

open field lines are excluded at the eigenvalue μ_1. Figure (5.8) shows an equilibrium with $\mu_{max} < \mu < \mu_1$. For the force free quilibrium, with $a = 1$ and $L = 1$, $\mu_1 = 4.95$.

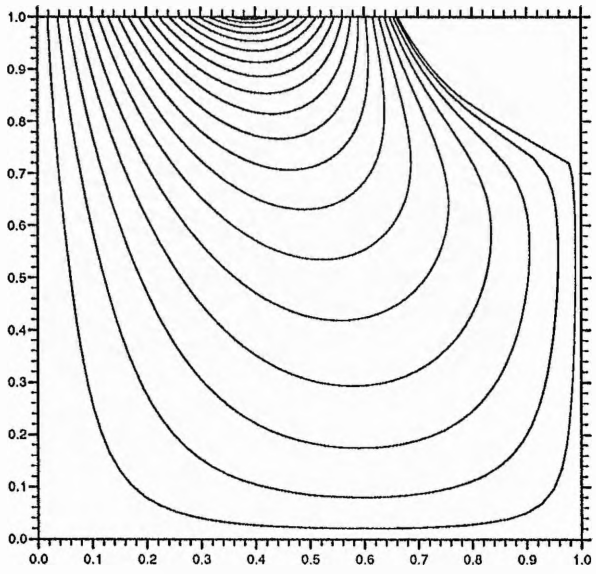

Figure 5.6: Contours of constant A for the "complex" boundary condition for $\mu = 3.0$, $\gamma = 5/3$, $\beta P_0 = \beta P_1 = 0$, $B_2/B_1 = 9/5$, $a = 1$ and $L = 1$.

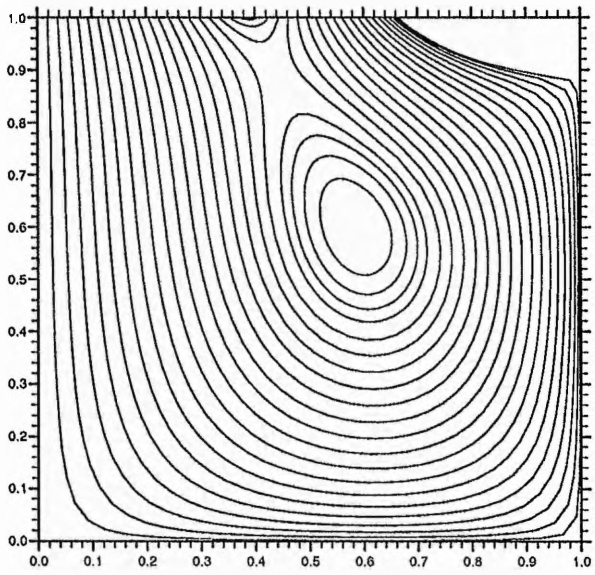

Figure 5.7: Contours of constant A for the "complex" boundary condition for $\mu = 4.6$, $\gamma = 5/3$, $\beta P_0 = \beta P_1 = 0$, $B_2/B_1 = 9/5$, $a = 1$ and $L = 1$.

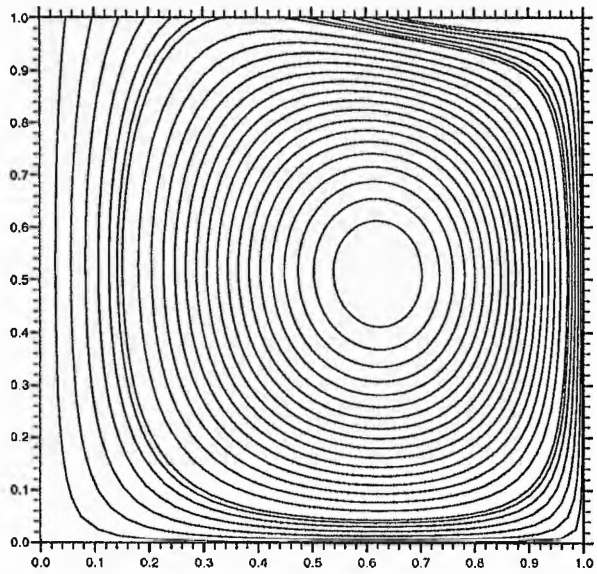

Figure 5.8: Contours of constant A for the "complex" boundary condition for $\mu = 4.9$, $\gamma = 5/3$, $\beta P_0 = \beta P_1 = 0$ and $B_2/B_2 = 9/5$.

5.2 Simple tests for MHD stability of 2D cylindrical equilibria

The energy principle discussed in Chapter 1 offers three lines of approach for determining stability (Hood, 1983). Firstly, one can use trial functions in an attempt to show that $\delta W < 0$, which gives necessary conditions for stability. Secondly, sufficient conditions for stability can be obtained by peforming a partial minimization, neglecting some positive terms in the energy integral. Thirdly, one can solve the full Euler-lagrange equations, which would give both necessary and sufficient conditions. However, the solution of the Euler-Lagrange equations involves solving a system of three coupled partial differential equations, a non-trivial problem.

As mentioned in the introduction, De Bruyne and Hood (1989a,b) and De Bruyne (1990) developed methods for two dimensional equilibria based on the first two approaches. To do this, they rewrote the perturbed potential energy integral in a suitable form

$$\delta W = \frac{1}{2\mu_0}(\mathcal{I} + \mathcal{J})$$

where $\mathcal{J}$ is positive definite and has all the perpendicular derivatives of the plasma displacement.

Firstly, ballooning modes are used as trial functions in an attempt to minimize δW, resulting in necessary conditions for stability (sufficient for instability). The localized modes are driven by the interaction of a strong outward pressure gradient and an unfavourable field line curvature. They tend to be highly localized about the flux surface where this interplay is most pronounced, so reducing the stabilizing effect of the neighbouring plasma. In nuclear fusion research they are often referred to as "ballooning modes" because they

force the plasma to "balloon out" where the destabilizing curvature is strongest. Secondly, a partial minimization of δW lead to sufficient conditions for stability to global modes. The main advantage of this method is that it does not require the solution of a system of coupled partial differential equations. Instead there are two sets of equations that consist of ordinary differential equations integrated along field lines. Combining these two approaches yields a parameter region of definite stability to localized modes, a parameter region of definite stability to all modes, and a parameter region in which the technique is unable to resolve the question of stability. We can apply these methods to axisymmetric, cylindrical Spheromak equilibria. The sets of ordinary differential equations that determine the necessary and sufficient conditions are derived below.

5.2.1 The energy integral

We can rewrite the axisymmetric, ideal, magnetostatic equilibrium equations (5.1) and (5.3) as

$$\mathbf{B} = \mathbf{B}_p + B_\theta \mathbf{e}_\theta, \quad \mathbf{B}_p = \nabla A \times \frac{\mathbf{e}_\theta}{r}, \quad p = p(A), \quad G = G(A), \tag{5.10}$$

and

$$\nabla \cdot \left(\frac{\nabla A}{r} \right) + r^2 J(A, r) = 0, \tag{5.11}$$

where

$$J(A, r) = GG' + r^2 \beta \frac{dp}{dA}$$

and

$$G' = \frac{dG}{dA}.$$

As the Jacobian

$$\frac{\partial(A,r)}{\partial(r,z)} \neq 0$$

we may use A, r as independent variables instead of r, z (Low,1975, Hu, 1987).

For the Spheromak, the anchoring of the field lines to the plasma gun is modeled by the "rigid-plate" conditions

$$\xi = 0 \quad \text{at the gun,} \tag{5.12}$$

i.e. all displacements vanish on the wall of the Spheromak. The perturbed potential energy, δW, given by

$$\begin{aligned} \delta W &= C\int[|\nabla\times(\xi\times\mathbf{B})|^2+(\nabla\times\mathbf{B})\cdot[\xi\times\nabla\times(\xi\times\mathbf{B})] \\ &+ \beta(\xi\cdot\nabla p)(\nabla\cdot\xi)+\beta\gamma p(\nabla\cdot\xi)^2]dV \end{aligned} \tag{5.13}$$

where C is a constant, can then be used.

Following Hu (1987), this can be rewritten in a form suitable for manipulation (see Appendix B):

$$\begin{aligned} \delta W &= C\int[\frac{1}{r^2B_p^2}|\mathbf{B}\cdot\nabla A_1|^2+\frac{V}{r^2}|A_1|^2+r^2\left|G\nabla\cdot\left(\frac{\xi_p}{r^2}\right)-\mathbf{B}_p\cdot\nabla\left(\frac{\xi_\theta}{r^2}\right)\right|^2 \\ &+ \frac{1}{r^2}\left|\frac{1}{rB_p}(\nabla A\cdot\nabla A_1+JA_1)+G\frac{\partial\xi_{\|p}}{\partial\theta}-B_p\frac{\partial\xi_\theta}{\partial\theta}\right|^2 \\ &+ \gamma\beta p|\nabla\cdot\xi|^2]dV \end{aligned} \tag{5.14}$$

where

$$V = r^2\nabla\cdot\left(\frac{J\nabla A}{r^4B_p^2}\right)-\frac{J^2}{r^2B_p^2}-r^2\frac{\partial}{\partial A}\left(\frac{J}{r^2}\right), \tag{5.15}$$

$$A_1 = -\xi_p\cdot\nabla A, \tag{5.16}$$

$$\xi = \xi_p+\xi_\theta \tag{5.17}$$

and

$$\xi_{\|p} = \frac{\xi_p \cdot \mathbf{B}_p}{B_p}. \tag{5.18}$$

Note that $\partial/\partial A$ stands for the derivative with respect to A while r is kept constant and $\partial/\partial r$ stands for the derivative with respect to r while A is kept constant.

For equilibria with magnetic surfaces defined by constant A, it is convenient to write the plasma displacement ξ in terms of the variables

$$\xi_A = B_p\tilde{\xi}_A = \frac{\nabla A}{B_p} \cdot \xi, \tag{5.19}$$

$$\xi_{\|} = B\tilde{\xi}_{\|} = \frac{\mathbf{B}}{B} \cdot \xi, \tag{5.20}$$

$$\xi_n = BB_p\tilde{\xi}_n = \frac{\nabla A \times \mathbf{B}}{r^2 B B_p} \cdot \xi. \tag{5.21}$$

So then

$$\xi = \tilde{\xi}_A \frac{\nabla A}{r^2} + \tilde{\xi}_{\|}\mathbf{B} + \tilde{\xi}_n \nabla A \times \mathbf{B}, \tag{5.22}$$

and

$$\nabla \cdot \xi = B_p \frac{\partial \tilde{\xi}_A}{\partial a} + B\frac{\partial \tilde{\xi}_{\|}}{\partial s} + BB_p \frac{\partial \tilde{\xi}_n}{\partial n} + \nabla \cdot \left(\frac{\nabla A}{r^2}\right)\tilde{\xi}_A, \tag{5.23}$$

where the derivatives are defined as

$$B_p \frac{\partial}{\partial a} = \frac{\nabla A}{r^2} \cdot \nabla, \tag{5.24}$$

$$B\frac{\partial}{\partial s} = \mathbf{B} \cdot \nabla, \tag{5.25}$$

$$BB_p \frac{\partial}{\partial n} = \nabla A \times \mathbf{B} \cdot \nabla. \tag{5.26}$$

Using transformations similar to those in De Bruyne (1990), we may rewrite the change in potential energy δW, (see Appendix C), as

$$\delta W = C(\mathcal{I} + \mathcal{J}) \tag{5.27}$$

where

$$\begin{aligned}\mathcal{I} &= \int[\frac{B^2}{r^2B_p^2}\left[\frac{\partial}{\partial s}(B_p^2\tilde{\xi}_A)\right]^2 - \left(\frac{2J}{r^2}\left(\frac{J}{r^2}+\frac{\partial B_p}{\partial a}\right)+\frac{2GG'}{r^3}B_p\frac{\partial r}{\partial a}\right)\xi_A^2 \\ &+ \frac{\gamma\beta p}{B^2+\gamma\beta p}\left[B^2\frac{\partial\tilde{\xi}_{||}}{\partial s}-\frac{1}{B}\left(\left(2\beta\frac{dp}{dA}B_p+\frac{\partial B^2}{\partial a}\right)\xi_A+\frac{\partial B^2}{\partial n}\xi_n\right)\right]^2 \\ &+ r^2\left[B_p\frac{\partial}{\partial s}(B^2\tilde{\xi}_n)-\frac{G}{BB_pr^2}\left(2\beta\frac{dp}{dA}B_p+\frac{1}{r^2}\frac{\partial}{\partial a}\left(r^2B^2\right)\right)\xi_A\right]^2]dV, \qquad (5.28)\end{aligned}$$

and

$$\begin{aligned}\mathcal{J} = \int(B^2+\gamma\beta p)[B_p\frac{\partial\tilde{\xi}_A}{\partial a}+BB_p\frac{\partial\tilde{\xi}_n}{\partial n}-\frac{J}{r^2}\tilde{\xi}_A+\frac{\gamma\beta p}{B^2+\gamma\beta p}\left(B\frac{\partial\tilde{\xi}_{||}}{\partial s}\right) \\ +\frac{1}{B^2+\gamma\beta p}\left(\left(2\beta\frac{dp}{dA}B_p+\frac{\partial B^2}{\partial a}\right)\xi_A+\frac{\partial B^2}{\partial n}\xi_n\right)]^2dV. \qquad (5.29)\end{aligned}$$

5.2.2 Necessary conditions for stability

Consider perturbations that vary rapidly across the field and slowly along it so reducing the stabilizing effect of magnetic tension. Following Hood (1986), we take ξ to be of the form

$$\xi(r,\theta,z) = \xi(r,z)\cos(mS), \qquad (5.30)$$

with

$$m \gg 1, \qquad (5.31)$$

where m is the ratio of the equilibrium length-scale to the perpendicular length-scale, and to eliminate stable modes S is chosen such that

$$\mathbf{B}_0 \cdot \nabla S = 0, \qquad (5.32)$$

with $\cos(mS)$ periodic in θ. If one is only interested in the least stable mode, a simple solution to (5.32) is

$$S = \theta - \int^s \left(\frac{B_\theta}{rB}\right)_{A=const.} ds, \qquad (5.33)$$

where s is the distance along a field line.

Now, expanding the displacement in inverse powers of m, that is, if

$$\xi = \xi_0 + \frac{1}{m}\xi_1 + \frac{1}{m^2}\xi_2 + ...$$

we can minimize $\mathcal{J}$ by taking

$$\xi_{n0} = \frac{B_p}{B}\frac{\partial S}{\partial a}\xi_{A0}, \tag{5.34}$$

as this eliminates the leading order, O(m), contribution to $\mathcal{J}$.

Substituting this into the expression for δW and choosing ξ_1 such that there is no O(1) contribution from $\mathcal{J}$, one gets to, leading order, the ballooning integral

$$\begin{aligned}\delta W_{ball} &= C\int dV\cos^2(mS)[\frac{B^2}{r^2B_p^2}\left[\frac{\partial y_1}{\partial s}\right]^2 - \left[\frac{2J}{r^2}\left(\frac{J}{r^2}+\frac{\partial B_p}{\partial a}\right)+\frac{2GG'}{r^3B_p}\frac{\partial r}{\partial a}\right]\frac{y_1^2}{B_p^2} \\ &+ \frac{\gamma\beta p}{B^2+\gamma\beta p}\left[B^2\frac{\partial y_2}{\partial s} - \frac{1}{B}\left(2\beta\frac{dp}{dA}B_p + \frac{\partial B^2}{\partial a} + \frac{\nabla A\cdot\nabla S}{r^2B}\frac{\partial B^2}{\partial n}\right)\frac{y_1}{B_p}\right]^2 \\ &+ r^2\left[B_p\frac{\partial}{\partial s}\left(\frac{\nabla A\cdot\nabla S}{r^2B_p^2}y_1\right) - \frac{G}{BB_p^2r^2}\left(2\beta\frac{dp}{dA}B_p + \frac{1}{r^2}\frac{\partial}{\partial a}\left(r^2B^2\right)\right)y_1\right]^2][5.35)\end{aligned}$$

where we have written the variables as

$$y_1 = \tilde{\xi}_A B_p^2$$

and

$$y_2 = \tilde{\xi}_{||}.$$

The minimisation of this integral, subject to the normalizing condition

$$\int y_1^2\frac{f^2}{B_p^2r^2}dV = \text{ constant}, \tag{5.36}$$

where f^2 is a strictly positive function produces a set of two second-order Euler-Lagrange equations containing a Lagrange multiplier λ that has the same sign as δW (the minimisation is outlined in Appendix D, and the Euler-Lagrange equations stated). This set

can be transformed into a system of four coupled equations that are first order, homogeneous and ordinary, plus an auxiliary equation (see Appendix F), suitable for numerical computation:

$$\frac{\partial y_1}{\partial s} = \left(\frac{B}{r^2 B_p^2} + \frac{r^2 B_p^2}{B} y_5^2\right)^{-1} y_3, \tag{5.37}$$

$$\frac{\partial y_2}{\partial s} = \frac{1}{B}\left[\frac{B^2 + \gamma\beta p}{\gamma\beta p B^2} y_4 + \frac{1}{B^2 B_p}\left(2\beta \frac{dp}{dA} B_p + \frac{\partial B^2}{\partial a} + \frac{B_p^2}{B}\frac{\partial B^2}{\partial n} y_5\right) y_1\right], \tag{5.38}$$

$$\begin{aligned}\frac{\partial y_3}{\partial s} &= \frac{-1}{B B_p}\left[\lambda \frac{f^2}{B_p r^2} y_1 + \beta \frac{dp}{dA}\left(2\beta \frac{dp}{dA} B_p + \frac{\partial B^2}{\partial a} + \frac{B_p^2}{B}\frac{\partial B^2}{\partial n} y_5\right) y_1\right] \\ &\quad - \frac{1}{B B_p}\left[2\beta \frac{dp}{dA} B_p + \frac{\partial B^2}{\partial a} + \frac{B_p^2}{B}\frac{\partial B^2}{\partial n} y_5\right] y_4,\end{aligned} \tag{5.39}$$

$$\frac{\partial y_4}{\partial s} = 0, \tag{5.40}$$

$$\frac{\partial y_5}{\partial s} = \frac{1}{B}\left[-\frac{1}{r^2}\frac{dG}{dA} + \frac{G}{r^2 B_p^2}\left(J + 2\frac{\partial B_p}{\partial a} - r^2 B_p \frac{\partial}{\partial a}\left(\frac{1}{r^2}\right)\right)\right], \tag{5.41}$$

where

$$y_5 = \frac{\nabla A \cdot \nabla S}{r^2 B_p^2}. \tag{5.42}$$

Equations (5.39) and (5.40) define y_3 and y_4 respectively, while equations (5.37) and (5.38) represent the Euler-Lagrange equations. The auxiliary equation (5.41) needed to compute $\partial S/\partial a$ comes from relation (5.42) (see Appendix F).

5.2.3 Sufficient conditions for stability

We can perform a partial minimization of δW by neglecting its non-negative $\mathcal{J}$ part. We minimize $\mathcal{I}$ with respect to the variables

$$y_1 = \frac{\tilde{\xi}_A}{B_p^2},$$

$$y_2 = \tilde{\xi}_{||},$$

and

$$y_5 = B^2\tilde{\xi}_n,$$

subject to the same normalizing condition (5.36). This results in three second order Euler-Lagrange equations that are derived in Appendix E. These equations can be rearranged into a system of six coupled first order homogeneous ordinary differential equations:

$$\frac{\partial y_1}{\partial s} = \frac{r^2 B_p^2}{B} y_3, \tag{5.43}$$

$$\frac{\partial y_2}{\partial s} = \frac{1}{B}\left[\frac{B^2+\gamma\beta p}{\gamma\beta p B^2} y_4 + \frac{1}{B^2 B_p}\left(2\beta\frac{dp}{dA}B_p + \frac{\partial B^2}{\partial a}\right) y_1 + \frac{G}{B^3}\frac{\partial B^2}{\partial s} y_5\right], \tag{5.44}$$

$$\begin{aligned}\frac{\partial y_3}{\partial s} &= \frac{-1}{B}\left[\lambda\frac{f^2}{B_p^2 r^2} y_1 + \frac{1}{B_p^2}\left(2J\left(J + \frac{\partial B_p}{\partial a}\right) - GG' B_p \frac{\partial}{\partial a}\left(\frac{1}{r^2}\right)\right) y_1\right] \\ &- \left[\left(2\beta\frac{dp}{dA}B_p + \frac{\partial B^2}{\partial a}\right)\frac{y_4}{B^3 B_p} + \frac{G}{B_p^3}\left(\frac{2\beta}{r^2}\frac{dp}{dA}B_p + \frac{1}{r^4}\frac{\partial}{\partial a}\left(r^2 B^2\right)\right)\frac{y_6}{B}\right],\end{aligned} \tag{5.45}$$

$$\frac{\partial y_4}{\partial s} = 0, \tag{5.46}$$

$$\frac{\partial y_5}{\partial s} = \frac{B}{r^2 B_p^2} y_6 + \frac{G}{r^2 B B_p^3}\left(2\beta\frac{dp}{dA}B_p + \frac{1}{r^2}\frac{\partial}{\partial a}\left(r^2 B^2\right)\right) y_1, \tag{5.47}$$

$$\frac{\partial y_6}{\partial s} = -\frac{G}{B^4}\frac{\partial B^2}{\partial s} y_4. \tag{5.48}$$

Equations (5.45), (5.46) and (5.48) define y_3, y_4 and y_6 respectively. Equations (5.43), (5.44) and (5.47) are the three Euler-Lagrange equations.

When the field is shearless (i.e. $B_\theta = 0$) it follows from the last two equations and the boundary condition (5.12) that $y_5 = y_6 = 0$ and so $\xi_n = 0$. The remaining equations then reduce to the equations (5.37) to (5.40) with $y_5 = 0$. This shows that for shearless fields, the ballooning modes are the most unstable (see e.g. Hood, 1986).

Note that when the equilibria is force-free, the expression for $\mathcal{I}$ transforms to

$$\begin{aligned}\mathcal{I} &= \int[\frac{B^2}{r^2 B_p^2}\left[\frac{\partial}{\partial s}(B_p^2\tilde{\xi}_A)\right]^2 - \left(\frac{2J}{r^2}\left(\frac{J}{r^2} + \frac{\partial B_p}{\partial a}\right) + \frac{2GG'}{r^3}B_p\frac{\partial r}{\partial a}\right)\xi_A^2 \\ &+ r^2\left[B_p\frac{\partial}{\partial s}(B^2\tilde{\xi}_n) - \frac{G}{BB_p r^2}\frac{1}{r^2}\frac{\partial}{\partial a}\left(r^2 B^2\right)\xi_A\right]^2]dV.\end{aligned} \tag{5.49}$$

The system of coupled Euler-Lagrange equations (5.43) to (5.48) reduces to

$$\frac{\partial y_1}{\partial s} = \frac{r^2 B_p^2}{B} y_3, \tag{5.50}$$

$$\frac{\partial y_3}{\partial s} = \frac{-1}{B}\left[\lambda \frac{f^2}{B_p^2 r^2} y_1 + \frac{1}{B_p^2}\left(2J\left(J + \frac{\partial B_p}{\partial a}\right) - GG' B_p \frac{\partial}{\partial a}\left(\frac{1}{r^2}\right)\right) y_1\right]$$
$$- \frac{1}{B}\frac{G}{r^2 B_p^3}\frac{1}{r^2}\frac{\partial}{\partial a}\left(r^2 B^2\right) y_6, \tag{5.51}$$

$$\frac{\partial y_5}{\partial s} = \frac{B}{r^2 B_p^2} y_6 + \frac{G}{r^2 B B_p^3}\frac{1}{r^2}\frac{\partial}{\partial a}\left(r^2 B^2\right) y_1, \tag{5.52}$$

$$\frac{\partial y_6}{\partial s} = 0. \tag{5.53}$$

5.3 Application to Spheromak equilibria

5.3.1 Numerical method

To integrate the systems (5.37) to (5.41), (5.43) to (5.48) and (5.50) to (5.53) we proceed as follows. As the integration is along a field line on which A is fixed, for lines projected onto the r, z-plane we can replace the independent variable s by a polar coordinate ϕ, for

$$B\frac{\partial}{\partial s} = \frac{B_\phi}{R}\frac{\partial}{\partial \phi},$$

where ϕ is the angular variable in a polar coordinate system, R, ϕ. The integration is performed along a field line from footpoint to footpoint. The boundary condition (5.12) requires that at $z = L$, $y_1 = y_2 = 0$ for the system (5.37) to (5.41), $y_1 = y_2 = y_5 = 0$ for the system (5.43) to (5.48) and that $y_1 = y_5 = 0$ for the system (5.50) to (5.53). The sign of δW is then determined by the sign of the Lagrange multiplier λ.

The most efficient way of integrating the system (5.37) to (5.41) for the Spheromak equilibria is as follows. Assume values for μ, γ, β, P_0, P_1, B_1, B_2 and select a value for A. To find a value for y_5, we first integrate equation (5.41) from $\phi = 0$ (where $y_5 = 0$) to the

boundary $z = L$. To be able to satisfy the boundary condition (5.12) at both ends of the open field lines the system (5.37) to (5.40) is then integrated twice from one end for two different sets of boundary values at this end, both having $y_1 = y_2 = 0$, simultaneously with equation (5.41). The normalizing constraint is chosen to be

$$f^2 = B^2 B_p^2.$$

This results in two linearly independent solutions. Demanding that a linear combination of these two solutions vanishes at the other end of the field line determines a value for the Lagrange multiplier λ. The stability of the field line is determined by the sign of λ, which has the same sign as δW.

The integration of system (5.43) to (5.48) is very similar. There is no variable for which the starting value has to be determined before the integration can start. This system is integrated three times simultaneously with boundary values $y_1 = y_2 = y_5 = 0$, resulting in three linearly independent solutions. Again, the normalizing constraint is chosen to be

$$f^2 = B^2 B_p^2.$$

The value of λ for which a linear combination of these vanishes at the boundary determines the stability of the field line.

The same procedure is followed for the integration of the force-free system (5.50) to (5.53). It is integrated twice simultaneously, for two different sets of boundary conditions satisfying $y_1 = y_5 = 0$. The normalizing constraint is chosen to be as above. The value of λ for which a linear combination of these vanishes at the boundary determines the stability of the field line.

In all these procedures a Bulirsch-Stoer shooting method was used to integrate the equations. This embodies Richardson polynomial function extrapolation (see, e.g. Press

et al., 1987). This technique is highly accurate and usually faster than a Runge-Kutta scheme. The iteration process to determine a critical value for λ makes use of a Van Wijngaarden-Dekker-Brent root-finding method (see, e.g. Press *et al.*, 1987).

5.4 Results

We started by integrating the system (5.50) to (5.53) for the force free equilibria. For a given value of the ratio B_2/B_1, we can find a critical value of μ which gives a bound on the definite stability of the equilibrium. For values of μ less than this critical value (called μ_{crit}), the equilibrium is definitely stable. For values of μ larger than μ_{crit} one or more of the magnetic field lines are unstable. Figure (5.9) shows how this value of μ_{crit} changes as B_2/B_1 is varied (with $a = 1$ and $L = 1$). The "entrance region" is narrower than the width of the cylinder for $B_2/B_1 > 0.73$. As B_2/B_1 increases from this value (the entrance region becomes narrower) the value of μ_{crit} decreases. The system appears to be becoming less stable as the entrance region narrows, and this is probably because the length of the field lines increases as the entrance region narrows, and so the stabilizing effect of line-tying is reduced. Note that for all the values of μ_{crit} found, only open field lines are present in the equilibria. When $B_2/B_1 = 0$, the equilibrium is no longer definitely stable at $A \approx 0.05$, for $\mu = \mu_{crit}$. The value of A at which the equilibrium is no longer definitely stable (i.e. at $\mu = \mu_{crit}$), slowly decreases as B_2/B_1 increases, and the equilibrium is no longer definitely stable for $A \approx 0.02$ when $B_2/B_1 = 16/5$, (A varies from 0 at $r = 0$ and $r = a$ to a maximum of 1 across the entrance region, as it has been non-dimensionalized). So the field lines that may become unstable when $\mu = \mu_{crit}$ are near to the edge of the equilibria, but are not themselves the outermost field lines.

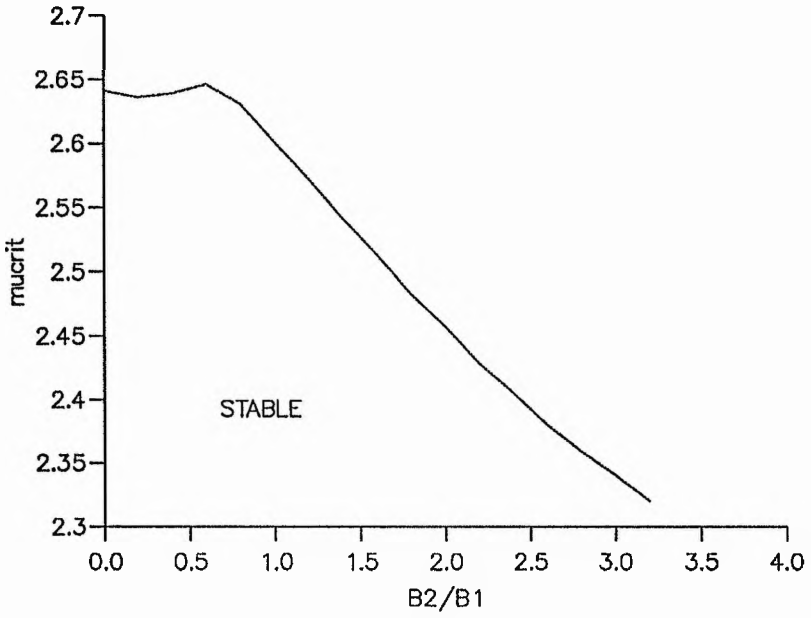

Figure 5.9: μ_{crit} against B_2/B_1 for the force free equilibria, with $a = 1$ and $L = 1$. Equilibria with $\mu < \mu_{crit}$ are definitely stable.

Before integrating the system (5.43) to (5.48) to find bounds on the definite stability of the Spheromak equilibria under investigation, we first have to choose values for the parameters. We let $P_0 = 1$, $P_1 = 1$, $a = 1$, $L = 1$ and $B_2/B_1 = 9/5$. Figure (5.10) demonstrates how μ_{crit} varies as β changes, for these parameter values, as we integrate the system (5.43) to (5.48) along the field lines. The value of μ_{crit} found for very small β agrees to three significant figures with the value found from integrating the system (5.50) to (5.53) for these values of the parameters. We can see from Figure (5.10) that, as β increases from 0 to 0.01, μ_{crit} initially shows a sharp increase. For these values of μ_{crit} the field lines are no longer definitely stable for values of A of approximately 0.06. As β increases further, μ_{crit} slowly decreases, until $\beta \approx 0.25$, when μ_{crit} begins to fall sharply. For this region ($\beta > 0.01$) the outermost field lines ($A \approx 0$) are no longer definitely stable at $\mu = \mu_{crit}$. So, for $\beta < 0.25$, ther is a region of definite stability, but this region has

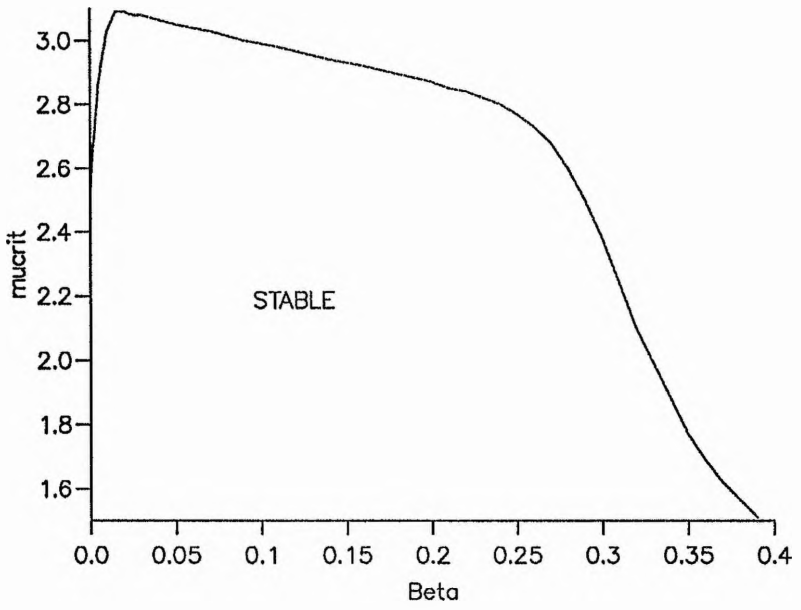

Figure 5.10: μ_{crit} against β for $B_2/B_1 = 9/5$, with $P_0 = 1$, $P_1 = 1$, $a = 1$ and $L = 1$. Equilibria with $\mu < \mu_{crit}$ are definitely stable.

values of μ below those required for closed field lines to appear in the system. (This value μ_{min} does decrease as the plasma pressure increases, but only slowly. It falls from 4.46 at $\beta = 0$ to 4.39 at $\beta = 1$.) For $\beta > 0.3$ the equilibria are definitely stable only for very low values of μ. Again, note that for all the values of μ_{crit} that we have found, there are no closed field lines present in the equilibria. We also found that the short, open field lines are always definitely stable for any value of μ and β.

Figure (5.11) illustrates how μ_{crit} varies with β for three different values of B_2/B_1 (with $a = 1$, $L = 1$, $P_0 = 1$ and $P_1 = 1$). The shape of all three graphs is similar, but they indicate that narrowing the entrance region reduces the stability of the system.

We integrated the system (5.37) to (5.41) for open field lines only, mainly because the boundary condition (5.12) does not apply to closed field lines ($A > 1$). Figure (5.12) shows μ_{crit} plotted against β for $B_2/B_1 = 9/5$, $a = 1$, $L = 1$, $P_0 = 1$ and $P_1 = 1$. For this

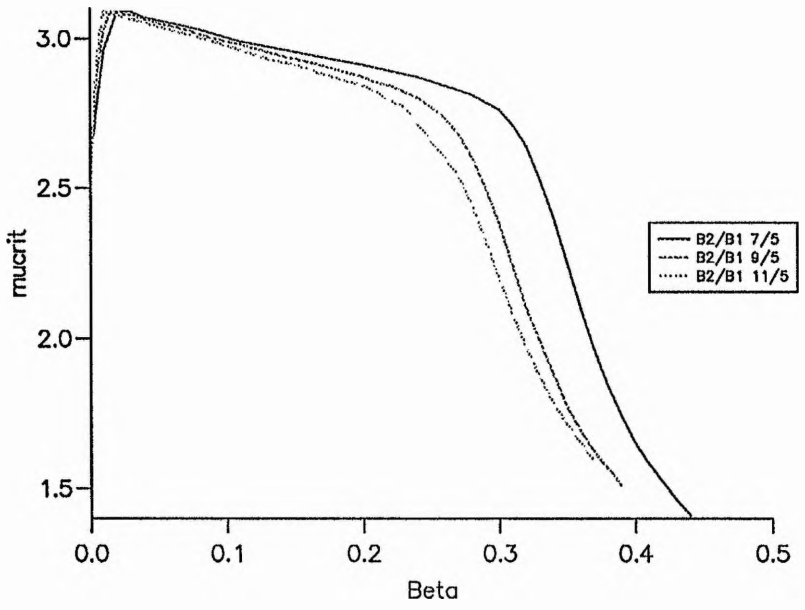

Figure 5.11: μ_{crit} against β for $B_2/B_1 = 7/5$, $B_2/B_1 = 9/5$ and $B_2/B_1 = 11/5$, with $P_0 = 1$, $P_1 = 1$, $a = 1$ and $L = 1$. Equilibria with $\mu < \mu_{crit}$ are definitely stable.

system, values of μ greater than μ_{crit} are definitely unstable. We can see that for values of β of approximately 1.8 or greater, the system is definitely unstable, except for small values of μ. But for $\beta < 1.77$ we have been unable to find any unstable field lines for any value of μ. This would indicate that, for these parameter values, the open field lines are stable to this particular class of disturbances for all values of μ when $\beta < O(1)$. At $\mu = \mu_{crit}$, the field lines which become unstable have $A \approx 0.07$, and the outer field lines do not become unstable first for any value of β.

Figure (5.13) shows μ_{crit} against β for three different values of B_2/B_1. The results again indicate that narrowing the entrance region reduces the stability of the system, as the value of β below which the open field lines are stable to the ballooning modes decreases as B_2/B_1 increases.

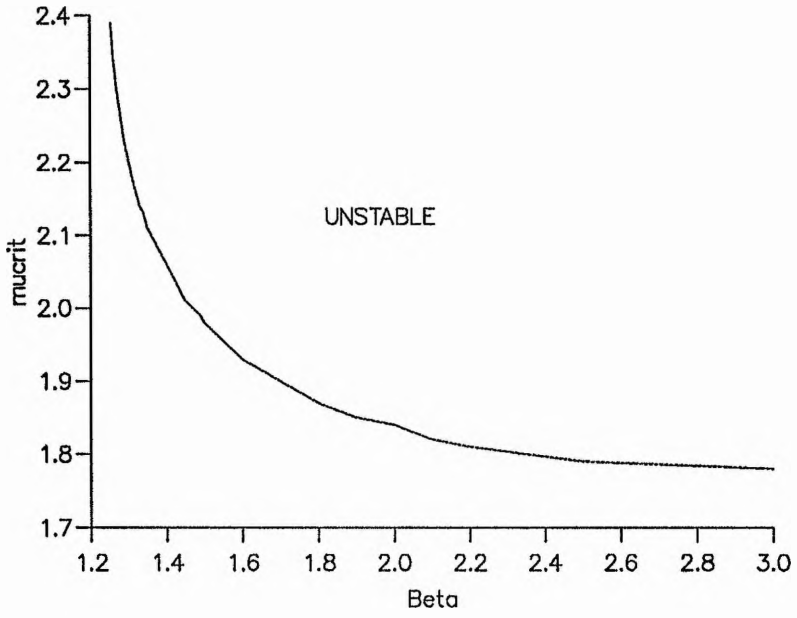

Figure 5.12: μ_{crit} against β for $B_2/B_1 = 9/5$, with $P_0 = 1$, $P_1 = 1$, $a = 1$ and $L = 1$. Equilibria with $\mu > \mu_{crit}$ are definitely unstable.

5.5 Discussion

We have used the analysis of De Bruyne and Hood (1989a, 1989b) and De Bruyne (1990), who recast the perturbed potential energy equation for dimensional equilibria in the form

$$\delta W = \frac{1}{2\mu_0}(\mathcal{I} + \mathcal{J})$$

where $\mathcal{I}$ depends only on derivatives along the field lines and $\mathcal{J}$ is positive definite, to find sufficient and necessary conditions for the stability of cylindrically symmetric Spheromak equilibria.

To find necessary conditions for stability, the ballooning modes of Connor, Hastie and Taylor (1979) are used as trial functions, these functions being particularly relevant to study instabilities which arise due to plasma pressure as they minimize the effect of magnetic tension (Suydam, 1958). To find sufficient conditions for stability, the integral $\mathcal{J}$ is neglected and a minimization of $\mathcal{I}$ is performed. These two approaches require only the

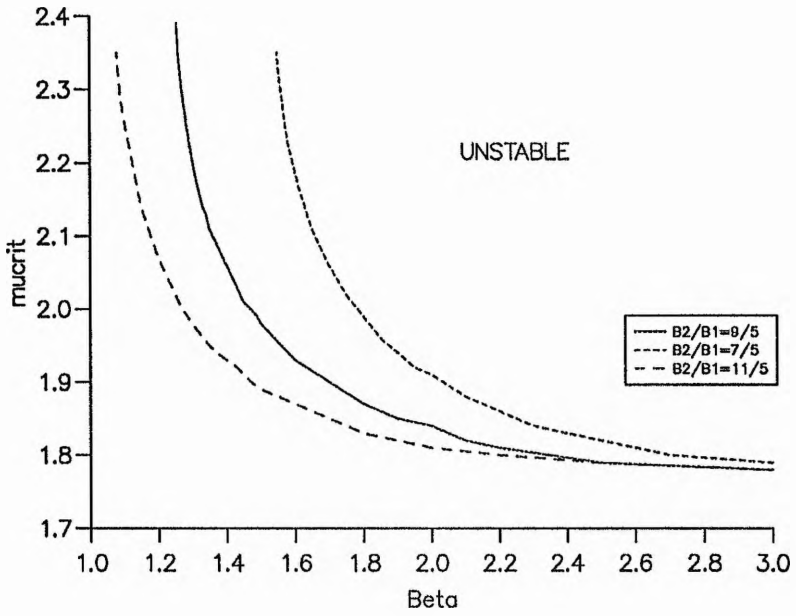

Figure 5.13: μ_{crit} against β for $B_2/B_1 = 7/5$, $B_2/B_1 = 9/5$ and $B_2/B_1 = 11/5$, with $P_0 = 1$, $P_1 = 1$, $a = 1$ and $L = 1$. Equilibria with $\mu > \mu_{crit}$ are definitely unstable.

solution of two systems of coupled ordinary differential equatons, subject to the boundary condition

$$\xi = 0,$$

the integration being performed along field lines.

The method yields three regions in parameter space, one in which the equilibrium is definitely stable, a second in which it is definitely unstable to localized modes and a third in which the stability is undetermined. When we applied the method to analytic Spheromak equilibria, this third region occupied a relatively large part of parameter space as illustrated in Figure (5.14). The application of the method to this particular equilibrium was not, therfore, particularly successful, although the size of the third region may be reduced if the stability of closed field lines is investigated.

Nevertheless, we can still draw some conclusions from our results:

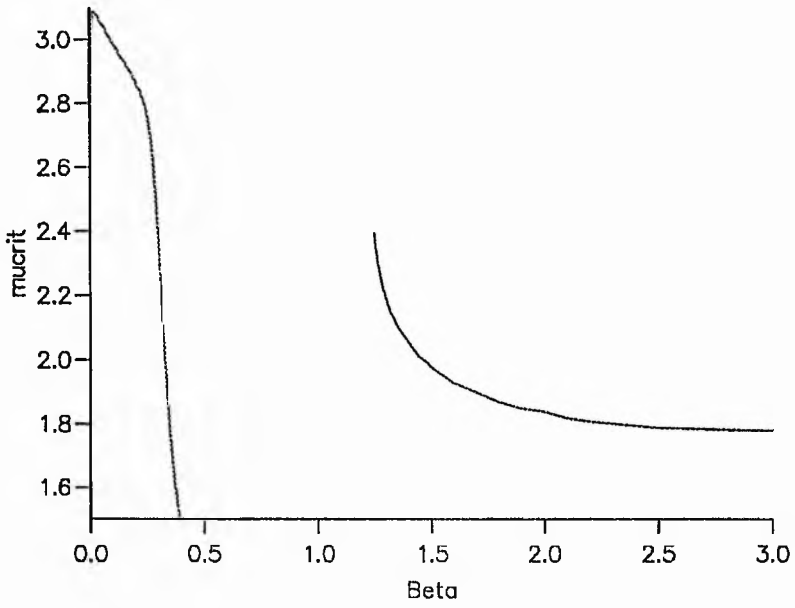

Figure 5.14: μ_{crit} against β for $B_2/B_1 = 9/5$, with $P_0 = 1$, $P_1 = 1$, $a = 1$ and $L = 1$, for both sufficient and necessary conditions.

- Short, open field lines lying across the mouth of the magnetized gun are always stable.

- As the entrance region narrows the stability of the system decreases, probably because of the increased length of the field lines, which reduces the stabilizing effect of the line-tied boundary.

- For small values of β (order (1/10) or less) there is a region of definite stability, but only for values of μ below those needed for closed lines to appear in the equilibria.

- The equilibria are definitely unstable to localised modes for values of β of O(1) or greater, except for equilibria with small values of μ.

Chapter 6

Conclusion

In Chapters 2 and 3 we studied the thermal instability in an equilibrium including two features which exist in coronal plasmas and which may be important in any model describing prominence formation, that is, the finite extent of the magnetic fields and anisotropical thermal conduction. Our investigations led us to the following conclusions:

- The inclusion of thermal conduction perpendicular to the magnetic field lines does not change the conclusions of Cargill and Hood (1989) concerning the thermal instability in line-tied Cartesian fields, namely that increasing the length of the field lines and increasing the magnetic shear help to stabilize the instability. However, we have found that introducing perpendicular thermal conduction into the analysis means that condensations are restricted to a narrow layer around the region where the local isobaric growth rate is largest.

- The thermal instability gives rise to condensations that are highly localized about the plane where the isobaric instability criterion is largest.

- The most unstable thermal mode grows almost isobarically and is decoupled from the magneto-acoustic modes.

- The growth rate of the system is largely unaffected by including the perpendicular conduction, the growth rate being close to the local isobaric growth rate with $\kappa_\perp = 0$.

- The width of the condensations is proportional to $(\kappa_\perp/\kappa_\parallel)^{\frac{1}{4}}$ when the perpendicular conduction coefficient is small. This relationship does not hold for larger values of $\kappa_\perp$, but these larger values are well above the classical value of $\kappa_\perp$. This means that perpendicular thermal conduction gives rise to length-scales across the magnetic field lines that are of the same order as the observed fine-scale structure in prominences. This implies that fine-structure could be a result of the formation process and does not occur after the prominence has been formed.

- The fundamental mode is the most unstable but other modes have growth rates very close to that of the fundamental mode for small values of the perpendicular conduction coefficient $\kappa_\perp$.

The linear time-dependent numerical code we developed to study the thermal instability gave extremely accurate results. This code could be extended to study other geometries (such as cylindrical), more complicated equilibria (such as magnetic shear) or even a non-linear system. The accuracy of the results presented in this Thesis would give us confidence in the results of these further investigations.

In Chapter 4 we showed that a wall of finite conductivity can destabilize ideal MHD instabilities in an analytic RFP equilibrium, which, were the wall perfectly conducting, would be stable. The calculated growth rates of these instabilities give qualitatively the

same results as those found by Hender, Gimblett and Robinson (1989) who investigated these modes using a numerical RFP profile. However, for an analytical Spheromak equilibrium, we did not find any unstable modes using our method. Further research is needed to investigate the nature and growth rates of modes made unstable by a conducting wall surrounding a Spheromak. Possible approaches might include allowing a vacuum to exist between the plasma and the wall.

In Chapter 5 we applied the analysis of De Bruyne (1990), who derived easy tests for necessary and sufficient conditions for the linear stability of two dimensional equilibria, to analytic, spherically symmetric Spheromak equilibria. The size of the region of parameter space in which stability was undetermined was fairly large, but from our results it was possible to arrive at the following conclusions:

- Short, open field lines, lying across the mouth of the magnetized gun, are always stable.

- As the entrance region narrows the stability of the system decreases, probably because of the increased length of the field lines, which reduces the stabilizing effect of the line-tied boundary.

- For small values of β (order (1/10) or less) there is a region of definite stability, but only for values of μ below those needed for closed lines to appear in the equilibria.

- The equilibria are definitely unstable to localised modes for values of β of O(1) or greater, except for equilibria with small values of μ.

Tighter bounds on the stability conditions may be found by investigating closed magnetic field lines, or by using a numerical equilibrium, with a more realistic model of the

pressure and μ profiles within the plasma. A sufficient and necessary condition could be found by solving the full Euler-Lagrange equations of the system bur this would be a very time-consuming process.

Appendix A

Numerical scheme for the MHD equations

One reason for writing a time-dependent numerical code to investigate thermal instabilities was to enable us to move on to an analysis of the non-linear problem. With this in mind, we chose a Lax-Wendroff scheme. In this Appendix, we outline the method of solving the non-linear problem. This also provides the best way to explain our approach to the linear set of differential equations.

A.1 Non-linear scheme

The MHD equations with the non-adiabatic terms included in the energy equation, using a two dimensional Cartesian geometry (axes x and z), can be rewritten in component form as:

$$\frac{\partial \rho}{\partial t} + \frac{\partial}{\partial x}(\rho v_x) + \frac{\partial}{\partial z}(\rho v_z) = 0, \tag{A.1}$$

$$\frac{\partial B_x}{\partial t} + \frac{\partial}{\partial z}(B_x v_z) = \frac{\partial}{\partial z}(B_z v_x), \tag{A.2}$$

$$\frac{\partial B_z}{\partial t} + \frac{\partial}{\partial x}(B_z v_x) = \frac{\partial}{\partial x}(B_x v_z), \tag{A.3}$$

$$\begin{aligned}\frac{\partial}{\partial t}(\rho v_x) + \frac{\partial}{\partial x}\left(\rho v_x^2\right) + \frac{\partial}{\partial z}(\rho v_x v_z) &= -\frac{\partial p}{\partial x} - \frac{\partial}{\partial x}\left(\frac{B^2}{2\mu}\right) \\ &+ \frac{B_x}{\mu}\frac{\partial B_z}{\partial x} + \frac{B_z}{\mu}\frac{\partial B_x}{\partial z},\end{aligned} \tag{A.4}$$

$$\begin{aligned}\frac{\partial}{\partial t}(\rho v_z) + \frac{\partial}{\partial x}(\rho v_x v_z) + \frac{\partial}{\partial z}\left(\rho v_z^2\right) &= -\frac{\partial p}{\partial z} - \frac{\partial}{\partial z}\left(\frac{B^2}{2\mu}\right) \\ &+ \frac{B_x}{\mu}\frac{\partial B_z}{\mu} + \frac{B_z}{\mu}\frac{\partial B_z}{\partial z},\end{aligned} \tag{A.5}$$

$$\begin{aligned}\frac{\partial T}{\partial t} + \frac{\partial}{\partial x}(T v_x) + \frac{\partial}{\partial z}(T V_z) &= -\gamma T\left(\frac{\partial v_z}{\partial x} + \frac{\partial v_x}{\partial z}\right) - \\ \frac{\gamma - 1}{\rho R}\rho^2 \chi T^\alpha &+ \frac{\gamma - a}{\rho R}\left(\frac{\partial}{\partial x}Q_x + \frac{\partial}{\partial z}Q_z\right)\end{aligned} \tag{A.6}$$

where

$$\mathbf{Q} = \left(\kappa_{\|} + \kappa_{\perp}\right)\frac{\mathbf{B}}{\mathbf{B^2}}\left[B_x\frac{\partial T}{\partial x} + B_z\frac{\partial T}{\partial z}\right] + \kappa_{\perp}\nabla T \tag{A.7}$$

and

$$p = R\rho T. \tag{A.8}$$

All the partial differential equations consist of advection terms and source terms, with the energy equation (A.6) also having diffusion terms. For the nonlinear equations we have a Lagrangian system. To illustrate how we can reduce the problem to one-dimensional numerical equations, consider the continuity equation (A.1)

$$\frac{\partial \rho}{\partial t} + \frac{\partial}{\partial x}(\rho v_x) + \frac{\partial}{\partial z}(\rho v_z) = 0$$

This can be solved as two one-dimensional advection equations:

$$\frac{\partial \rho}{\partial t} + \frac{\partial}{\partial x}(\rho v_x) = 0$$

and

$$\frac{\partial \rho}{\partial t} + \frac{\partial}{\partial z}(\rho v_z) = 0$$

if we invoke the concept of operator splitting, which could be written as

$$\rho^{n+1} = L_x \rho^n \qquad (L_x = x \text{ advection operator})$$

$$\rho^{n+2} = L_z \rho^{n+1} \qquad (L_z = z \text{ advection operator})$$

where ρ^n is the value of ρ after the n^{th} time step. This scheme is second order accurate in time if we carry out the operations in the sequence

$$L_x L_z L_z L_x,$$

where L_x and L_z are one-dimensional Lax-Wendroff operators.

The other equations can be solved similarly. The momentum equation can be written as four one-dimensional equations with Lagrangian source terms

$$\begin{aligned}
\frac{\partial}{\partial t}(\rho v_x) + \frac{\partial}{\partial x}\left(\rho v_x^2\right) &= -\frac{\partial p}{\partial x} - \frac{\partial}{\partial x}\left(\frac{B_z^2}{2\mu}\right), \\
\frac{\partial}{\partial t}(\rho v_x) + \frac{\partial}{\partial z}(\rho v_x v_z) &= \frac{B_z}{\mu}\frac{\partial B_x}{\partial x}, \\
\frac{\partial}{\partial t}(\rho v_z) + \frac{\partial}{\partial x}(\rho v_x v_z) &= -\frac{B_x}{\mu}\frac{\partial B_z}{\partial x}, \\
\frac{\partial}{\partial t}(\rho v_z) + \frac{\partial}{\partial z}\left(\rho v_z^2\right) &= -\frac{\partial p}{\partial z} - \frac{\partial}{\partial z}\left(\frac{B_x^2}{2\mu}\right).
\end{aligned}$$

The induction is already in the form of an advection equation.

The energy equation can be written as two one dimensional advection equations and one diffusion equation

$$\begin{aligned}
\frac{\partial T}{\partial t} + \frac{\partial}{\partial x}(T v_x) &= -\gamma T \frac{\partial v_x}{\partial x} - \frac{\gamma - 1}{\rho R}\left(\rho^2 \chi T^{\alpha}\right), \\
\frac{\partial T}{\partial t} + \frac{\partial}{\partial z}(T v_z) &= -\gamma T \frac{\partial v_x}{\partial z}, \\
\frac{\partial T}{\partial t} &= \frac{\gamma - 1}{\rho R}\frac{\partial}{\partial x}(Q_x) + \frac{\partial}{\partial z}(Q_z).
\end{aligned}$$

Thus, we have reduced the equations to a set of one dimensional operators.

If we represent the x,z-plane by a rectangular grid with J cells in the z direction and I cells in the x direction, then the problem can be split into three parts:

1. x scan. J one dimensional advection problems with sources

2. z scan. I one dimensional advection problems with sources

3. Diffusion.

For the linearized case, with Eulerian variables, the diffusion terms can be included in the advection problems as source terms. This avoids the need to include artificial viscosity in the energy equation.

A.2 Linear discretized equations

This section sets out the full discretized equations of the system (3.18) to (3.23). We have an x-scan and a z-scan of one-dimensional advection equations with source terms. The equations include the numerical diffusion that we add. The equilibrium has been assumed to be isothermal, but a non-constant equilibrium temperature could be easily incorporated. We can represent the Lax-Wendroff method as a two-step process involving an intermediate timestep $n + \frac{1}{2}$.

A.2.1 x-scan

In the x scan we advance the variables from the n^{th} timestep to the $n + 1^{th}$ by a two stage process.

First stage

The discretized equations are

$$
\begin{aligned}
\rho_{i,j}^{n+\frac{1}{2}} &= \rho_{i,j}^{n} - \frac{\Delta t}{4\Delta x}(\rho_{i+1,j}^{0} v x_{i+1,j}^{n} - \rho_{i-1,j}^{0} v x_{i-1,j}^{n}) + \xi \frac{\Delta t}{2\Delta x^2}(\rho_{i+1,j}^{n} - 2\rho_{i,j}^{n} + \rho_{i-1,j}^{n}), \\
Bz_{i,j}^{n+\frac{1}{2}} &= Bz_{i,j}^{n} - \frac{\Delta t}{4\Delta x}(B_{i+1,j}^{0} v x_{i+1,j}^{n} - B_{i-1,j}^{0} v x_{i-1,j}^{n}) \\
&+ \xi \frac{\Delta t}{2\Delta x^2}(Bz_{i+1,j}^{n} - 2Bz_{i,j}^{n} + Bz_{i-1,j}^{n}), \\
v x_{i,j}^{n+\frac{1}{2}} &= v x_{i,j}^{n} - \frac{1}{\epsilon^2}\frac{1}{\rho_{i,j}^{0}}\frac{\beta}{2}\left[\frac{\Delta t}{4\Delta x}(\rho_{i+1,j}^{n} - \rho_{i-1,j}^{n}) + \frac{\Delta t}{4\Delta x}(\rho_{i+1,j}^{0} T_{i+1,j}^{n} - \rho_{i-1,j}^{0} T_{i-1,j}^{n})\right] \\
&- \frac{1}{\epsilon^2}\frac{1}{\rho_0}\frac{\Delta t}{4\Delta x}(B_{i+1,j}^{0} Bz_{i+1,j}^{n} - B_{i-1,j}^{0} Bz_{i-1,j}^{n}) \\
&+ \xi \frac{\Delta t}{2\Delta x^2}(v x_{i+1,j}^{n} - 2v x_{i,j}^{n} + v x_{i-1,j}^{n}), \\
v z_{i,j}^{n+\frac{1}{2}} &= v z_{i,j}^{n} + \frac{1}{\epsilon^2}\frac{1}{\rho_{i,j}^{0}} Bx_{i,j}^{n}\frac{\Delta t}{4\Delta x}(B_{i+1,j}^{0} - B_{i-1,j}^{0}) \\
&+ \xi \frac{\Delta t}{2\Delta x^2}(v z_{i+1,j}^{n} - 2v z_{i,j}^{n} + v z_{i-1,j}^{n}), \\
T_{i,j}^{n+\frac{1}{2}} &= T_{i,j}^{n} - (\gamma - 1)\frac{\Delta t}{4\Delta x}(v x_{i+1,j}^{n} - v x_{i-1,j}^{n}) - \alpha \rho_{i,j}^{0} T_{i,j}^{n} + 2\rho_{i,j}^{n} \\
&+ \frac{1}{\rho_{i,j}^{0}}\frac{\tau_{rad}}{\tau_{\perp}}\frac{\Delta t}{2\Delta x^2}(T_{i+1,j}^{n} - 2T_{i,j}^{n} + T_{i-1,j}^{n}).
\end{aligned}
$$

Second stage

The intermediate values of the variables are now used to find the values at the time step $n+1$ using the equations

$$
\begin{aligned}
\rho_{i,j}^{n+1} &= \rho_{i,j}^{n} - \frac{\Delta t}{4\Delta x}(\rho_{i+1,j}^{0} v x_{i+1,j}^{n} - \rho_{i-1,j}^{0} v x_{i-1,j}^{n}) \\
&+ \xi \frac{\Delta t}{2\Delta x^2}(\rho_{i+1,j}^{n} - 2\rho_{i,j}^{n} + \rho_{i-1,j}^{n}), \\
Bz_{i,j}^{n+\frac{1}{2}} &= Bz_{i,j}^{n} - \frac{\Delta t}{4\Delta x}(B_{i+1,j}^{0} v x_{i+1,j}^{n+\frac{1}{2}} - B_{i-1,j}^{0} v x_{i-1,j}^{n+\frac{1}{2}}) \\
&+ \xi \frac{\Delta t}{2\Delta x^2}(Bz_{i+1,j}^{n+\frac{1}{2}} - 2Bz_{i,j}^{n+\frac{1}{2}} + Bz_{i-1,j}^{n+\frac{1}{2}}), \\
v x_{i,j}^{n} &= v x_{i,j}^{n} - \frac{1}{\epsilon^2}\frac{1}{\rho_{i,j}^{0}}\frac{\beta}{2}\left[\frac{\Delta t}{4\Delta x}(\rho_{i+1,j}^{n+\frac{1}{2}} - \rho_{i-1,j}^{n+\frac{1}{2}}) + \frac{\Delta t}{4\Delta x}(\rho_{i+1,j}^{0} T_{i+1,j}^{n+\frac{1}{2}} - \rho_{i-1,j}^{0} T_{i-1,j}^{n+\frac{1}{2}})\right]
\end{aligned}
$$

$$
\begin{aligned}
&- \frac{1}{\epsilon^2}\frac{1}{\rho^0_{i,j}}\frac{\Delta t}{4\Delta x}(B^0_{i+1,j}Bz^{n+\frac{1}{2}}_{i+1,j} - B^0_{i-1,j}Bz^{n+\frac{1}{2}}_{i-1,j}) \\
&+ \xi\frac{\Delta t}{2\Delta x^2}(vx^{n+\frac{1}{2}}_{i+1,j} - 2vx^{n+\frac{1}{2}}_{i,j} + vx^{n+\frac{1}{2}}_{i-1,j}), \\
vz^n_{i,j} &= vz^n_{i,j} + \frac{1}{\epsilon^2}\frac{1}{\rho^0_{i,j}}Bx^{n+\frac{1}{2}}_{i,j}\frac{\Delta t}{4\Delta x}(B^0_{i+1,j} - B^0_{i-1,j}) \\
&+ \xi\frac{\Delta t}{2\Delta x^2}(vz^{n+\frac{1}{2}}_{i+1,j} - 2vz^{n+\frac{1}{2}}_{i,j} + vz^{n+\frac{1}{2}}_{i-1,j}), \\
T^n_{i,j} &= T^n_{i,j} - (\gamma-1)\frac{\Delta t}{4\Delta x}(vx^{n+\frac{1}{2}}_{i+1,j} - vx^{n+\frac{1}{2}}_{i-1,j}) - \alpha\rho^0_{i,j}T^{n+\frac{1}{2}}_{i,j} \\
&+ 2\rho^{n+\frac{1}{2}}_{i,j} + \frac{1}{\rho^0_{i,j}}\frac{\tau_{rad}}{\tau_\perp}\frac{\Delta t}{2\Delta x^2}(T^{n+\frac{1}{2}}_{i+1,j} - 2T^{n+\frac{1}{2}}_{i,j} + T^{n+\frac{1}{2}}_{i-1,j}).
\end{aligned}
$$

B_x is not involved in the x-scan, so

$$Bx^{n+1}_{i,j} = Bx^n_{i,j}$$

A.2.2 z-scan

The z-scan is written similarly, here going from the $(n+1)^{th}$ timestep to the $(n+2)^{th}$.

First stage

The discretized equations are

$$
\begin{aligned}
\rho^{n+\frac{3}{2}}_{i,j} &= \rho^{n+1}_{i,j} - \rho^0_{i,j}\frac{\Delta t}{4\Delta z}(vz^{n+1}_{i+1,j} - vz^{n+1}_{i-1,j}) + \xi\frac{\Delta t}{2\Delta z^2}(\rho^{n+1}_{i+1,j} - 2\rho^{n+1}_{i,j} + \rho^{n+1}_{i-1,j}), \quad \text{(A.9)} \\
Bx^{n+\frac{3}{2}}_{i,j} &= Bx^{n+1}_{i,j} + \frac{\Delta t}{4\Delta z}B^0_{i,j}(vx^{n+1}_{i+1,j} - vx^{n+1}_{i-1,j}) \\
&+ \xi\frac{\Delta t}{2\Delta z^2}(Bx^{n+1}_{i+1,j} - 2Bx^{n+1}_{i,j} + Bx^{n+1}_{i-1,j}), \\
vx^{n+\frac{3}{2}}_{i,j} &= vx^{n+1}_{i,j} = \frac{1}{\epsilon^2}\frac{1}{\rho^0_{i,j}}B^0_{i,j}\frac{\Delta t}{4\Delta z}(Bx^{n+1}_{i+1,j} - Bx^{n+1}_{i-1,j}) \\
&+ \xi\frac{\Delta t}{2\Delta z^2}(vx^{n+1}_{i+1,j} - 2vx^{n+1}_{i,j} + vx^{n+1}_{i-1,j}), \\
vz^{n+\frac{3}{2}}_{i,j} &= vz^{n+1}_{i,j} - \frac{1}{\epsilon^2}\frac{1}{\rho^0_{i,j}}\frac{\beta}{2}\left[\frac{\Delta t}{4\Delta z}(\rho^{n+1}_{i+1,j} - \rho^{n+1}_{i-1,j}) + \rho^0_{i,j}\frac{\Delta t}{4\Delta z}(T^{n+1}_{i+1,j} - T^{n+1}_{i-1,j})\right] \\
&+ \xi\frac{\Delta t}{2\Delta z^2}(vz^{n+1}_{i+1,j} - 2vz^{n+1}_{i,j} + vz^{n+1}_{i-1,j}),
\end{aligned}
$$

$$
\begin{aligned}
T_{i,j}^{n+\frac{3}{2}} &= T_{i,j}^{n+1} - (\gamma-1)\frac{\Delta t}{4\Delta z}(vz_{i+1,j}^{n+1} - vz_{i-1,j}^{n+1}) \\
&+ \frac{1}{\rho_{i,j}^0}\frac{\tau_{rad}}{\tau_{\|}}\frac{\Delta t}{2\Delta z^2}(T_{i+1,j}^{n+1} - 2T_{i,j}^{n+1} + T_{i-1,j}^{n+1}).
\end{aligned}
$$

Second stage

The intermediate values of the variables are now used to find the values at the time step $n+2$ using the equations

$$
\begin{aligned}
\rho_{i,j}^{n+2} &= \rho_{i,j}^{n+1} - \rho_{i,j}^0\frac{\Delta t}{4\Delta z}(vz_{i+1,j}^{n+\frac{3}{2}} - vz_{i-1,j}^{n+\frac{3}{2}}) + \xi\frac{\Delta t}{2\Delta z^2}(\rho_{i+1,j}^{n+\frac{3}{2}} - 2\rho_{i,j}^{n+1} + \rho_{i-1,j}^{n+1}), \\
Bx_{i,j}^{n+2} &= Bx_{i,j}^{n+1} + \frac{\Delta t}{4\Delta z}B_{i,j}^0(vx_{i+1,j}^{n+\frac{3}{2}} - vx_{i-1,j}^{n+\frac{3}{2}}) \\
&+ \xi\frac{\Delta t}{2\Delta z^2}(Bx_{i+1,j}^{n+\frac{3}{2}} - 2Bx_{i,j}^{n+\frac{3}{2}} + Bx_{i-1,j}^{n+1}), \\
vx_{i,j}^{n+2} &= vx_{i,j}^{n+1} = \frac{1}{\epsilon^2}\frac{1}{\rho_{i,j}^0}B_{i,j}^0\frac{\Delta t}{4\Delta z}(Bx_{i+1,j}^{n+\frac{3}{2}} - Bx_{i-1,j}^{n+\frac{3}{2}}) \\
&+ \xi\frac{\Delta t}{2\Delta z^2}(vx_{i+1,j}^{n+\frac{3}{2}} - 2vx_{i,j}^{n+\frac{3}{2}} + vx_{i-1,j}^{n+\frac{3}{2}}), \\
vz_{i,j}^{n+2} &= vz_{i,j}^{n+1} - \frac{1}{\epsilon^2}\frac{1}{\rho_{i,j}^0}\frac{\beta}{2}\left[\frac{\Delta t}{4\Delta z}(\rho_{i+1,j}^{n+\frac{3}{2}} - \rho_{i-1,j}^{n+\frac{3}{2}}) + \rho_{i,j}^0\frac{\Delta t}{4\Delta z}(T_{i+1,j}^{n+\frac{3}{2}} - T_{i-1,j}^{n+\frac{3}{2}})\right] \\
&+ \xi\frac{\Delta t}{2\Delta z^2}(vz_{i+1,j}^{n+\frac{3}{2}} - 2vz_{i,j}^{n+\frac{3}{2}} + vz_{i-1,j}^{n+\frac{3}{2}}), \\
T_{i,j}^{n+2} &= T_{i,j}^{n+1} - (\gamma-1)\frac{\Delta t}{4\Delta z}(vz_{i+1,j}^{n+\frac{3}{2}} - vz_{i-1,j}^{n+\frac{3}{2}}) \\
&+ \frac{1}{\rho_{i,j}^0}\frac{\tau_{rad}}{\tau_{\|}}\frac{\Delta t}{2\Delta z^2}(T_{i+1,j}^{n+\frac{3}{2}} - 2T_{i,j}^{n+\frac{3}{2}} + T_{i-1,j}^{n+\frac{3}{2}})
\end{aligned}
$$

B_z is not involved in the x-scan, so

$$
Bz_{i,j}^{n+2} = Bz_{i,j}^{n+1}
$$

Appendix B

The two-dimensional energy principle

Following Hu (1987), we start by resolving ξ_p as follows:

$$\xi_p = \xi_{\|p} + \xi_{\perp p}, \quad \xi_{\|p} = \frac{\xi_p \cdot \mathbf{B}_p}{B_p}\mathbf{B}_p, \quad \xi_{\perp p} = -\frac{A_1}{r^2 B_p^2}\nabla A, \quad A_1 = -\xi_p \cdot \nabla A, \tag{B.1}$$

and letting

$$\mathbf{e}_1 = \frac{\mathbf{B}}{B}, \qquad \mathbf{e}_2 = \frac{\nabla A}{|\nabla A|}.$$

Using the equations of two dimensional magnetostatic equilibrium (5.10) and (5.11) we can derive each term in the integrand of equatiun (5.13) as follows

$$\begin{aligned} |\nabla \times (\xi \times \mathbf{B})|^2 &= \left|\nabla A_1 \times \frac{\mathbf{e}_\theta}{r} + \frac{G}{r^2}\left(\mathbf{e}_1 \frac{\partial \xi_r}{\partial \theta} + \mathbf{e}_2 \frac{\partial \xi_z}{\partial \theta}\right) - \frac{\mathbf{B}_p}{r}\frac{\partial \xi_\theta}{\partial \theta}\right|^2 \\ &+ \left|\frac{1}{r}\left(G' A_1 - G\nabla \cdot \xi_p\right) + \frac{2G}{r^2}\xi_p \cdot \nabla r + r\mathbf{B}_p \cdot \nabla \frac{\xi_\theta}{r}\right|^2, \end{aligned} \tag{B.2}$$

$$\begin{aligned} \nabla \times \mathbf{B} \cdot [\xi \times \nabla \times (\xi \times \mathbf{B})] &= -\frac{J}{r^2}\left[\xi_p \cdot \nabla A_1 + \mathbf{B}_\theta \cdot \left(\frac{\partial \xi_p}{\partial \theta} \times \xi_p\right) + \frac{A_1}{r}\frac{\partial \xi_\theta}{\partial \theta}\right] \\ &- \frac{G' A_1}{r^2}\left[G' A_1 - G\nabla \cdot \xi_p + \frac{2G}{r}\xi_p \cdot \nabla r + r^2 \mathbf{B}_p \cdot \nabla \frac{\xi_\theta}{r}\right] \end{aligned}$$

$$+ \quad \frac{G'\xi_\theta}{r^2}\left(r\mathbf{B}_p\cdot\nabla A_1+\frac{G}{r}\frac{\partial A_1}{\partial\theta}\right), \tag{B.3}$$

so

$$\begin{aligned}|\nabla\times(\xi\times\mathbf{B})|^2 \;+\; & \nabla\times\mathbf{B}\cdot[\xi\times\nabla\times(\xi\times\mathbf{B})]\\ =\;& \left|\nabla A_1\times\frac{\mathbf{e}_\theta}{r}+\frac{G}{r^2}\left(\mathrm{e}_1\frac{\partial\xi_r}{\partial\theta}+\mathrm{e}_2\frac{\partial\xi_z}{\partial\theta}\right)-\frac{\mathbf{B}_p}{r}\frac{\partial\xi_\theta}{\partial\theta}\right|^2\\ +\;& \left|rG\nabla\cdot\frac{\xi_p}{r^2}-r\mathbf{B}_p\cdot\nabla\frac{\xi_\theta}{r}\right|^2+\frac{GG'\xi_\theta}{r^3}\frac{\partial A_1}{\partial\theta}\\ -\;& \frac{J}{r^2}\left[\xi_p\cdot\nabla A_1+\mathbf{B}_\theta\cdot\left(\frac{\partial\xi_p}{\partial\theta}\times\xi_p\right)+\frac{A_1}{r}\frac{\partial\xi_\theta}{\partial\theta}\right]\\ +\;& \frac{G'A_1}{r^2}\left[-G\nabla\cdot\xi_p+\frac{2G}{r}\xi_p\cdot\nabla r\right]+\nabla\cdot\left(\frac{G'}{r}\xi_\theta A_1\mathbf{B}_p\right),\end{aligned} \tag{B.4}$$

and

$$\begin{aligned}\beta_0(\xi\cdot\nabla p)(\nabla\cdot\xi) \;+\; & \beta_0\gamma p(\nabla\cdot\xi)^2=\gamma\beta_0 p|\nabla\cdot\xi|^2-\beta_0A_1\frac{dp}{dA}\nabla\cdot\xi_p\\ -\;& \beta_0\frac{A_1}{r}\frac{dp}{dA}\frac{\partial\xi_\theta}{\partial\theta},\end{aligned} \tag{B.5}$$

$$\begin{aligned}\frac{J}{r^2}\xi_p\cdot\nabla A_1+\frac{GG'}{r^2}A_1\nabla\cdot\xi_p+\beta_0A_1\frac{dp}{dA}\nabla\cdot\xi_p \;=\;& \nabla\cdot\left(\frac{1}{r^2}JA_1\xi_p\right)+|A_1|^2\frac{\partial}{\partial A}\left(\frac{J}{r^2}\right)\\ -\;& A_1\frac{\partial}{\partial r}\left(\frac{J}{r^2}\right)\xi_p\cdot\nabla r,\end{aligned} \tag{B.6}$$

$$\frac{1}{r^3}GG'\xi_\theta\frac{\partial A_1}{\partial\theta}-\beta_0\frac{A_1}{r}\frac{dp}{dA}\frac{\partial\xi_\theta}{\partial\theta}=-\frac{JA_1}{r^3}\frac{\partial\xi_\theta}{\partial\theta}+\frac{\partial}{\partial\theta}\left(\frac{1}{r^3}GG'\xi_\theta A_1\right), \tag{B.7}$$

and

$$\frac{2}{r^3}GG'A_1\xi_p\cdot\nabla r+A_1\frac{\partial}{\partial r}\left(\frac{J}{r^2}\right)\xi_p\cdot\nabla r=0. \tag{B.8}$$

Note, that from the boundary condition (5.12), the volume integrals of the last term in (B.4), (B.6) and (B.7) vanish after transforming into surface integrals. Inserting (B.4) to (B.6) into equation (5.13) leads to

$$\delta W \;=\; C\int[\left[\frac{1}{B_p^2r^2}|\mathbf{B}_p\cdot\nabla A_1|^2+\frac{|\nabla A\cdot\nabla A_1|^2}{r^4B_p^2}+\left|\frac{B_\theta}{r^2}\left(\mathrm{e}_1\frac{\partial\xi_{\parallel p}}{\partial\theta}+\mathrm{e}_2\frac{\partial\xi_{\perp p}}{\partial\theta}\right)-\frac{\mathbf{B}_p}{r^2}\frac{\partial\xi_\theta}{\partial\theta}\right|^2\right]$$

$$+ \quad r^2 \left| G\nabla \cdot \frac{\xi_p}{r^2} - \mathbf{B}_p \cdot \nabla \frac{\xi_\theta}{r} \right|^2 - \frac{J}{r^2} \mathbf{B}_\theta \cdot \left(\frac{\partial \xi_p}{\partial \theta} \times \xi_p \right)$$

$$- \quad \frac{2}{r^3} \frac{\partial \xi_\theta}{\partial \theta} \left(\nabla A \cdot \nabla A_1 + J A_1 \right) - \frac{\partial}{\partial A} \left(\frac{J}{r^2} \right) |A_1|^2 - \gamma \beta_0 p \, |\nabla \cdot \xi|^2$$

$$+ \frac{2}{r^2} \left[\frac{B_\theta}{r B_p} \frac{\partial \xi_{\| p}}{\partial \theta} \nabla A \cdot \nabla A_1 + \frac{B_\theta}{r B_p^2} \frac{\partial A_1}{\partial \theta} \mathbf{B}_p \cdot \nabla A_1 \right]] dV \tag{B.9}$$

and we also have

$$\left| B_\theta \left(\mathbf{e}_1 \frac{\partial \xi_{\| p}}{\partial \theta} + \mathbf{e}_2 \frac{\partial \xi_{\perp p}}{\partial \theta} \right) - \mathbf{B}_p \frac{\partial \xi_\theta}{\partial \theta} \right|^2 = \left| B_\theta \frac{\partial \xi_{\| p}}{\partial \theta} - B_p \frac{\partial \xi_\theta}{\partial \theta} \right|^2 + \frac{B_\theta^2}{r^2 B_p^2} \left| \frac{\partial A_1}{\partial \theta} \right|^2, \tag{B.10}$$

$$\left| B_\theta \frac{\partial \xi_{\| p}}{\partial \theta} - B_p \frac{\partial \xi_\theta}{\partial \theta} \right|^2 - \frac{2}{r} \frac{\partial \xi_\theta}{\partial \theta} \left(\nabla A \cdot \nabla A_1 + J A_1 \right) =$$

$$\left| \frac{1}{r B_p} \left(\nabla A \cdot \nabla A_1 + J A_1 \right) + B_\theta \frac{\partial \xi_{\| p}}{\partial \theta} - B_p \frac{\partial \xi_\theta}{\partial \theta} \right|^2 - \frac{2 B_\theta}{r B_p} \frac{\partial \xi_{\| p}}{\partial \theta} \left(\nabla A \cdot \nabla A_1 + J A_1 \right)$$

$$- \frac{1}{r^2 B_p^2} \left| \nabla A \cdot \nabla A_1 + J A_1 \right|^2, \tag{B.11}$$

$$\mathbf{B}_\theta \cdot \left(\frac{\partial \xi_p}{\partial \theta} \times \xi_p \right) = \frac{B_\theta}{r^2 B_p} \left[\frac{\partial}{\partial \theta} (\xi_{\| p} A_1) - 2 A_1 \frac{\partial \xi_{\| p}}{\partial \theta} \right], \tag{B.12}$$

$$- \frac{1}{r^2 B_p^2} \left| \nabla A \cdot \nabla A_1 + J A_1 \right|^2 = - \frac{1}{r^2 B_p^2} \left| \nabla A \cdot \nabla A_1 \right|^2 - \frac{J^2}{r^2 B_p^2} |A_1|^2 - \frac{2J}{r^2 B_p^2} A_1 \left[\nabla A \cdot \nabla A_1 \right], \tag{B.13}$$

and

$$\frac{1}{r^2 B_p^2} \left| \nabla A \cdot \nabla A_1 \right|^2 + \frac{B_\theta^2}{r^2 B_p^2} \left| \frac{\partial A_1}{\partial \theta} \right|^2 - \frac{1}{r^2 B_p^2} \left| \nabla A \cdot \nabla A_1 + J A_1 \right|^2 + \frac{2 B_\theta}{r B_p^2} \frac{\partial A_1}{\partial \theta} \mathbf{B}_p \cdot \nabla A_1 =$$

$$- \frac{J^2}{r^2 B_p^2} |A_1|^2 + r^2 |A_1|^2 \nabla \cdot \left(\frac{J \nabla A}{r^4 B_p^2} \right) - r^2 \nabla \cdot \left[\frac{J |A_1|^2}{r^4 B_p^2} \nabla A \right]. \tag{B.14}$$

The volume integral of the last term in equation (B.14) vanishes after being transformed into a surface integral and the two dimensional energy integral (5.14) is obtained by substitution.

Appendix C

An expression for δW

We wish to rewrite the expression for δW in the form $\mathcal{I} + \mathcal{J}$. Our starting point is equation (5.14), which is

$$\begin{aligned}\delta W &= C\int[\frac{1}{r^2B_p^2}\left|\mathbf{B}\cdot\nabla A_1\right|^2+\frac{V}{r^2}\left|A_1\right|^2+r^2\left|G\nabla\cdot\left(\frac{\xi_p}{r^2}\right)-\mathbf{B}_p\cdot\nabla\left(\frac{\xi_\theta}{r}\right)\right|^2 \\ &+ \frac{1}{r^2}\left|\frac{1}{rB_p}\left(\nabla A\cdot\nabla A_1+JA_1\right)+\frac{G}{r}\frac{\partial\xi_{\|p}}{\partial\theta}-B_p\frac{\partial\xi_\theta}{\partial\theta}\right|^2 \\ &+ \gamma\beta_0 p\left|\nabla\cdot\xi\right|^2]dV\end{aligned}$$

with

$$V = r^2\nabla\cdot\left(\frac{J\nabla A}{r^4B_p^2}\right)-\frac{J^2}{r^2B_p^2}-r^2\frac{\partial}{\partial A}\left(\frac{J}{r^2}\right)$$

$$A_1 = -\xi_p\cdot\nabla A$$

$$\xi = \xi_p + \xi_\theta \mathbf{e}_\theta$$

and

$$\xi_{\|p} = \frac{\xi_p\cdot\mathbf{B}_p}{B_p}.$$

Note that $\partial/\partial A$ stands for the derivative with respect to A while r is kept constant and $\partial/\partial r$ stands for the derivative with respect to r while A is kept constant.

Now we introduce the notations (see De Bruyne, 1990)

$$\begin{aligned}
\tilde{F} &= B_p\frac{\partial\tilde{\xi}_A}{\partial a} + BB_p\frac{\partial\tilde{\xi}_n}{\partial n} - \frac{J}{r^2}\tilde{\xi}_A,\\
a_1 &= -B\frac{\partial}{\partial s}(B_p^2\tilde{\xi}_n) - GB_p\left(\frac{\partial}{\partial a}\left(\frac{1}{r^2}\right)\tilde{\xi}_A + B\frac{\partial}{\partial n}\left(\frac{1}{r^2}\right)\tilde{\xi}_n\right),\\
a_2 &= -2B_p\left(\frac{J}{r^2} + \frac{\partial B_p}{\partial a}\right)\tilde{\xi}_A + GB_pB\frac{\partial\tilde{\xi}_n}{\partial s},\\
a_3 &= B\frac{\partial\tilde{\xi}_{||}}{\partial s},
\end{aligned}$$

and use the transformations

$$A_1 = B_p\xi_A,$$

$$\frac{\partial}{\partial A}\left(\frac{J}{r^2}\right) = \frac{1}{B_p}\frac{\partial}{\partial a}\left(\frac{J}{r^2}\right) - \frac{1}{B_p}\frac{\partial r}{\partial a}\frac{\partial}{\partial r}\left(\frac{J}{r^2}\right),$$

$$\frac{V}{r^2} = -\frac{2J}{r^2B_p^2}\left(\frac{J}{r^2} + \frac{\partial B_p}{\partial a}\right) + \frac{GG'}{B_p}\frac{\partial}{\partial a}\left(\frac{1}{r^2}\right),$$

$$-G\nabla\cdot(\frac{1}{r^2}\xi_p) + \mathbf{B}_p\cdot\nabla\left(\frac{\xi_0}{r}\right) = -\frac{G}{r^2}\tilde{F} + a_1,$$

$$-\frac{1}{B_p}\left(\frac{\nabla A\cdot\nabla A_1}{r^2} + \frac{JA_1}{r^2}\right) - \frac{B_p}{r}\frac{\partial\xi_0}{\partial 0} + \frac{G}{r^2}\frac{\partial\xi_{||p}}{\partial 0} = -B_p\tilde{F} + a_2,$$

$$\nabla\cdot\xi = \tilde{F} + a_3.$$

Noting that for an equilibrium quantity h,

$$\frac{G}{r}\frac{\partial h}{\partial s} = B_p\frac{\partial h}{\partial n},$$

we can rewrite the final three terms in the integrand of equation (5.14) as

$$\begin{aligned}
r^2\left(-\frac{G}{r^2}\tilde{F} + a_1\right)^2 + \left(-B_p\tilde{F} + a_2\right)^2 + \gamma\beta_0 p\left(\tilde{F} + a_3\right)^2 &= r^2a_1^2 + a_2^2 + \gamma\beta_0 pa_3^2 +\\
(B^2 + \gamma\beta_0 p)\left[\tilde{F} + \frac{-Ga_1 - B_pa_2 + \gamma\beta_0 pa_3}{B^2 + \gamma\beta_0 p}\right]^2 &- \frac{(-Ga_1 - B_pa_2 + \gamma\beta_0 pa_3)^2}{B^2 + \gamma\beta_0 p}.
\end{aligned}$$

Now making use of the formulae

$$-Ga_1 - B_pa_2 + \gamma\beta_0 pa_3 = \gamma\beta_0 pB\frac{\partial\tilde{\xi}_{||}}{\partial s} + \left(2\beta_0\frac{dp}{dA}B_p + \frac{\partial B^2}{\partial a}\right)\xi_A + \frac{\partial B^2}{\partial n}\xi_n,$$

and

$$2\frac{G}{r^2}\left(\frac{J}{r^2}+\frac{\partial B_p}{\partial a}\right)-GB_p\frac{\partial}{\partial a}\left(\frac{1}{r^2}\right)=\frac{G}{r^2B_p}\left(2\beta_0\frac{dp}{dA}B_p+\frac{1}{r^2}\frac{\partial}{\partial a}(r^2B^2)\right),$$

and completing the squares in $\partial\tilde{\xi}_{\|}/\partial s$ and $\partial\tilde{\xi}_n/\partial s$, δW finally takes the form

$$\delta W = C(\mathcal{I}+\mathcal{J}),$$

where

$$\begin{aligned}\mathcal{I} &= \int[\frac{B^2}{r^2E_p^2}\left[\frac{\partial}{\partial s}(B_p^2\tilde{\xi}_A)\right]^2-\left[\frac{2J}{r^2}\left(\frac{J}{r^2}+\frac{\partial B_p}{\partial a}\right)+\frac{2GG'}{r^3}B_p\frac{\partial r}{\partial a}\right]\xi_A^2\\ &+ \frac{\gamma\beta_0 p}{B^2+\gamma\beta_0 p}\left[B^2\frac{\partial\tilde{\xi}_{\|}}{\partial s}-\frac{1}{B}\left(\left(2\beta_0\frac{dp}{dA}B_p+\frac{\partial B^2}{\partial a}\right)\xi_A+\frac{\partial B^2}{\partial n}\xi_n\right)\right]^2\\ &+ r^2\left[B_p\frac{\partial}{\partial s}(B^2\tilde{\xi}_n)-\frac{G}{BB_pr^2}\left(2\beta_0\frac{dp}{dA}B_p+\frac{1}{r^2}\frac{\partial}{\partial a}\left(r^2B^2\right)\right)\xi_A\right]^2]dV, \qquad \text{(C.1)}\end{aligned}$$

and

$$\begin{aligned}\mathcal{J} &= \int(B^2+\gamma\beta_0 p)[B_p\frac{\partial\tilde{\xi}_A}{\partial a}+BB_p\frac{\partial\tilde{\xi}_n}{\partial n}\\ &- \frac{J}{r^2}\tilde{\xi}_A+\frac{\gamma\beta_0 p}{B^2+\gamma\beta_0 p}\left(B\frac{\partial\tilde{\xi}_{\|}}{\partial s}\right)\\ &+ \frac{1}{B^2+\gamma\beta_0 p}\left[\left(2\beta_0\frac{dp}{dA}B_p+\frac{\partial B^2}{\partial a}\right)\xi_A+\frac{\partial B^2}{\partial n}\xi_n\right]]^2dV. \qquad \text{(C.2)}\end{aligned}$$

Appendix D

The Euler-Lagrange equations for the ballooning approximation

The leading order contribution to δW in the ballooning ordering gives:

$$\begin{aligned}\delta W_{ball} &= C\int dV\cos^2(mS)[\frac{B^2}{r^2B_p^2}\left[\frac{\partial y_1}{\partial s}\right]^2-\left[\frac{2J}{r^2}\left(\frac{J}{r^2}+\frac{\partial B_p}{\partial a}\right)+\frac{2GG'}{r^3B_p}\frac{\partial r}{\partial a}\right]\frac{y_1^2}{B_p^2}\\ &+ \frac{\gamma\beta_0 p}{B^2+\gamma\beta_0 p}\left[B^2\frac{\partial y_2}{\partial s}-\frac{1}{B}\left(2\beta_0\frac{dp}{dA}B_p+\frac{\partial B^2}{\partial a}+\frac{\nabla A\cdot\nabla S}{r^2B}\frac{\partial B^2}{\partial n}\right)\frac{y_1}{B_p}\right]^2\\ &+ r^2\left[B_p\frac{\partial}{\partial s}\left(\frac{\nabla A\cdot\nabla S}{r^2B_p^2}y_1\right)-\frac{G}{BB_p^2r^2}\left(2\beta_0\frac{dp}{dA}B_p+\frac{1}{r^2}\frac{\partial}{\partial a}\left(r^2B^2\right)\right)y_1\right]^2\text{]}\end{aligned} \tag{D.1}$$

This can be rearranged as

$$\begin{aligned}\delta W_{ball} &= C\int dV\cos^2 mS[\frac{B^2}{r^2B_p^2}\left[\frac{\partial y_1}{\partial s}\right]^2-\left[\frac{2J}{r^2}\left(\frac{J}{r^2}+\frac{\partial B_p}{\partial a}\right)+\frac{2GG'}{r^3B_P}\frac{\partial r}{\partial a}\right]\frac{y_1^2}{B_p^2}\\ &+ \frac{\gamma\beta_0 p}{B^2+\gamma\beta_0 p}\left[B^2\frac{\partial y_2}{\partial s}-\frac{1}{B}\left(2\beta_0\frac{dp}{dA}B_p+\frac{\partial B^2}{\partial a}+\frac{B_p^2}{B}y_5\frac{\partial B^2}{\partial n}\right)\frac{y_1}{B_p}\right]^2\\ &+ r^2\left[B_py_5\frac{\partial y_1}{\partial s}-y_1\left(\frac{B_p}{B}\frac{G'}{r^2}+\frac{GJ}{r^4BB_p}\right)\right]^2\text{]},\end{aligned} \tag{D.2}$$

where

$$y_5=\frac{\nabla A\cdot\nabla S}{r^2B_p^2}.$$

This expression is integrated with respect to the volume element dV, where $dV = da\ dn\ ds$. We can easily integrate in the flux surfaces (integration by dn) and across the flux surfaces (integration by da) if we assign Dirac Delta properties to a:

$$\text{e.g.} \quad \int_{-\infty}^{\infty} \xi_n^2 \mathrm{da} = 1 \quad \text{etc.}$$

this highlights a specific field line. We are left with a one-dimensional integral that can be minimized using calculus of variations with respect to y_1 and y_2, subject to the normalizing condition

$$L = \int y_1^2 \frac{f^2}{B_p^2 r^2} dV = \text{ constant}$$

where f^2 is a positive function (this excludes the trivial solution $\xi = 0$).

To minimize, let

$$Y_1(s) = y_1(s) + \epsilon\eta(s)$$

and

$$Y_2(s) = y_2(s) + \epsilon\zeta(s)$$

where

$$\int \eta(s)ds = \int \zeta(s)ds = 0$$

on the surface.

Then let

$$I(\epsilon) = \int f(s, Y_1, Y_2, Y_5')ds,$$

$$L(\epsilon) = \int g(s, Y_1)ds,$$

and then let

$$I^* = I(\epsilon) + \lambda L(\epsilon),$$

where λ is a Lagrange multiplier. Now

$$\frac{\partial I^*}{\partial \epsilon} = 0 \quad \text{when} \quad \epsilon = 0$$

will give the minimum, and I^* can be written as

$$\begin{aligned}
I^* &= C \int ds [\frac{1}{r^2 B_p^2} [\mathbf{B} \cdot \nabla (Y_1 - \epsilon\eta)]^2 \\
&- \left[\frac{2J}{r^2}\left(\frac{J}{r^2} + \frac{\partial B_p}{\partial a}\right) + \frac{2GG'}{r^3} B_p \frac{\partial r}{\partial a}\right] \frac{(Y_1 - \epsilon\eta)^2}{B_p^2} \\
&+ \frac{\gamma\beta_0 p}{B^2 + \gamma\beta_0 p} \frac{1}{B^2 B_p^2} \left[2\beta_0 \frac{dp}{dA} + \frac{\partial B^2}{\partial a} + \frac{B_p^2}{B}\frac{\partial B^2}{\partial n} y_5\right]^2 (Y_1 - \epsilon\eta)^2 \\
&+ r^2 \left[\frac{B_p G'}{B r^2} + \frac{GJ}{r^4 B B_p}\right]^2 (Y_1 - \epsilon\eta)^2 \\
&+ \frac{\gamma\beta_0 p B^2}{B^2 + \gamma\beta_0 p} [\mathbf{B} \cdot \nabla (Y_2 - \epsilon\zeta)]^2 + \frac{r^2 B_p^2}{B^2} y_5^2 [\mathbf{B} \cdot \nabla (Y_1 - \epsilon\eta)]^2 \\
&- \frac{2}{B_p} \frac{\gamma\beta_0 p}{B^2 + \gamma\beta_0 p} \left(2\beta_0 \frac{dp}{dA} B_p + \frac{\partial B^2}{\partial a} + \frac{B_p^2}{B}\frac{\partial B^2}{\partial n} y_5\right) \mathbf{B} \cdot \nabla (Y_2 - \epsilon\zeta)(Y_1 - \epsilon\eta) \\
&- 2\frac{r^2 B_p}{B} y_5 \left(\frac{B_p}{B}\frac{G'}{r^2} + \frac{GJ}{r^4 B B_p}\right) \mathbf{B} \cdot \nabla (Y_1 - \epsilon\eta)(Y_1 - \epsilon\eta). \qquad \text{(D.3)}
\end{aligned}$$

Using the identities

$$\begin{aligned}
\frac{\partial}{\partial \epsilon} a [\mathbf{B} \cdot \nabla (Y_1 - \epsilon\eta)]^2 |_{\epsilon=0} &= 2\eta \mathbf{B} \cdot \nabla [a \mathbf{B} \cdot \nabla (y_1)], \\
\frac{\partial}{\partial \epsilon} (Y_1 - \epsilon\eta)^2 |_{\epsilon=0} &= -2\eta y_1, \\
\frac{\partial}{\partial \epsilon} a [\mathbf{B} \cdot \nabla (Y_1 - \epsilon\eta)(Y_1 - \epsilon\eta)] |_{\epsilon=0} &= \eta y_1 \mathbf{B} \cdot \nabla a, \\
\frac{\partial}{\partial \epsilon} [(Y_1 - \epsilon\eta)(Y_2 - \epsilon\zeta)] |\epsilon = 0 &= -\zeta y_1 - \eta y_2, \\
\frac{\partial}{\partial \epsilon} a [\mathbf{B} \cdot \nabla (Y_1 - \epsilon\eta)(Y_2 - \epsilon\zeta)] |_{\epsilon=0} &= -\zeta a \mathbf{B} \cdot \nabla y_1 + \eta \mathbf{B} \cdot \nabla (a y_2), \\
\frac{\partial}{\partial \epsilon} a [\mathbf{B} \cdot \nabla (Y_2 - \epsilon\zeta)(Y_1 - \epsilon\eta)] |_{\epsilon=0} &= -\eta a \mathbf{B} \cdot \nabla y_2 + \zeta \mathbf{B} \cdot \nabla (a y_1),
\end{aligned}$$

and equating the terms in η to 0 and the terms in ζ to 0 we get the Euler-Lagrange equations:

$$\mathbf{B} \cdot \nabla \left(\frac{1}{r^2 B_p^2} \mathbf{B} \cdot \nabla y_1\right) + \mathbf{B} \cdot \nabla \left(\frac{r^2 B_p^2}{B^2} y_5^2 \mathbf{B} \cdot \nabla y_1\right) - r^2 \left[\frac{B_p G'}{B r^2} + \frac{GJ}{r^4 B B_p}\right]^2 y_1$$

$$
\begin{aligned}
&+ \quad \frac{1}{B_p}\frac{\gamma\beta_0 p}{B^2+\gamma\beta_0 p}\left(2\beta_0\frac{dp}{dA}B_p + \frac{\partial B^2}{\partial a} + \frac{B_p^2}{B}\frac{\partial B^2}{\partial n}y_5\right)\mathbf{B}\cdot\nabla y_2 \\
&+ \quad \left[\frac{2J}{r^2}\left(\frac{J}{r^2}+\frac{\partial B_p}{\partial a}\right) + \frac{2GG'}{r^3}B_p\frac{\partial r}{\partial a}\right]\frac{y_1}{B_p^2} \\
&- \quad y_1\mathbf{B}\cdot\nabla\left[\frac{r^2B_p}{B}y_5\left(\frac{B_p}{B}\frac{G'}{r^2}+\frac{GJ}{r^4BB_p}\right)\right] \\
&- \quad \frac{\gamma\beta_0 p}{B^2+\gamma\beta_0 p}\frac{1}{B^2B_p^2}\left[2\beta_0\frac{dp}{dA} + \frac{\partial B^2}{\partial a} + \frac{B_p^2}{B}\frac{\partial B^2}{\partial n}y_5\right]^2 y_1 \\
&= \quad 0 \qquad\qquad (D.4)
\end{aligned}
$$

and

$$
\begin{aligned}
\mathbf{B}\cdot\nabla\left(\frac{1}{B_p}\frac{\gamma\beta_0 p}{B^2+\gamma\beta_0 p}\left(2\beta_0\frac{dp}{dA}B_p + \frac{\partial B^2}{\partial a} + \frac{B_p^2}{B}\frac{\partial B^2}{\partial n}y_5\right)y_1\right) \quad - \\
\mathbf{B}\cdot\nabla\left(\frac{\gamma\beta_0 pB^2}{B^2+\gamma\beta_0 p}\mathbf{B}\cdot\nabla y_2\right) \quad = \quad 0. \qquad (D.5)
\end{aligned}
$$

These two equations can be rewritten as a set of four coupled first order ordinary differential equations.

Appendix E

The Euler-Lagrange equations for minimization of $\mathcal{I}$

The non-negative $\mathcal{I}$-part of δW is

$$\begin{aligned}\mathcal{I} &= \int[\frac{B^2}{r^2 B_p^2}\left[\frac{\partial}{\partial s}y_1\right]^2 - \left[\frac{2J}{r^2}\left(\frac{J}{r^2}+\frac{\partial B_p}{\partial a}\right)+\frac{2GG'}{r^3}B_p\frac{\partial r}{\partial a}\right]\frac{y_1^2}{B_p^2} \\ &+ \frac{\gamma\beta_0 p}{B^2+\gamma\beta_0 p}\left[B^2\frac{\partial y_2}{\partial s}-\frac{1}{B}\left(\left(2\beta_0\frac{dp}{dA}B_p+\frac{\partial B^2}{\partial a}\right)\frac{y_1}{B_p}+\frac{\partial B^2}{\partial n}\frac{B_p y_5}{B}\right)\right]^2 \\ &+ r^2\left[B_p\frac{\partial}{\partial s}y_5-\frac{G}{BB_p r^2}\left(2\beta_0\frac{dp}{dA}B_p+\frac{1}{r^2}\frac{\partial}{\partial a}\left(r^2B^2\right)\right)\frac{y_1}{B_p}\right]^2]dV, \end{aligned} \tag{E.1}$$

This expression is integrated with respect to the volume element dV, where $dV = da\,dn\,ds$. We can easily integrate in the flux surfaces (integration by dn) and across the flux surfaces (integration by da) if we assign Dirac Delta properties to a:

$$\text{e.g.} \quad \int_{-\infty}^{\infty}\xi_n^2\,\mathrm{da} = 1 \quad \text{etc.}$$

This highlights a specific field line. We are left with a one-dimensional integral that can be minimized using calculus of variations with respect to y_1, y_2 and y_5 subject to the

normalizing condition

$$L = \int y_1^2 \frac{f^2}{r^2 B_p^2} dV = \text{ constant}$$

where f^2 is a positive function (this excludes the trivial solution $\xi = 0$).

To minimize, let

$$Y_1(s) = y_1(s) + \epsilon\eta(s),$$

$$Y_2(s) = y_2(s) + \epsilon\zeta(s)$$

and

$$Y_5(s) = y_5(s) + \epsilon\nu(s),$$

where

$$\int \eta(s)ds = \int \zeta(s)ds = \int \nu(s)ds = 0$$

on the surface.

Then let

$$I(\epsilon) = \int f(s, Y_1, Y_2, Y_5)ds,$$

$$L(\epsilon) = \int g(s, Y_1)ds,$$

and then let

$$I^* = I(\epsilon) + \lambda L(\epsilon),$$

where λ is a Lagrange multiplier. Now

$$\frac{\partial I^*}{\partial \epsilon} = 0 \quad \text{when} \quad \epsilon = 0$$

will give the minimum, and I^* can be written as

$$I^* = C \int [\frac{1}{r^2 B_p^2} [\mathbf{B} \cdot (Y_1 - \epsilon\eta)]^2$$

$$
\begin{aligned}
&- \left[\frac{2J}{r^2}\left(\frac{J}{r^2}+\frac{\partial B_p}{\partial a}\right)+\frac{2GG'}{r^3}B_p\frac{\partial r}{\partial a}\right]\frac{(Y_1-\epsilon\eta)^2}{B_p^2}\\
&+ \frac{\gamma\beta_0 p}{B^2+\gamma\beta_0 p}\left[B^2\left[\mathbf{B}\cdot(Y_2-\epsilon\zeta)\right]^2+\frac{1}{B^2B_p^2}\left(2\beta_0\frac{dp}{dA}B_p+\frac{\partial B^2}{\partial a}\right)^2(Y_1-\epsilon\eta)^2\right]\\
&+ \frac{\gamma\beta_0 p}{B^2+\gamma\beta_0 p}\left[\frac{B_p^2}{B^4}\left(\frac{\partial B^2}{\partial n}\right)^2(Y_5-\epsilon\nu)^2-\left(4\beta_0\frac{dp}{dA}+\frac{2}{B_p}\frac{\partial B^2}{\partial a}\right)\mathbf{B}\cdot(Y_2-\epsilon\zeta)(Y_1-\epsilon\eta)\right]\\
&- \frac{\gamma\beta_0 p}{B^2+\gamma\beta_0 p}\left[\frac{2B_p}{B}\frac{\partial B^2}{\partial n}\mathbf{B}\cdot(Y_2-\epsilon\zeta)(Y_5-\epsilon\nu)\right]\\
&+ \frac{\gamma\beta_0 p}{B^2+\gamma\beta_0 p}\left[\frac{2}{B^3}\left(2\beta_0\frac{dp}{dA}B_p+\frac{\partial B^2}{\partial a}\right)\frac{\partial B^2}{\partial n}(Y_1-\epsilon\eta)(Y_5-\epsilon\nu)\right]\\
&+ \left[\frac{B_p^2r^2}{B^2}\left[\mathbf{B}\cdot(Y_5-\epsilon\nu)\right]^2-\frac{2G}{B^2}\left(2\beta_0\frac{dp}{dA}+\frac{1}{r^2B_p}\frac{\partial}{\partial a}\left(r^2B^2\right)\right)\mathbf{B}\cdot(Y_5-\epsilon\nu)(Y_1-\epsilon\eta)\right]\\
&+ r^2\left[\frac{G^2}{r^4B^2B_p^4}\left(2\beta_0\frac{dp}{dA}B_p+\frac{1}{r^2}\frac{\partial}{\partial a}\left(r^2B^2\right)\right)(Y_1-\epsilon\eta)^2\right]]ds, \qquad \text{(E.2)}
\end{aligned}
$$

Using the identities

$$
\begin{aligned}
\frac{\partial}{\partial\epsilon}a\left[\mathbf{B}\cdot\nabla(Y_1-\epsilon\eta)\right]^2|_{\epsilon=0} &= 2\eta\mathbf{B}\cdot\nabla\left[a\mathbf{B}\cdot\nabla(y_1)\right],\\
\frac{\partial}{\partial\epsilon}\left(Y_1-\epsilon\eta\right)^2|_{\epsilon=0} &= -2\eta y_1,\\
\frac{\partial}{\partial\epsilon}a\left[\mathbf{B}\cdot\nabla(Y_1-\epsilon\eta)(Y_1-\epsilon\eta)\right]|_{\epsilon=0} &= \eta y_1\mathbf{B}\cdot\nabla a,\\
\frac{\partial}{\partial\epsilon}\left[(Y_1-\epsilon\eta)(Y_2-\epsilon\zeta)\right]|_{\epsilon=0} &= -\zeta y_1-\eta y_2,\\
\frac{\partial}{\partial\epsilon}a\left[\mathbf{B}\cdot\nabla(Y_1-\epsilon\eta)(Y_2-\epsilon\zeta)\right]|_{\epsilon=0} &= -\zeta a\mathbf{B}\cdot\nabla y_1+\eta\mathbf{B}\cdot\nabla(ay_2),\\
\frac{\partial}{\partial\epsilon}a\left[\mathbf{B}\cdot\nabla(Y_2-\epsilon\zeta)(Y_1-\epsilon\eta)\right]|_{\epsilon=0} &= -\eta a\mathbf{B}\cdot\nabla y_2+\zeta\mathbf{B}\cdot\nabla(ay_1),
\end{aligned}
$$

and equating the terms in η, ζ and ν to 0 we get the Euler-Lagrange equations:

$$
\begin{aligned}
\mathbf{B}\cdot\nabla\left(\frac{1}{r^2B_p^2}\mathbf{B}\cdot\nabla y_1\right) &+ \left[\frac{2J}{r^2}\left(\frac{J}{r^2}+\frac{\partial B_p}{\partial a}\right)+\frac{2GG'}{r^3}B_p\frac{\partial r}{\partial a}\right]\frac{y_1}{B_p^2}\\
&- \frac{\gamma\beta_0 p}{B^2+\gamma\beta_0 p}\frac{1}{B^2B_p^2}\left(2\beta_0\frac{dp}{dA}B_p+\frac{\partial B^2}{\partial a}\right)^2y_1\\
&+ \frac{\gamma\beta_0 p}{B^2+\gamma\beta_0 p}\frac{1}{B_p}\left(2\beta_0\frac{dp}{dA}B_p+\frac{\partial B^2}{\partial a}\right)\mathbf{B}\cdot\nabla y_2\\
&+ \frac{G}{B^2B_p}\left(2\beta_0\frac{dp}{dA}B_p+\frac{1}{r^2}\frac{\partial}{\partial a}\left(r^2B^2\right)\right)\mathbf{B}\cdot\nabla y_5
\end{aligned}
$$

$$+ \quad \frac{\gamma\beta_0 p}{B^2+\gamma\beta_0 p}\frac{1}{B_p}\frac{1}{B^3}\frac{\partial B^2}{\partial n}\left(2\beta_0\frac{dp}{dA}B_p+\frac{\partial B^2}{\partial a}\right)y_5$$
$$- \quad \frac{G^2}{r^2B^2B_p^4}\left(2\beta_0\frac{dp}{dA}B_p+\frac{1}{r^2}\frac{\partial}{\partial a}\left(r^2B^2\right)\right)y_1=0, \qquad \text{(E.3)}$$

$$\mathbf{B}\cdot\nabla\left(\frac{\gamma\beta_0 p}{B^2+\gamma\beta_0 p}B^2\mathbf{B}\cdot\nabla y_2\right) - \mathbf{B}\cdot\nabla\left(\frac{\gamma\beta_0 p}{B^2+\gamma\beta_0 p}\frac{1}{B_p}\left(2\beta_0\frac{dp}{dA}B_p+\frac{\partial B^2}{\partial a}\right)y_1\right)$$
$$- \mathbf{B}\cdot\nabla\left(\frac{\gamma\beta_0 p}{B^2+\gamma\beta_0 p}\frac{B_p}{B}\frac{\partial B^2}{\partial n}y_5\right)=0, \qquad \text{(E.4)}$$

and

$$\mathbf{B}\cdot\nabla\left(\frac{r^2B_p^2}{B^2}\mathbf{B}\cdot\nabla y_5\right) - \mathbf{B}\cdot\nabla\left[\frac{G}{B^2B_p}y_1\left(2\beta_0\frac{dp}{dA}B_p+\frac{1}{r^2}\frac{\partial}{\partial a}\left(r^2B^2\right)\right)\right]+$$
$$\frac{\gamma\beta_0 p}{B^2+\gamma\beta_0 p}\frac{B_p}{B}\frac{\partial B^2}{\partial n}\mathbf{B}\cdot\nabla y_2 + \frac{\gamma\beta_0 p}{B^2+\gamma\beta_0 p}\frac{1}{B^3}\frac{\partial B^2}{\partial n}\left(2\beta_0\frac{dp}{dA}B_p+\frac{\partial B^2}{\partial a}\right)y_1 -$$
$$\frac{\gamma\beta_0 p}{B^2+\gamma\beta_0 p}\frac{B_p^2}{B^4}\left(\frac{\partial B^2}{\partial n}\right)^2 y_5 = 0. \qquad \text{(E.5)}$$

These three equations can be rewritten as a set of six coupled first order ordinary differential equations.

Appendix F

Derivation of the auxiliary equation

We start of with the transformation

$$\begin{aligned}\nabla \times \left(S\frac{\mathbf{e}_\theta}{r}\right) &= \nabla S \times \frac{\mathbf{e}_\theta}{r} \\ &= \frac{\nabla A \cdot \nabla S}{|\nabla A|^2}\nabla A \times \frac{\mathbf{e}_\theta}{r} + \frac{\mathbf{B}_p \cdot \nabla S}{B_p^2}\mathbf{B_p} \times \frac{\mathbf{e}_\theta}{\mathbf{r}} \\ &= \frac{\nabla A \cdot \nabla S}{r^2 B_p^2}\mathbf{B}_p - \frac{\mathbf{B}_p \cdot \nabla S}{r^2 B_p^2}\nabla A\end{aligned}$$

where S is defined by Equation (5.33). We take the divergence of the above to give

$$\nabla \cdot \nabla \times \left(S\frac{\mathbf{e}_\theta}{r}\right) = 0 = \nabla \cdot \left(\frac{\nabla A \cdot \nabla S}{r^2 B_p^2}\mathbf{B}_p\right) - \nabla\left(\frac{\mathbf{B}_p \cdot \nabla S}{r^2 B_p^2}\nabla A\right).$$

So,

$$\mathbf{B}_p \cdot \nabla\left(\frac{\nabla A \cdot \nabla S}{r^2 B_p^2}\right) = -\nabla \cdot \left(\frac{G}{r^4 B_p^2}\nabla A\right),$$

since $\nabla \cdot \mathbf{B}_p = 0$ and $\mathbf{B} \cdot \nabla S = 0 = G/r^2 + \mathbf{B}_p \cdot \nabla S$. Therefore

$$\mathbf{B} \cdot \nabla\left(\frac{\nabla A \cdot \nabla S}{r^2 B_p^2}\right) = -\frac{G}{r^2 B_p^2}\nabla \cdot \left(\frac{\nabla A}{r^2}\right) - \frac{\nabla A}{r^2} \cdot \nabla\left(\frac{G}{r^2 B_p^2}\right),$$

i.e.

$$\mathbf{B} \cdot \nabla\left(\frac{\nabla A \cdot \nabla S}{r^2 B_p^2}\right) = -\frac{1}{r^2}\frac{dG}{dA} + \frac{G}{r^2 B_p^2}\left(\frac{J}{r^2} + 2\frac{\partial B_p}{\partial a} - r^2 B_p \frac{\partial}{\partial a}\left(\frac{1}{r^2}\right)\right).$$

Use of the definitions

$$B\frac{\partial}{\partial s} = \mathbf{B} \cdot \nabla$$

and

$$y_5 = \frac{\nabla A \cdot \nabla S}{r^2 B_p^2}$$

then results in the desired equation.

Appendix G

References

Aleskin, V. F. and Romanov, S. S. 1974, *Zhurnal Tech. Fiz.* **44**, 1877.

An, C. H. 1982, *Solar Phys.* **75**, 19.

An, C. H. 1984, *Astrophys. J.* **281**, 419.

An, C. H. 1986, *Astrophys. J.* **304**, 532.

An, C. H., Wu, S. T. and Boa, J. J. 1988, in J. L. Ballester and E. R. Priest (eds) *Proc. Mallorca Workshop on Dynamics and Structure of Solar Prominences.* University of the Balearic isles, Palma.

Antiochos, S. 1979, *Astrophys. J.* **232**, L125.

Antiochos, S., Shoub, E. C., An, C. H. and Emslie, A. G. 1985, *Astrophys. J.* **298**, 876.

Babcock, H. and Babcock, H. 1955, *Astrophys. J.* **121**, 349.

Bateman, G. 1978, *MHD Instabilities*, MIT Press, Cambridge, Massachusetts.

Berger, M. A. and Field, G. B. 1984, *J. Fluid Mech.* **147**, 133.

Bernstein, I. B., Frieman, E. A. and Kulsrud, R. M. 1958, *Proc. Royal Soc.* **A244**, 17.

Birn, J. and Schindler, K. 1981, in E. R. Priest (ed), *Solar Flare Magnetohydrodynamics*,

Gordon and Breach Science publishers, New York.

Bodin, H. A. B. and Newton, A. A. 1980, *Nuclear Fusion* **20**, 1255.

Bommier, V. 1986, in A. Poland (ed) *Coronal and prominence Plasmas* NASA Conf. Pub.

Browning, P. K. 1988, *Plasma Phys.* **30**, 1.

Bruhns, H. 1986, *Plasma Phys.* **28**, 1389.

Bussac, M. N., Furth, H. P., Okabayashi, M., Rosenbluth, M. N. and Todd, A. M. 1978, PPPL Report 1472..

Cargill, P. J. and Hood, A. W. 1989, *Solar Physics* **124**, 101.

Cargill, P. J. and Hood, A. W. 1993, in preperation.

Chandrasekhar, S. and Kendall, P. C. 1957, *Astrophys. J.* **126**, 457.

Chiuderi, C. and Van Hoven, G. 1979, *Astrophys. J.* **232**, L69.

Clegg, J. C., Browning, P. K. and Rusbridge, M. G. 1989, preprint.

Connor, J. W., Hastie R. J. and Taylor J. B. 1979, *Proc. Royal Soc.* **A365**, 1.

Craig, I. J. D. and McClymont, A. N. 1987, *Astrophys. J.* **318**, 421.

De Bruyne, P. and Hood, A. W. 1989a, *Solar Phys.* **119**, 87.

De Bruyne, P. and Hood, A. W. 1989b, *Solar Phys.* **1123**, 241.

De Bruyne, P. 1990, *PhD Thesis*, St Andrews University.

Dewar, R. L. and Glasser A. H. 1983, *Phys. Fluids* **26**, 3039.

Einaudi, G. and Van Hoven, G. 1981, *Phys. Fluids* **31**, 813.

Einaudi, G. and Van Hoven, G. 1983, *Solar Phys.* **88**, 163.

Field, G. B. 1962, in L. Woltjer (ed), *Interstellar Matter in Galaxies*, W. A. Benjamin Inc., New York.

Field, G. B. 1965, *Astrophys. J.* **142**, 531.

Freidberg, J. P. 1982, *Rev. Mod. Phys.* **54**, 801.

Gibson, R. D. and Whiteman, K. 1968, *Plasma Phys.* **10**, 1101.

Gimblett, C. G. 1986, *Nuclear Fusion* **26**, 617.

Gimblett, C. G. 1987, in *Physics of Mirrors, Reversed Field Pinches and Compact Tori.*

Goedbloed, J. P., Pfirsch, D. and Tasso, H. 1972, *Nuclear Fusion* **12**, 649.

Goedbloed, J. P. 1983, *Lecture Notes in Ideal Magnetohydrodynamics*, Rijnhuizen Report.

Gold, T. and Hoyle, F. 1959, in R. N. Bracewell (ed), *Paris Symposium on Radio Astronomy*, Stanford Univ. Press, California.

Habbal, S. and Rosner, R. 1978, *Astrophys. J.* **234**, 1113.

Hain K. Von, Lüst, R. and Schlüter, A. 1957, *Z. Naturforschg.* **12a**, 833.

Hart, G. W., Janos, A., Meyerhofer, D. D. and Yamada, M. 1985, *Phys. Fluids.*

Hender, T. C., Gimblett, C. G. and Robinson, D. C. 1989, *Nuclear Fusion* **29**, 1279.

Hender, T. C., Gimblett, C. G. and Robinson, D. C. 1986, *Contolled Fusion and Plasma Heating.*

Hermans, D., Hood, A. W. and Clifford, L. 1990, in *The Dynamic Sun,* Publ. Debrecen Obs. Vol. 7.

Hermans, D. 1988, *PhD Thesis*, Katholieke Universiteit Leuven.

Heyvaerts, J. 1974, *Astron. Astrophys.* **37**, 65.

Hildner, E. 1974, *Solar Physics* **35**, 123.

Hood, A. W. 1990, *Comp. Phys. Rep.* **12**, 177.

Hood, A. W. 1991, *Plasma Phys. and Conrollled Fusion* **34**, 411.

Hood, A. W. 1983, *Solar Phys.* **87**, 279.

Hood, A. W. 1986, *Solar Phys.* **103**, 329.

Hood, A. W., Cargill, P. J., Van der Linden, R. and Goossens, M. 1993, in preperation.

Hood, A. W., Van der Linden, R. and Goossens, M. 1989, *Solar Phys.* **87**, 261.

Hood, A. W. and Priest, E. R. 1980a, *Solar Phys.* **66**, 110.

Hood, A. W. and Priest, E. R. 1980b, *Astron. Astrophys.* **87**, 126.

Hood, A. W. and Priest, E. R. 1979, *Solar Phys.* **64**, 303.

Hu, Y. Q. 1987, *Scientia Sinica (Ser. A)* **30**, 509.

Jarboe, T. R., Henins, Sherwood, A. R., Barnes, C. W. and Hoida, H. W. 1983, *Phys. Rev. Lett.* **51**, 39.

Jensen, E. , Maltby, P. and Orrall, F. 1979, *Physics of Solar Prominences*, IAU Colloq No. 44.

Jensen, T. R. and Chu, M. S. 1983, *Plasma Phys.* **30**, 57.

Jensen, T. R. and Chu, M. S. 1984, *Phys. Fluids* **27**, 2881.

Klimchuk, J. A., Antiochos, S. K. and Mariska J. T. 1987, *Astrophys. J.* **320**, 409.

Kadomtsev, B. B. 1966, in M. A. Leontovich (ed), *Reviews of Plasma Physics*, Consultants Bureau, New York, **2**, 153.

Kiepenheuer, K. O. 1953, in G. Kuiper (ed) *The Sun* Chicago Univ. Press.

Laval, G., Mercier, C. and Pellat R. 1965, *Nuclear Fusion* **5**, 156.

Leroy, J. L. 1979, in Jensen *et al.* (1979), 56.

Lundquist, S. 1951 *Phys. Rev. (Ser. II)* **83**, 307.

Martin, T. J. and Taylor, J. B. 1974, *Helically deformed States in Toroidal Pinches*, Culham Laboratory Report (unpublished).

McClymont, A. N. and Craig, I. J. D. 1985a, *Astrophys. J.* **289**, 820.

McClymont, A. N. and Craig, I. J. D. 1985b, *Astrophys. J.* **289**, 834.

McWhirter, R. W. P., Thonemann, P. C. and Wilson, R. 1975, *Astron. Astrophys.* **40**, 63.

Mok, Y., Drake, J. F., Schnack, D. D. and Van Hoven G. 1990, *Astrophys. J.* **359**, 228.

Mok, Y., Schnack, D. D. and Van Hoven G. 1991, *Solar Phys.* **132**, 95.

Nalesso, G. F. and Costa, S. 1980, *Nuclear Fusion* **20**, 443.

Nayfeh, 1983. *Problems in Perturbation Theory.*

Newcomb, W. 1960 *Ann. Phys.* **10**, 232.

Oran, E. S., Mariska, J. T. and Boris, J. P. 1982, *Astrophys. J.* **254**, 349.

Parker, E. N. 1953, *Astrophys. J.* **117**, 431.

Parker, E. N. 1963, *Interplanetary Dynamical Processes*, Interscience Pub., New York.

Pfirsch, D. and Tasso, H. 1971, *Nuclear Fusion* **11**, 259.

Poland, A. and Mariska J. 1988, in J. L. Ballester and E. R. Priest (eds) *proc. Mallorca Workshop on Dynamics and Structure of Solar Prominences.* University of the Balearic isles, Palma.

Press, W. H., Flannery, B. P., Teukolsky, S. A. and Vetterling, W. T. 1987, *Numerical Recipes,* Cambridge University Press, Cambridge.

Priest, E. R. 1982, *Solar Magnetohydrodynamics*, D. Reidel Publ. Co., Dordrecht, Holland.

Priest, E. R. (ed.) 1989, *Dynamics and Structure of Quiescent Solar Prominences*, Kluwer Academic Publishers, Dordrecht, Holland.

Priest, E. R., Hood, A. W. and Anzer, U. 1989, *Astrophys. J.* **344**, 1010.

Raadu, M. 1972, *Solar Physics* **22**, 425.

Raymond, J. C. and Smith, B. W. 1977, *Astrophys. J. Suppl.* **35**, 419.

Robinson, D. C. 1978, *Nuclear Fusion* **18**, 939.

Rosenbluth, M. N. 1958, *Peaceful Uses of Atomic energy* (Proc. Int. Conf. Geneva, 1958).

Rosenbluth, M. N. and Bussac, M. N. 1979, *Nuclear Fusion* **19**, 489.

Rosner, R., Low, B. C. and Holzer, T. E. 1986, in P. Sturrock, T. Holzer, D. Mihalas and D. Ulrich (eds), *Physics of the Sun*, D. Reidel, Dordrecht, Holland.

Rosner, R., Tucker, W. H. and Vaiana, G. S. 1978, *Astrophys. J.* **220**, 643.

Rust, D. 1967, *Astrophys J.* **150**, 313.

Sato, T. and Kusano, K. 1985, *Plasma Physics and Controlled Nuclear Fusion Research 1984.*

Sparks, L. and Van Hoven, G. 1987, *Phys. Fluids* **30**, 2470.

Sparks, L. and Van Hoven, G. 1988, *Astrophys. J.* **333**, 953.

Sparks, L. Van Hoven G. and Schnack, D. D. 1990, *Astrophys. J.* **353**, 297.

Spitzer, L. 1962 *Physics of Fully Ionized Gasses*, Interscience, New York.

Steinolfson, R. S. 1984, *Astrophys. J.* **281**, 854.

Sykes, A. and Wesson, J. A. 1977, *Proc. of the 8th European Conference on Controlled Fusion and Plasma Physics*, Prague.

Tandberg-Hanssen, E. 1974, *Solar Prominences* D Reidel.

Taylor, J. B. 1974, *Phys. Rev. Lett.* **33**, 1139.

Taylor, J. B. 1976, in *Pulsed High Beta plasmas*, Pergamon, Oxford.

Taylor, J. B. 1986, *Reviews of Modern Physics*, **58**, 741.

Turner, L. 1984, *Phys. fluids* **27**, 1677.

Turner, W. C., Goldenbaum, G. C., Granneman, E. H. A., Hammer, J. H., Hartman, C.

W., Prono, D. S. and Taska, J. 1983, *Phys. Fluids* **26**, 1965.

Van der Linden, R. 1991, *PhD Thesis*, Katholieke Universiteit Leuven.

Van der Linden, R. 1992, preprint.

Van der Linden, R., Goossens, M. and Hood, A. W. 1991, *Solar Phys.* **140**, 317.

Van Hoven, G., Sparks, L. and Tachi, T. 1986, *Astrophys. J.* **300**, 249.

Van Hoven, G. 1981, in E. R. Priest (ed), *Solar Flare Magnetohydrodynamics*, Gordon and Breach Science Publishers, New York.

Van Hoven G., Sparks L. and Schnack, D. D. 1987, *Astrophys. J.* **317**, L91.

Wesson, J. A. 1978, *Nuclear Fusion* **18**, 87.

Whiteman, K. 1962, *Plasma Phys.* **7**, 293.